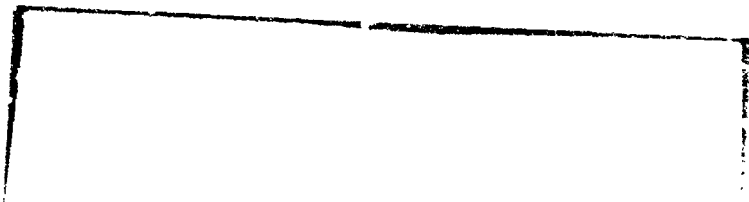


(NASA-CR-161972) GLASS SHELL MANUFACTURING  
IN SPACE Final Report, Dec. 1978 - Dec.  
1981 (KMS Fusion, Inc., Ann Arbor, Mich.)  
104 p HC A06/MP A01 CSCI 22A

N82-17233

Unclas  
08943

G3/12



**fusion** -kms  
inc.

**KMS FUSION, INC.  
3621 South State Road  
Ann Arbor, Michigan 48104  
Department of Materials Sciences**

**FINAL REPORT  
GLASS SHELL MANUFACTURING  
IN SPACE**

**From December 1978, to December 1981**

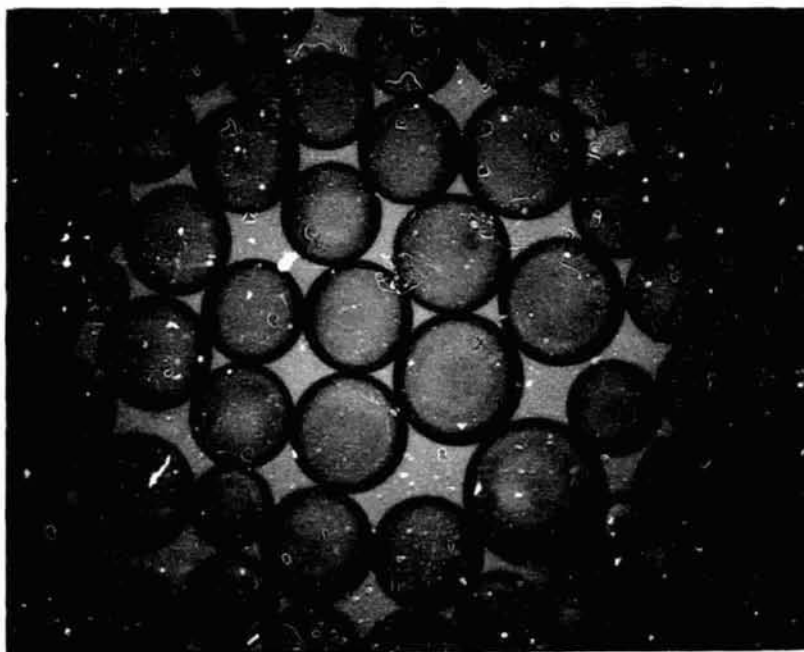
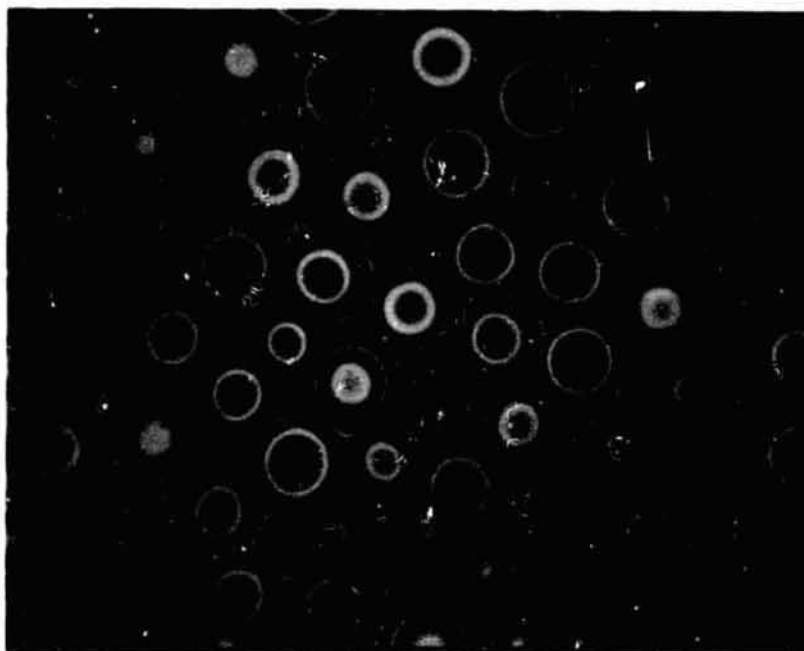
**Date of Publication: December 21, 1981**

**FINAL REPORT  
NAS8-33103**

*Raymond L. Downs, PI,  
Matthias A. Ebner, Co-I, and  
Robert L. Nolen, Jr., Co-I*

**Prepared for George C. Marshall Space Flight Center,  
Marshall Space Flight Center, Alabama 35812**

ORIGINAL PAGE  
COLOR PHOTOGRAPH



Optical and Interferometric photomicrographs of a batch of highly-uniform glass shells, having an average diameter of 250  $\mu$ m and wall thickness of 1  $\mu$ m.

## TABLE OF CONTENTS

ABSTRACT	1
1. INTRODUCTION	2
2. PYROLYSIS STUDY OF GELS	4
2.1 Gel Morphology	4
2.2 Mass/Dimensional Changes	12
2.3 Shells from Pyrolyzed Gels	16
2.4 Specific Heat	19
2.5 Gases Evolved by Gel Pyrolysis	23
3. NATURE AND SOURCE OF SHELL FORMING GASES	30
3.1 Residual Gases in Shells	30
3.2 Source of the Gases	32
4. FURNACE-TO-GEL HEAT TRANSFER MODEL	35
4.1 Mathematical Model	36
4.2 Model Predictions and Experimental Observations	38
5. EFFECT OF GRAVITY ON SHELL CONCENTRICITY	50
5.1 Shell-Decentering Model	50
5.2 Preliminary Model-Testing Experiments	52
6. CONCLUSIONS	62
7. RECOMMENDATIONS	65
7.1 Mass Transport Study	65
7.2 Shell Centering Study	65
7.3 Shell Decentering Study	66
ACKNOWLEDGEMENTS	67
REFERENCES	68
APPENDIX I	70
APPENDIX II	81
APPENDIX III	85
APPENDIX IV	90

## ILLUSTRATIONS

<u>Figures</u>	<u>Title</u>	
1.	a. Initial Expansion of Compacted Gel Powder, and Formation of Closed-cell Foam	7
	b. Gel Sintering and Expansion of Cell Structure	8
	c. Gel Spheroidization	9
	d. Hollow Glass Shell	10
2.	Foam Coalescence in Glass Spheroid	11
3.	a. Effect of Gel Pyrolysis	14
	b. Effect of Gel Pyrolysis	15
4.	TGA Thermograms of Metal-Organic Gel	18
5.	Shells from Pyrolyzed Gels	21
6.	Effect of Pyrolysis on the Specific Heat of Gels	22
7.	Pyrolysis-GC of Gel Powders	25
8.	DTA of Metal-Organic Gel	27
9.	DTA-TGA-PMS Correlation for Unhydrolyzed Gel	28
10.	Pellet Drop Distance as a Function of Pellet Mass	42
11.	Effect of Shell Diameter on Decentering Time	53
12.	Phase Separation in Shells Reheated to 1300°C	56
13.	Change in Surface Texture Upon Reheating Shells to 900°C	57
14.	Phase Separation in Shells Reheated to 800-900°C	58

## TABLES

<u>Tables</u>	<u>Title</u>	
1.	Gel Morphology from Hot Stage Microscopy	6
2.	Effect of Heat Treatment on Gel Pellets	13
3.	Pellet-to-Shell Mass Correlations	17
4.	Effect of Gel Pyrolysis on Shell Formation	20
5.	Pyrolysis-Gas Chromatography of Metal-Organic Gels	24
6.	Residual Gases in Shells of Several Compositions	31
7.	Residual Gases in Shells Exposed to Water Vapor During Shell Blowing	33
8.	Effect of Specific Heat on Pellet Heating	43
9.	Effect of Furnace Gas	45
10.	Effects of Hot Zone Length on Shell Characteristics	48
11.	EDXS Elemental Analysis of Remelted Glass Shells	59

## ABSTRACT

Highly-uniform, hollow glass spheres (shells), which are used for inertial confinement fusion targets, are formed from metal-organic gel powder feedstock in a vertical furnace. The modeling of this gel-to-shell transformation has consisted of three phases: a study of the effect of pyrolysis on gel morphology and thermochemistry; development and testing of a furnace-to-gel heat transfer model; and development and preliminary testing of a model describing the gravity-driven degradation of shell concentricity as a function of shell characteristics and time.

As a result of the rapid pyrolysis caused by the furnace, the gel is transformed to a shell in five distinct stages: a) surface closure of the porous gel, b) generation of a closed-cell foam structure in the gel, c) spheridization of the gel and further expansion of the foam, d) coalescence of the closed-cell foam to a single-void shell, and e) fining of the glass shell. Initial foaming is driven by the pyrolysis of the residual organics, such as the metal alkoxides and alcohol, and by the decomposition of silanols and the alkali bicarbonates in the gel. Further foam expansion is driven by the oxidation of the elemental carbon produced in the initial pyrolysis and by decomposition of the alkali carbonates in the gel. The sole shell-forming gases were identified from residual gas analyses as  $\text{CO}_2$ ,  $\text{H}_2\text{O}$ ,  $\text{O}_2$  and  $\text{N}_2$ . The  $\text{O}_2$  and  $\text{N}_2$  from the furnace ambience permeate into the shell during its formation.

The heat transfer from the furnace to the falling gel particle was modeled to determine the effective heating rate of the gel. The model predicts the temperature history for a particle as a function of mass, dimensions, specific heat, and absorptance as well as furnace temperature profile and thermal conductivity of the furnace gas. This model has been experimentally verified.

In the third phase, a model was developed that predicts the gravity-induced degradation of shell concentricity in falling molten shells as a function of shell characteristics and time. The model predicts negligible rates of decentering for glass shells smaller than 2 mm diameter. The validity of the model and initial efforts for testing the model are discussed.

## 1. INTRODUCTION

Targets currently used in inertial confinement fusion (ICF) include spherical glass shells filled with deuterium-tritium fuel. Currently these shells have diameters from 100 to 500  $\mu\text{m}$ . and wall thickness from 0.5 to 10  $\mu\text{m}$ . To meet the experimental requirements the non-concentricity<sup>†</sup> of the inner and outer surfaces of the shells must be less than 5%, asphericity less than 1% and surface irregularities less than 0.5  $\mu\text{m}$ . These specifications are becoming more stringent as the available laser power increases and laser fusion experiments become more sophisticated. In addition, the shells are required to have high strength, good chemical durability and be permeable to various diagnostic and fuel gases. Meeting these requirements becomes particularly difficult for the next generation of targets whose diameters are greater than 1mm, the effective size limit for current manufacturing methods. For such large glass shells, the force of gravity and the aerodynamic forces, acting upon falling molten shells, will increasingly manifest themselves, degrading the concentricity and sphericity of the shells, and by virtue of the relatively large terminal velocity of the gel, limit the glass fining time interval during which a falling particle is exposed to the heat of the furnace.

These shells are currently manufactured by several methods [1,2,3]. One of the more promising and versatile methods involves the use of metal-organic powder which is fed into an electrically-heated vertical tube furnace whereby glass shells are formed. Metal-organic gels as glass precursors permit the formation of hollow glass spheres with a variety of glass compositions [4,5,6].

In view of the limitations on shell size and quality that are imposed by the gravitation and aerodynamic forces on the current methods, the manufacture of shells in the near-weightless environment of space seems to be a viable alternative to earth-based manufacture of large-diameter highly-uniform shells. A necessary preliminary to any glass manufacturing experiments in space is a better understanding of the gel-to-glass-sphere

<sup>†</sup>Non-concentricity is defined by the ratio of  $\Delta d/d$  where  $d$  is the wall thickness. Asphericity is defined by the ratio  $\Delta R/R$ , that is the difference between the maximum and minimum external radii of the oblate, divided by the minimum radius. Surface irregularities are surface features, debris, or reaction products deposited on the surface.

transformation, and an assessment of the effects of gravity on these processes and upon the final molten glass shell. Such an understanding could be attained by a thorough investigation and modelling of the mechanisms that comprise the gel-to-glass shell transformation that occurs during the terrestrial manufacture of shells.

Our ground-based research has consisted of three phases: 1) determining the gel morphology and thermochemistry, 2) modelling furnace-to-gel heat transfer and 3) modelling the effects of gravity on the concentricity of the final glass shell. The results of these efforts are presented herein.

## 2. PYROLYSIS STUDY OF GELS

Since the transformation of the gel to glass involves both physical and chemical processes a study of this transformation involves both a study of the gel morphology and gel thermochemistry. Because the transformation is rapid and the furnace temperature high, monitoring in real-time is difficult. Consequently, we have performed experiments in which we examined stages of the process and typically at much lower heating rates than would occur in the vertical furnace. It should be noted that at the lower heating rates the gel responds more uniformly to temperature changes and internal stresses and the resulting volatiles have time to escape from the gel bulk by diffusion. In contrast to this, the rapid heating rates achieved in the vertical furnace can be expected to trap more volatiles. This difference in heating rate undoubtedly introduces other effects.

2.1 Gel Morphology. The changes that occur in the structure of the gel upon heating were studied by hot stage microscopy. Sodium silicate gels (e.g. 20 mole %  $\text{Na}_2\text{O}$ , 80 mole %  $\text{SiO}_2$ ) were examined extensively because they were simple in composition and were expected to exhibit most of the physical and chemical changes of other glasses of interest. In order to compare the shell-blowing behavior of metal-organic gels to gels having little or no organic constituents, two other gel samples were examined. The first of these was a metal-organic gel, prepared from sodium and silicon ethoxides, which after initial drying, crushing and sieving was exposed to moist air for extended periods. We refer to the gel as-made as "unhydrolyzed" and that exposed to moist air as "hydrolyzed". The second sample was prepared by the evaporation of water from an aqueous (inorganic) sodium silicate solution.

When the aqueous inorganic sodium silicate gel was heated it formed spheroids at  $150^\circ$ , and crude, transparent glass shells at  $300^\circ\text{C}$ . The hydrolyzed metal-organic gel, which like the inorganic silicate sample had a very low surface area ( $< 0.1 \text{ m}^2/\text{gm}$ ), also produced a foam spheroid at relatively low temperatures ( $250$  to  $400^\circ\text{C}$ ), but a similar crude hollow shell did not form until about  $800$  to  $900^\circ\text{C}$ . The unhydrolyzed gel, which contained significant amounts of organic species, was water-poor and had a high surface area ( $\sim 300 \text{ m}^2/\text{gm}$ ) compared to the other samples, remained rigid until about  $500^\circ\text{C}$ , but sporadic movement of the gel particles testified to some gas evolution. Near  $500^\circ\text{C}$ , the gel began to expand and to carbonize,

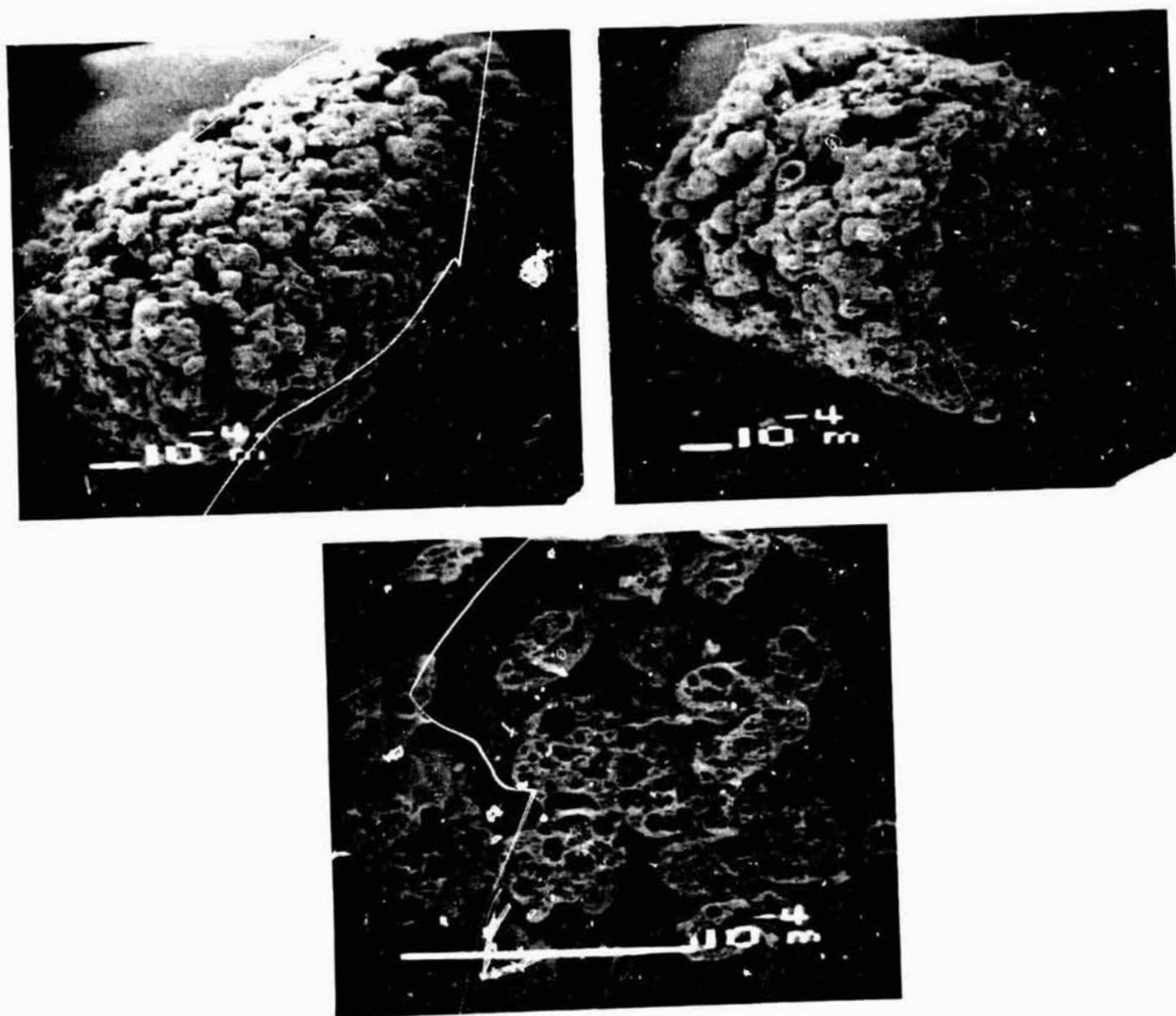
forming a closed-cell foam, and at 800 to 900°C finally formed a crude foam or multi-void spheroid. These observations are summarized in Table 1.

Other, more complex metal-organic gels behaved similarly when examined by hot stage microscopy, that is, the unhydrolyzed gels remained rigid and unchanged until 500 to 600°C, at which time the organic species comprising the gel carbonized. These unhydrolyzed gels then further experienced a volume increase due to foaming, much like pop-corn, followed by glass flow at the surface at 600 to 700°C. Melting of the "glass" and oxidation of carbon occurred at 800 to 1000°C. The oxidation of the trapped carbon probably provided a significant quantity of CO<sub>2</sub> for driving the shell expansion to completion in this temperature regime. The corresponding hydrolyzed gels generally formed a foam structure and expanded at 400°C; otherwise they behaved similarly. Shell intermediates that were recovered from shell-forming experiments have yielded further insight into the gel morphology. These intermediates, formed from 20 to 180 µm cylinders of compacted gel powder (gel pellets)[7] in a vertical furnace, ranged from partially-expanded gel pellets to black spheroids having an internal closed-cell structure to crude, carbon-laden spheres. Scanning electron microscope views of these intermediates, Figure 1a-1d, show the sequence of changes in the external and internal gel structure as the gel pellets transform into hollow glassshells. At relatively low particle temperatures (~ 500°C), before significant surface flow occurred, the gel grains that comprise the pellet were expanded by the gaseous pyrolysates generated in the gel; a closed-cell foam structure was formed in the gel. Upon heating the gel to approximately 600°C, further pellet expansion, sintering of the grains and significant surface flow occurred, consolidating the pellet surface. At higher temperatures, as the material became fluid, the surface tension became dominant, causing the spheridization of the gel particle and the subsequent collapse of the internal closed-cell foam structure into a crude hollow sphere (Fig. 1d). This consolidation of the internal closed-cell structure within the spheroid is more readily inferred from the decreasing number of voids in the spheres in Figure 2. The product of this process is a black spheroid whose thick walls contain bubbles and carbon inclusions. The last phase of the process is further expansion and fining of the hollow glass sphere, driven by the oxidation of these carbon inclusions. Experimental work in support of heat-transfer modelling (discussed later) indicated that the transformation of the gel to a hollow black spheroid occurs rapidly (within ~1 sec @ 1000-1300°C) for gel particles as massive

Table 1. Gel Morphology From Hot Stage Microscopy

Sodium Silicate Gel	Temperature for Structure Changes (°C)				
	Rigid Gel	Sintering	Foaming Expansion	Spheroid	Crude Shell Central Void
Aqueous-Based	25°	-	-	150°	300°
Metal-Organic Hydrolyzed	25°	-	150-200°	240-400°	800-900°
Metal-Organic	25°	400°	500	800-900°	

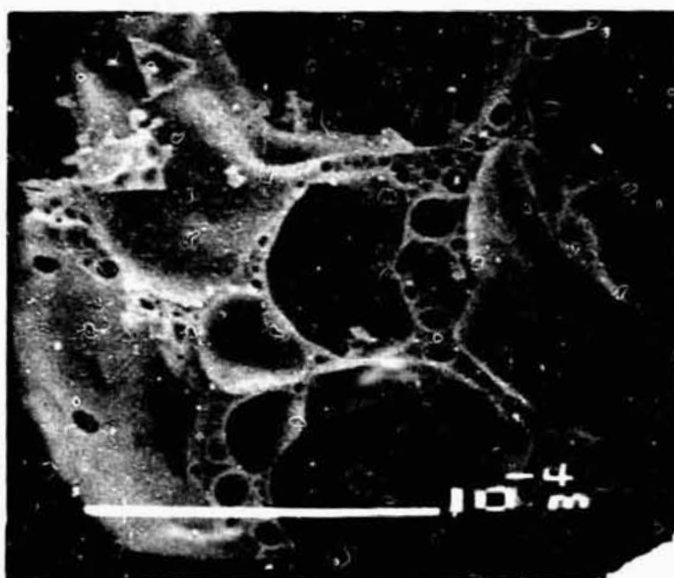
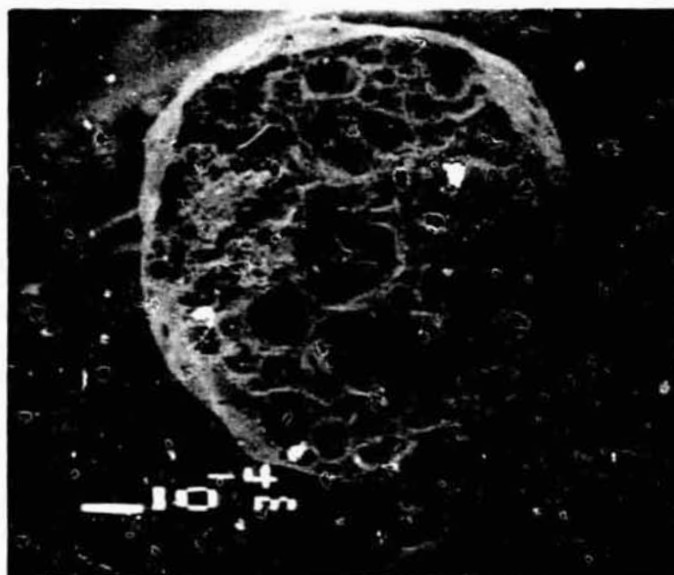
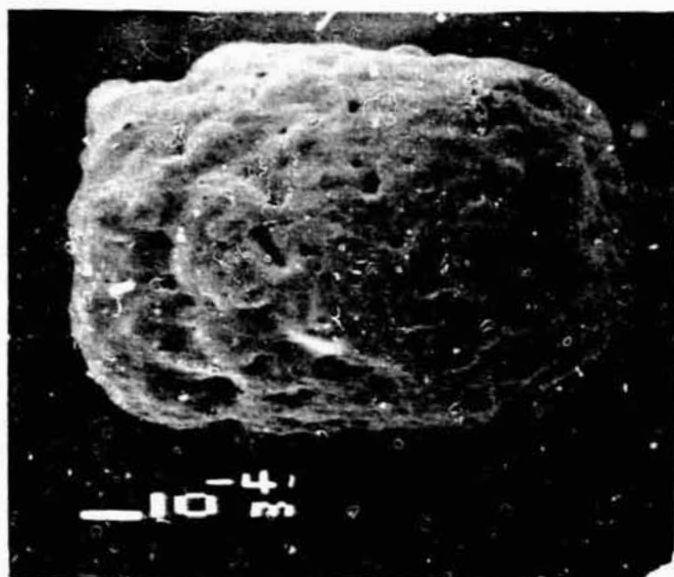
ORIGINAL PAGE  
BLACK AND WHITE PHOTOGRAPH



$T \approx 500^{\circ}\text{C}$

Figure 1 a. Initial Expansion of Compacted Gel Powder (Gel Pellet), and Formation of Closed-Cell Foam.

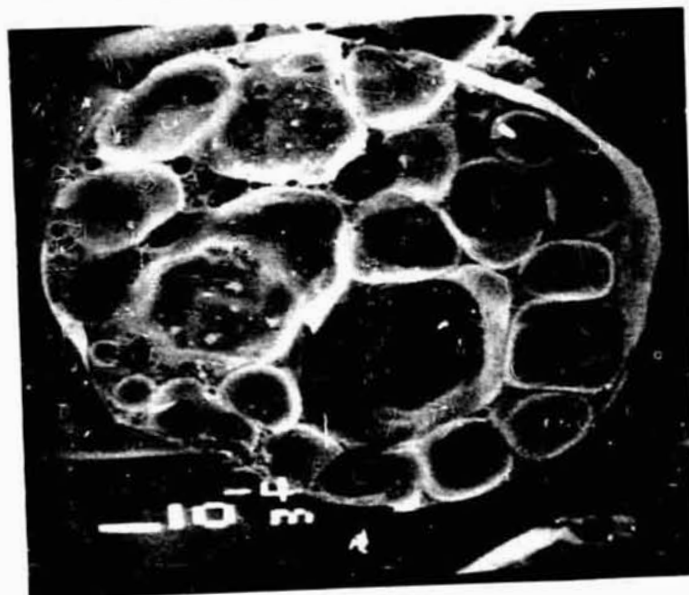
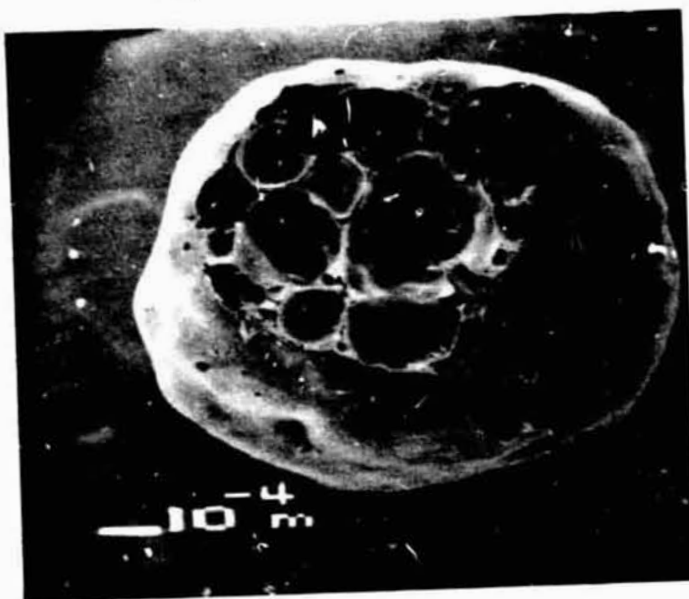
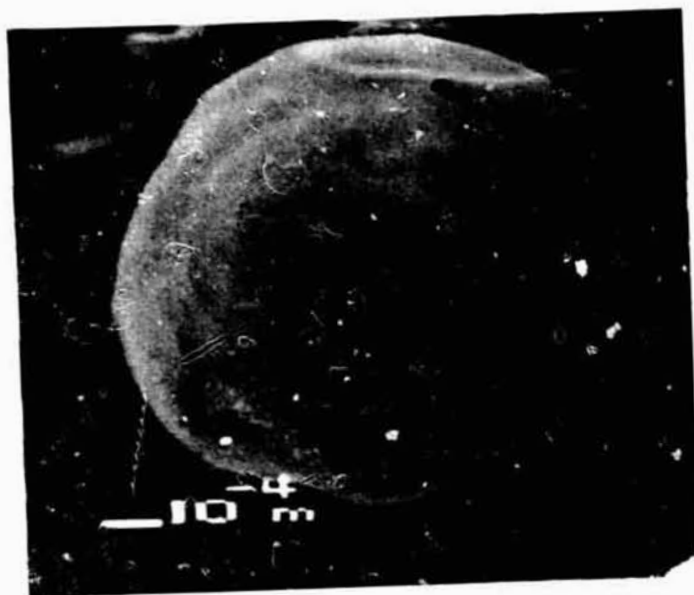
ORIGINAL PAGE  
BLACK AND WHITE PHOTOGRAPH



$T \approx 600^{\circ}\text{C}$

Figure 1 b. Gel Sintering and Expansion of Cell Structure.

ORIGINAL PAGE  
BLACK AND WHITE PHOTOGRAPH



$T \approx 800 - 1000^{\circ}\text{C}$

Figure 1 c. Gel Spheroidization.

ORIGINAL PAGE  
BLACK AND WHITE PHOTOGRAPH

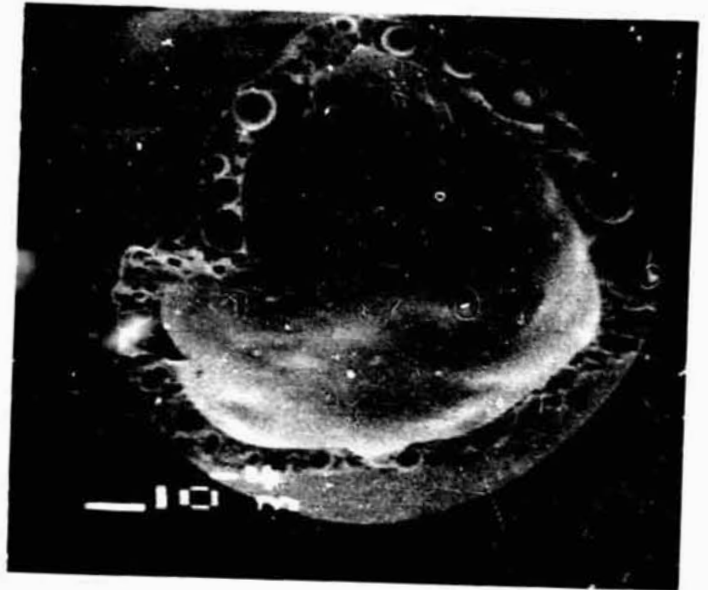
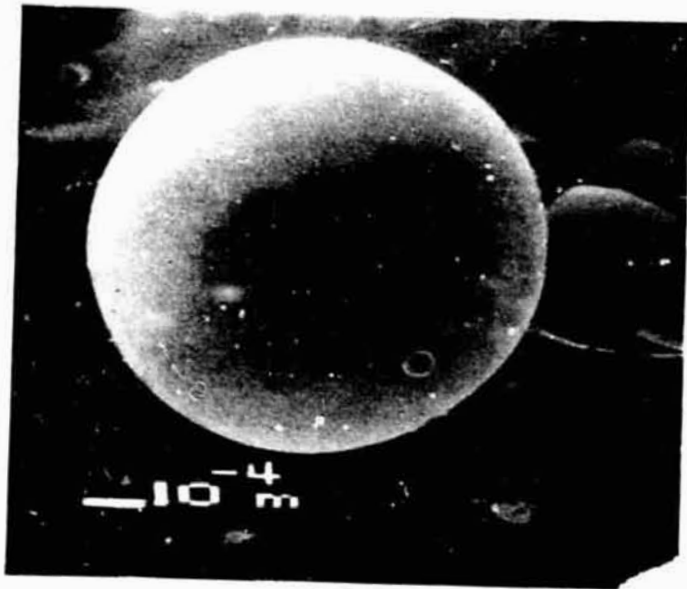


Figure 1 d. Hollow Glass Shell, Unfined.

ORIGINAL PAGE  
BLACK AND WHITE PHOTOGRAPH

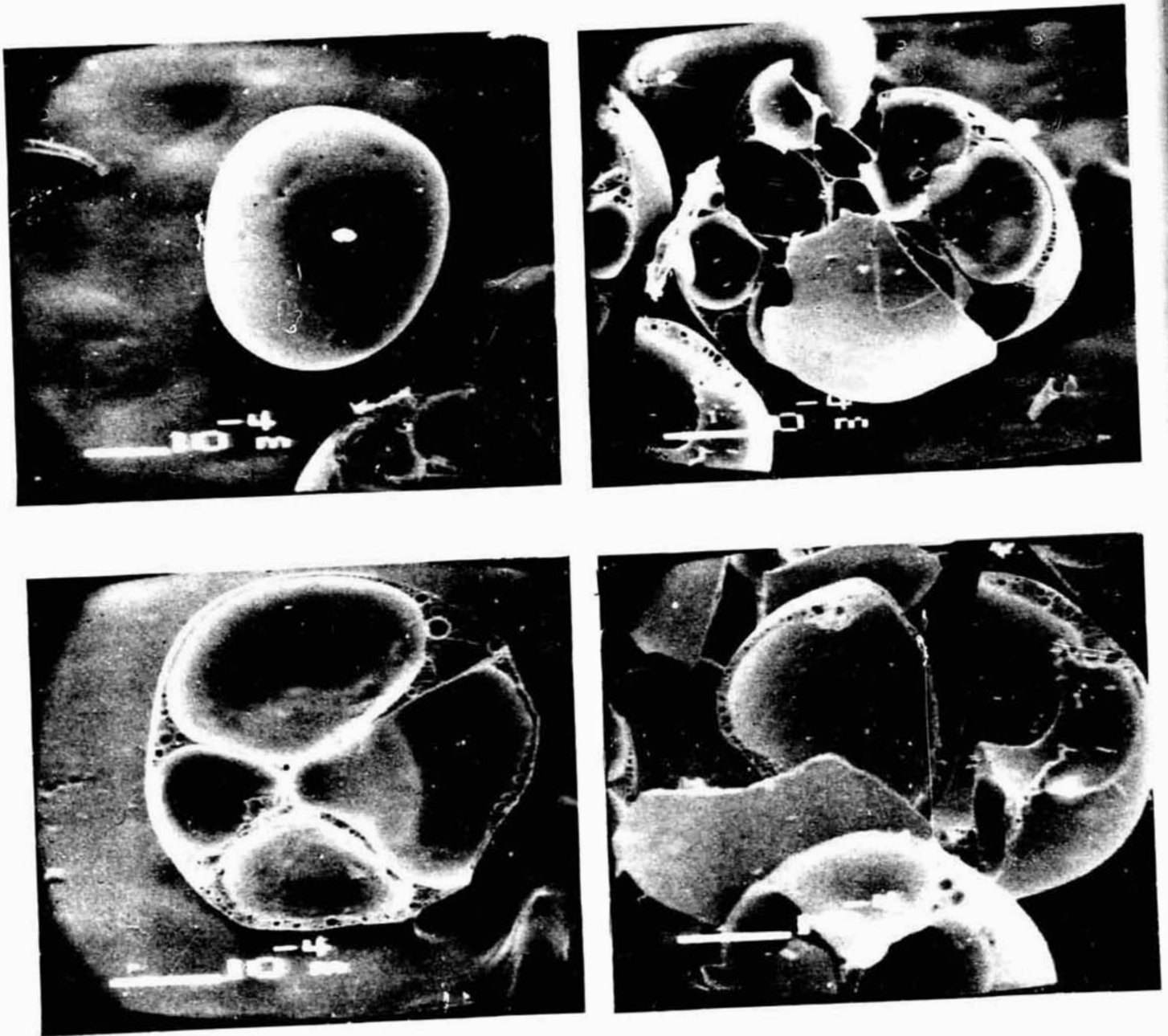


Figure 2. Foam Coalescence in Glass Spheroid.

as 20  $\mu\text{m}$ . However, subsequent fining of the carbon and gas bubble inclusions in the glass wall was incomplete even after an additional five seconds residence time in the furnace.

This morphology was deduced from gel particles that were partially transformed by heating in a vertical furnace, as well as by supplementary experiments in a box furnace. A similar morphology was evident in metal-organic gel that was heated to melting while levitated in an air jet. This work was done by Dr. Edwin Ethridge of MSFC using gel samples we provided [8].

On the basis of the above observations from shell-forming experiments in our vertical furnace, hot stage microscopy, and a limited number of levitation experiments, a general model for a transformation of the gel morphology can be visualized: a) closure of surface of the porous gel structure, such as by an initial sintering, b) low-temperature foam generation, c) particle spheridization and foam expansion, d) void consolidation (foam coalescence) and further expansion to a single-void spheroid, and e) final fining of glass wall of the shell to remove elemental carbon inclusions and gas bubbles. The model is a general one, and the characteristic temperatures of each state may vary substantially, depending on the composition and heating of the gel.

2.2 Mass/Dimensional Changes. The change in morphology, that is in gel mass and dimensions, resulting from pyrolysis of the gel was determined quantitatively as a function of temperature in the range of 20 to 600°C. Since irregularly-shaped gel particles were not suitable for this purpose, the unhydrolyzed gel was crushed into a fine powder and compacted into right circular cylinders (gel pellets), for which the diameter, length, and mass was accurately determined [7]. Thus a batch of sodium silicate gel pellets, 250  $\mu\text{m}$  in diameter and 250  $\mu\text{m}$  long, were fully characterized for dimensions, mass, composition of pyrolyzable volatiles and specific heat as a function of temperature. Platinum crucibles containing 50 mgm samples of these pellets were heated in air at 200°, 400°, 500°, 600°, and 800°C for one hour; these pellets were subsequently completely recharacterized to assess the changes in the gel. The results are summarized in Table 2. This dimensional analysis, and subsequent SEM inspection of the pyrolyzed samples, shown in Figures 3a and 3b, corroborated the observed initial expansion of gel pellets that were pyrolyzed at 400 to 600°C. Pellets that were pyrolyzed at 600° had expanded an average 20% in diameter and 20 to 50% in

Table 2. Effect of Heat Treatment on Gel Pellets

<u>Sample</u>	<u>Treatment</u>	<u>Diameter</u> ( $\mu\text{m}$ )	<u>Length</u> ( $\mu\text{m}$ )	<u>Mass</u> ( $\mu\text{gm}$ )	<u><math>\Delta\text{m},\%</math><sup>a)</sup></u>
1	untreated	261 $\pm$ 2	255 $\pm$ 5	19.9 $\pm$ .9	N/A
2	200°C	246 $\pm$ 2	242 $\pm$ 2	17.4 $\pm$ .4	12.8
3	400°C	254 $\pm$ 5	279 $\pm$ 5	15.7 $\pm$ .6	21.1
4	500°C	267 $\pm$ 2	275 $\pm$ 4	15.8 $\pm$ .4	20.8
5	600°C	301 $\pm$ 6	310 $\pm$ 12	14.6 $\pm$ .4	26.6
6	800°C	_____ b)	_____ b)	_____ b)	

a) Mass loss,  $\Delta\text{m}$ , is based on the mass ( $\bar{m}$ ) of the untreated pellets

b) Gel pellets were completely melted and not recoverable as pellets

ORIGINAL PAGE  
BLACK AND WHITE PHOTOGRAPH



T = 25°



200°



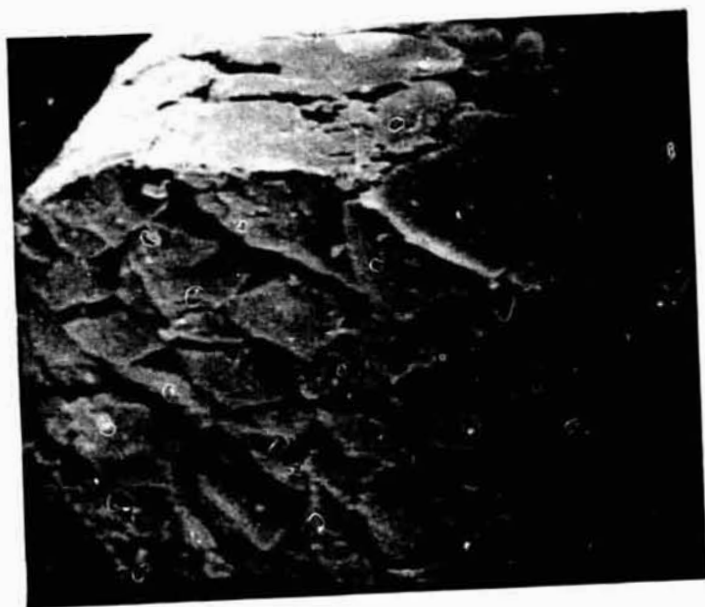
400°



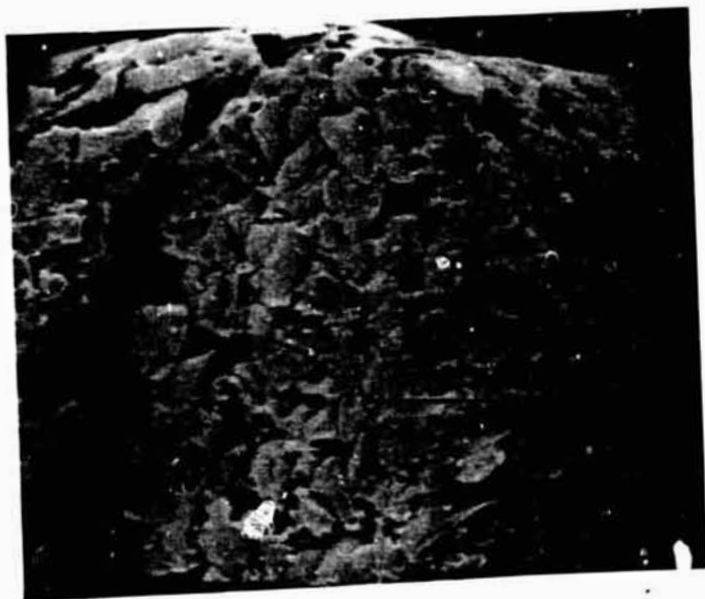
600°

Figure 3 a. Effect of Gel Pyrolysis.

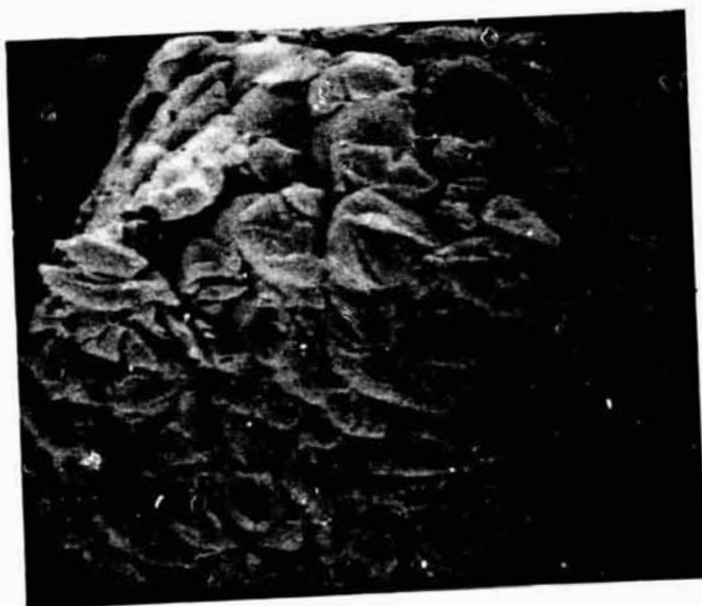
ORIGINAL PAGE  
BLACK AND WHITE PHOTOGRAPH



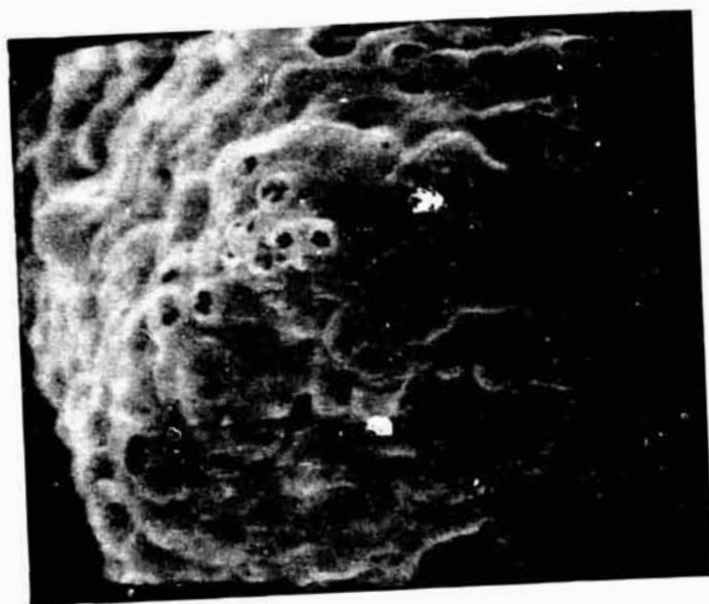
25°



200°



400°



600°

Figure 3 b. Effect of Gel Pyrolysis.

length depending on the extent of pellet densification during compaction, and had experienced a corresponding mass loss of 27%. SEM inspection showed the pellet surface had formed a continuous outer surface of rough texture due to underlying gas bubbles. Enough surface flow had occurred to firmly fuse contiguous pellets.

The 800°C sample had melted completely to puddles of black, foamed "glass" that firmly adhered to the platinum boat and were not recovered for a determination of the mass loss. Therefore, the mass loss was determined for the whole pellet-to-shell transformation, rather than for just the molten "glass" at 800°C, from shells formed at 1500°C from pellets. These data are shown in Table 3. These mass correlations were obtained initially from discrete pellet-shell pairs. This entailed a) pellet mass and size determination, b) formation of the shell from pellet, one at a time, in a 1500° furnace, and c) shell mass and size determination. (Once it was determined that the gel pellets did not fragment during heating, these data were obtained by statistical batch analyses, such as those in Table 4.) The average mass loss of 26.2% observed for these shells however, is similar to that found for pellets heated to 600° in a box furnace. This indicates that most of the mass lost in the gel-to-shell transformation is lost before the gel reaches 600°. This conclusion is corroborated by thermogravimetric analyses (TGA) of gel powder and gel pellets, wherein most of the evolved gases comprising the lost mass are lost prior to 500-600°C, and an essentially stable mass results beyond that, up to 1000°. A typical TGA thermogram illustrating this for both unhydrolyzed and hydrolyzed gel is shown in Figure 4. When dry gel is preheated by heating at 100°C to a constant weight to desorb H<sub>2</sub>O, the mass loss observed for the gel by TGA is approximately 15% of the dry gel mass. For the untreated dry gel, such as the above pellets, typical mass losses observed by TGA are 20-24% (of the dry gel mass) somewhat lower than losses resulting from heating pellets at 600°C or from the gel-to-shell transformation. Under certain conditions, e.g., low gel particle mass, high furnace temperatures and high shell surface area to glass mass, it is possible to lose appreciable amounts of the alkali and boron present in the glass shell formed from the pellet.

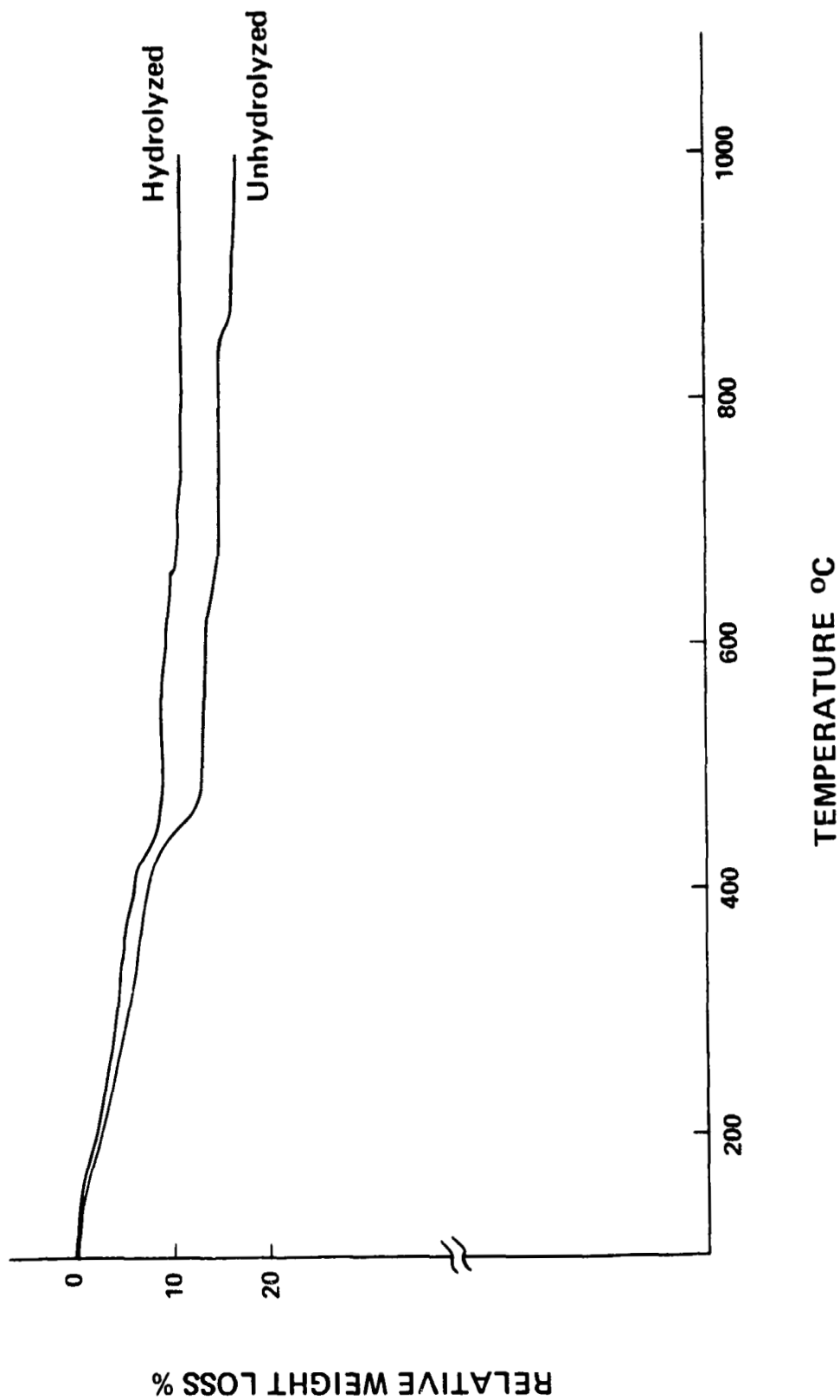
2.3 Shells From Pyrolyzed Pellets. To determine whether the heat-treated gel pellets still contained sufficient blowing agent to form shells, the pellets which were pyrolyzed as described above were dropped

Table 3. Pellet-to-Shell Mass Correlations

<u>Pellet</u>	<u>Mass (<math>\mu\text{gm}</math>)<sup>a)</sup></u>	<u>Shell</u>	<u>Mass (<math>\mu\text{gm}</math>)<sup>a)</sup></u>	<u>% Mass Loss</u>
1	13.5	1	9.2	31.8
2	12.7	2	9.9	22.0
3	12.7	3	8.8	30.7
4	13.4	4	9.6	28.4
5	13.0	5	9.9	23.8
6	14.5	6	11.3	22.1
7	11.1	7	8.4	24.3
8	12.1	8	9.0	25.6
9	9.6	9	7.0	27.1

a) Mass measurement uncertainty  $\pm$  5%.

Figure 4  
TGA THERMOGRAMS OF METAL - ORGANIC GEL



through the furnace at 1300°C (dry air environment). The shell produced from the unheated and the 200°-, 400°-, and 500°-pyrolyzed pellets were virtually identical in yield, quality, size, and mass, as shown in Table 4 and Figure 5. The average diameters of the shells from the 500°- and 600°-pyrolyzed gel pellets are larger than those for the other pellet samples, and also have a correspondingly wider standard deviation for the average diameter of the samples. While these data imply that the shell diameters increase with increasing pyrolysis temperature, the data actually reflect an increasing frequency of shell multipliers (~10%) in the shell sample. These multipliers had twice the average shell mass; they were dropped from the mass analysis. However their diameters were only slightly larger than the normal population and could not be positively identified, nor consequently eliminated from the size analysis on the basis of diameter. They therefore skewed the analysis to a larger average. It is presumed that these multipliers are the products of collision between gel pellets or shells in the furnace. Evidently the gases evolved by the pyrolyzing gels effectively disperse a gel charge in the furnace, reducing the chance of collision. A significant reduction of these evolved gases by prior pyrolysis of the gel results in ineffective particle dispersion and an increased collision frequency. The 600°C-pyrolyzed sample sintered and fused at contact points. These agglomerates, which were used without separating them, expanded at 1300°C, but due to their greater mass, formed only crude spheroids. The 800°C sample had formed "glass" puddles and was not recoverable. Thus the heat treatment, which stripped the gel of considerable amounts of volatiles, did not alter the pellets in any way that affected the shell-forming process. Evidently the residual elemental carbon and/or the  $\text{Na}_2\text{CO}_3$  in the gel (see below) are the sources of  $\text{CO}_2$  sufficient to form the shell.

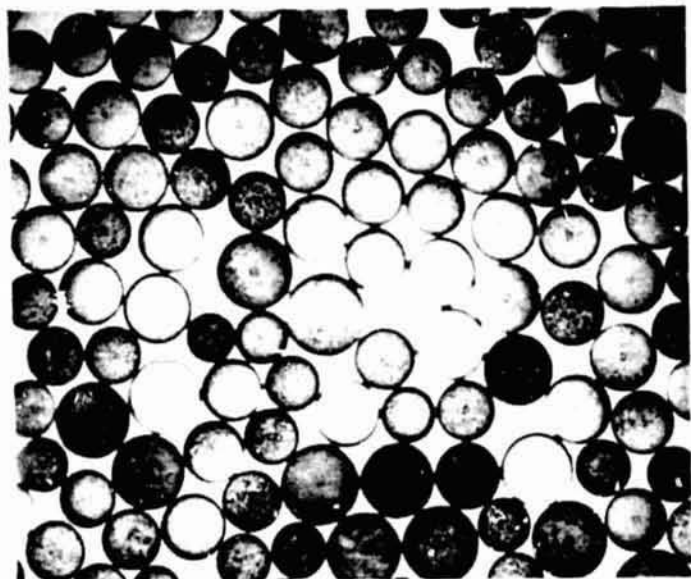
2.4 Specific Heat. The specific heat of the pellets, determined by differential scanning calorimetry, changed markedly as the organic and inorganic species in the gel were removed by pyrolysis. Figure 6 shows the specific heat ( $C_p$ ) as a function of temperature for two gel samples pyrolyzed at 400°C and 600°C, and for the unpyrolyzed gel. The figure also includes the  $C_p$  trace for the sapphire ( $\text{Al}_2\text{O}_3$ ) calibration standard. The unpyrolyzed gel in general exhibits a higher  $C_p$  due to the latent energy due to the silanol condensation, organic pyrolysis and  $\text{NaHCO}_3$  decomposition reactions. But superimposed on this is a strong endotherm

Table 4. Effect of Gel Pyrolysis on Shell Formation (Characteristics)

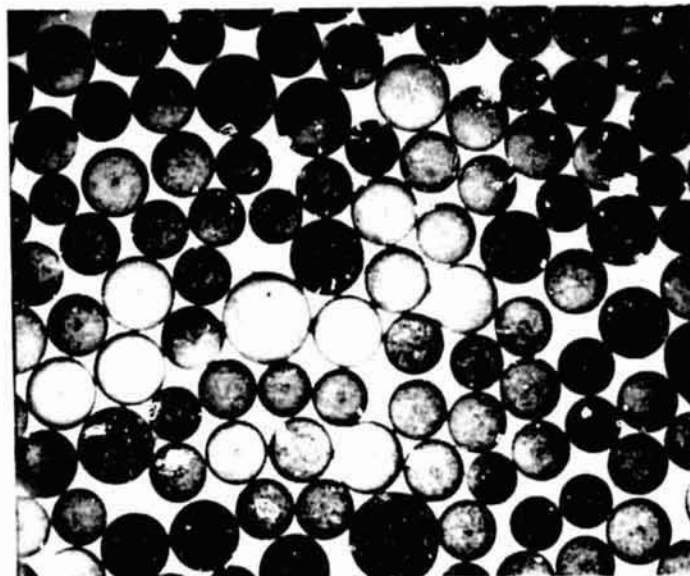
Gel Pellet Pyrolysis	Pellet Characteristics		Shell Characteristics	
	Diameter ( $\mu\text{m}$ )	Length ( $\mu\text{m}$ )	Mass ( $\mu\text{gm}$ )	Diameter ( $\mu\text{m}$ ) Mass ( $\mu\text{gm}$ )
None	261 $\pm$ 2	255 $\pm$ 5	19.9 $\pm$ .9	429 $\pm$ 47 15.4 $\pm$ .3
200°C	246 $\pm$ 2	242 $\pm$ 2	17.4 $\pm$ .4	425 $\pm$ 54 15.1 $\pm$ .7
400°C	264 $\pm$ 5	279 $\pm$ 5	15.7 $\pm$ .6	442 $\pm$ 68 14.7 $\pm$ .3
500°C	267 $\pm$ 2	274 $\pm$ 4	15.8 $\pm$ .4	464 $\pm$ 82 <sup>a</sup> 15.1 $\pm$ .4
600°C	301 $\pm$ 6	310 $\pm$ 12	14.6 $\pm$ .4	

a) The large average diameter, and the wider sample range ( $\sigma$ ) reflect the increased frequency of shell multipliers in the shell sample. The multipliers are the result of agglomeration or collision of shells/pellets in the furnace, as the reduced gas charge in the gel reduces the effective dispersion of the gel in the furnace. Shell mass values do not reflect this, since obvious mass multipliers were eliminated from the analysis.

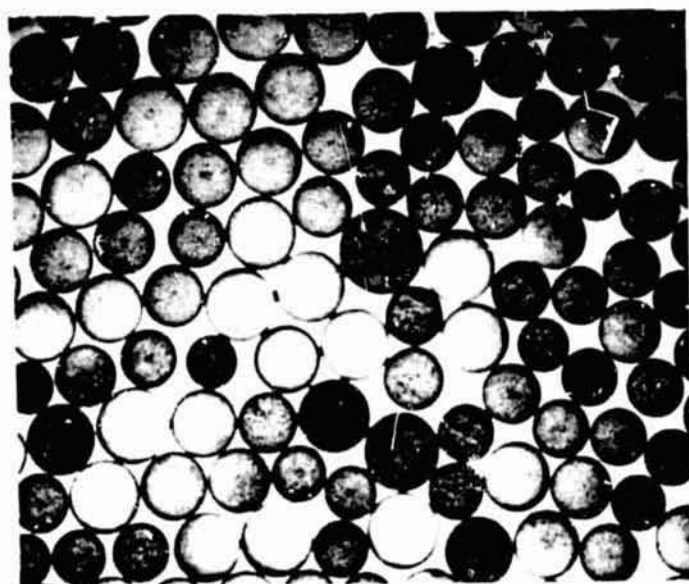
ORIGINAL PAGE  
BLACK AND WHITE PHOTOGRAPH



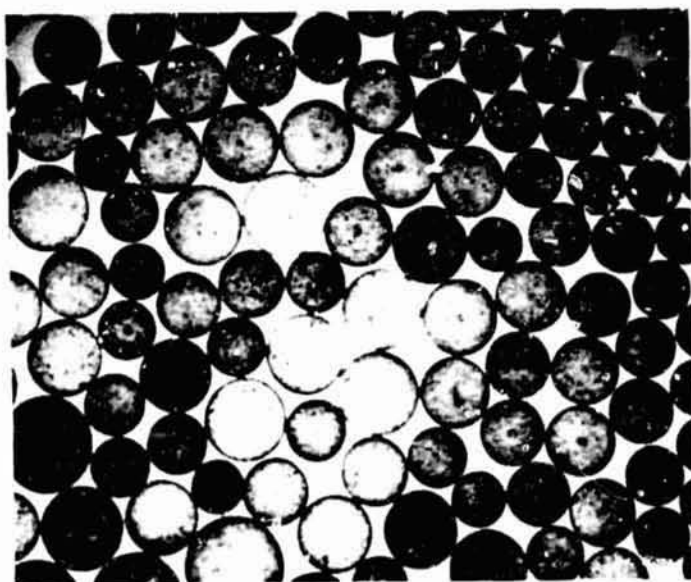
25° Gel



200° Gel



400° Gel

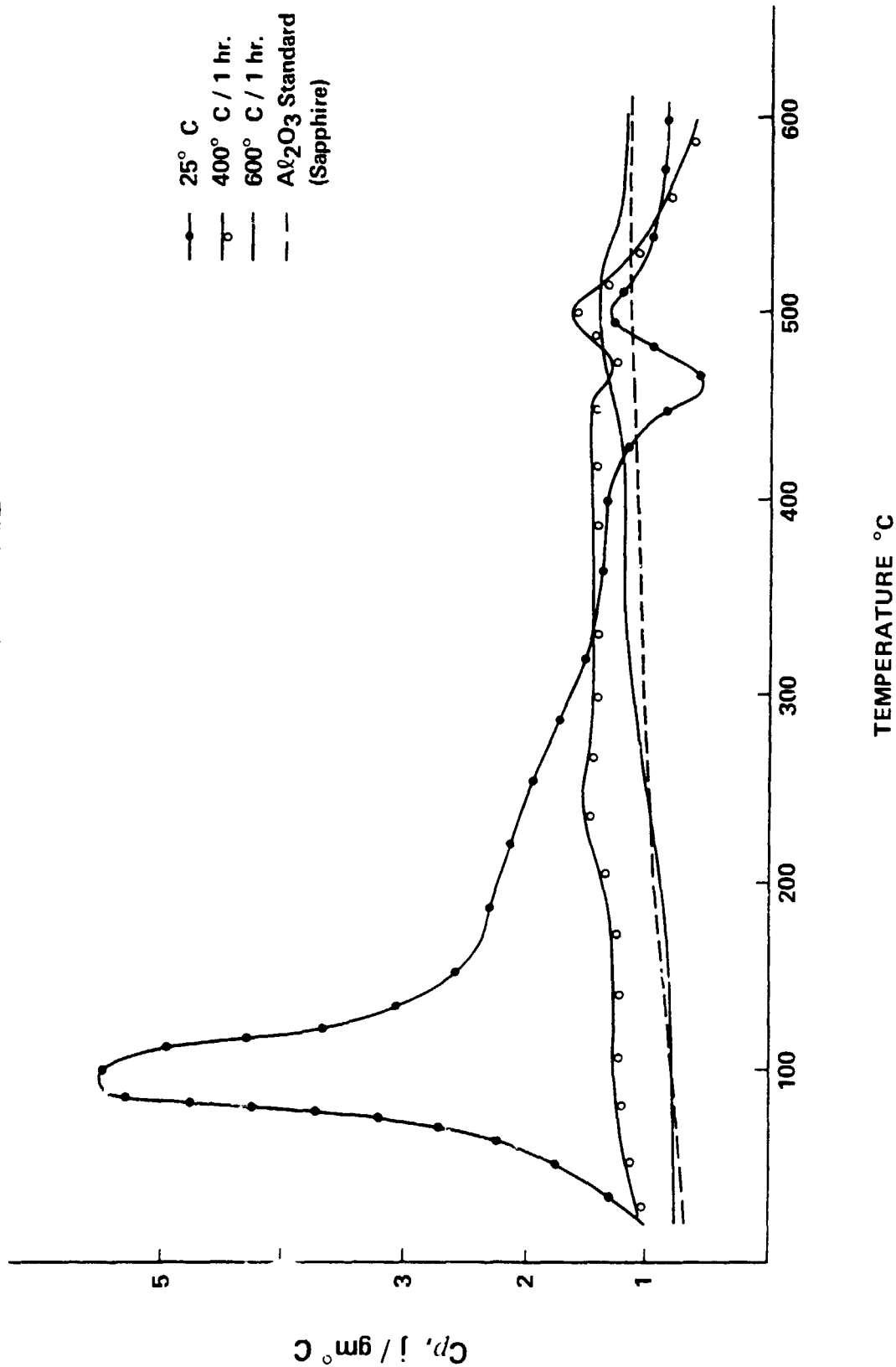


500° Gel

Figure 5. Shells From Pyrolyzed Gels.

Figure 6

EFFECT OF PYROLYSIS ON THE  
SPECIFIC HEAT OF GEL



at approximately 100°C, corresponding to the evaporation of adsorbed H<sub>2</sub>O and free ethanol, and exotherms at approximately 400°C and 600°C, corresponding to oxidation of evolved organic pyrolysates and gel sintering reactions. These are totally absent in the C<sub>p</sub> trace for the gel pyrolyzed at 600°C. The trace is similar to that of the sapphire standard (though somewhat endothermic) and to C<sub>p</sub> values for glass. Gel pyrolyzed at 400°C exhibits the expected features, i.e., below 400°C it exhibits C<sub>p</sub> values similar to sapphire and the 600°C-pyrolyzed gel, but above 400° exhibits the oxidation and sintering exotherm, similar to those of the unpyrolyzed gel. The pyrolysis of a gel produces a decrease in the specific heat, as measured at a sample temperature of 100°C, from 5.4 j/gm K to 8.4 j/gm K, due to the elimination of the endothermic pyrolytic reactions. It produces an increase in the specific heat at 600° from 0.85 j/gm K to 1.27 g/gm K due to the elimination of the exothermic reactions. Thus the specific heat of gel samples pyrolyzed at 600° and stripped of all endothermic and exothermic reactions ranges from 0.84 (at 100°C) to 1.27 j/gm K (at 600°C). This is comparable to that of glass, which ranges from 0.92 (at 100°C) to 1.30 j/gm K (at 600°C).

2.5 Gases Evolved by Gel Pyrolysis. Gases are generated in and evolved by the gel during pyrolysis, and are the agents that expand the closed-cell foam structure that eventually results in a hollow glass shell. As is evident from the above mass analyses and shell-forming experiments, most of these evolved gases escape from the gel, especially during the early stages of the pyrolysis prior to sintering of the porous gel. They presumably comprise most of the observed mass loss from the gel. These gases were identified by pyrolysis-gas chromatography (PGC), pyrolysis-mass spectrometry (PMS) and, indirectly, by differential thermal analysis (DTA). The identities of evolved gases obtained by PGC analyses, and the typical relative amounts of the evolved gases, are given in Table 5. Typical chromatograms of the evolved gases are shown in Figure 7 for sodium silicate gels made from aqueous silicate solution and from metal-organic solution. The traces also show graphically the difference in the evolved species from metal-organic gel that has been maintained dry (unhydrolyzed) and that exposed to ambient humidity (hydrolyzed). Thus, the evolved gases from all these gels consist typically of CO<sub>2</sub> and H<sub>2</sub>O; those gases evolved from unhydrolyzed

Table 5. Pyrolysis Gas Chromatography of Metal-Organic Gels

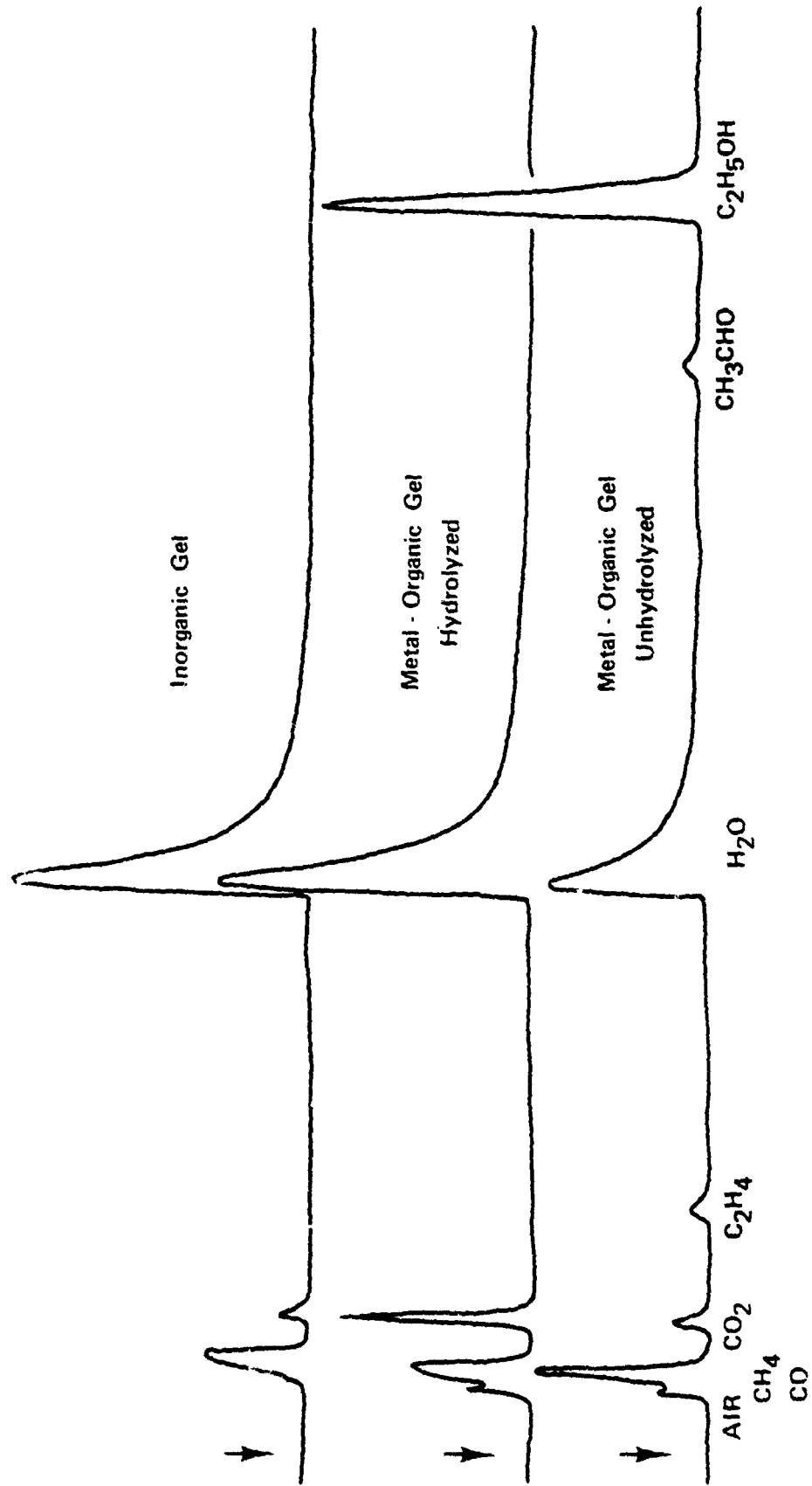
Sample <sup>a)</sup>	Gel History <sup>b)</sup>	Gas in Gel	Volatiles <sup>c)</sup> (by TGA)	CO <sub>2</sub>	H <sub>2</sub> O	EtOH	CH <sub>3</sub> CHO	CO	CH <sub>4</sub>	C <sub>2</sub> H <sub>2</sub>	C <sub>2</sub> H <sub>6</sub>
1	Unhydrolyzed	Air	17%	4.5	51.4	25.9	6.1	7.3	3.2	1.2	0.3
	Hydrolyzed	Air	13%	9.8	87.9			1.3	1.0		
2	Unhydrolyzed	Air	20%	2.4	45.6	39.6	6.4	2.5	1.7	1.3	0.3
	Hydrolyzed	Air	13%	8.9	88.6			1.5	1.0		
3	Unhydrolyzed	Argon	12%	1.6	17.8	64.0	4.4	6.5	3.3	2.2	0.2
	Hydrolyzed	Argon	15%	1.3	93.9	1.5	1.0	1.4	0.9		

a) The metal oxide glasses were prepared from dried metal-organic gels which were either subsequently kept dry (unhydrolyzed) or exposed to 80% RH for about 5 days (hydrolyzed).

b) Gels had been dried to constant weight at 100° prior to analysis.

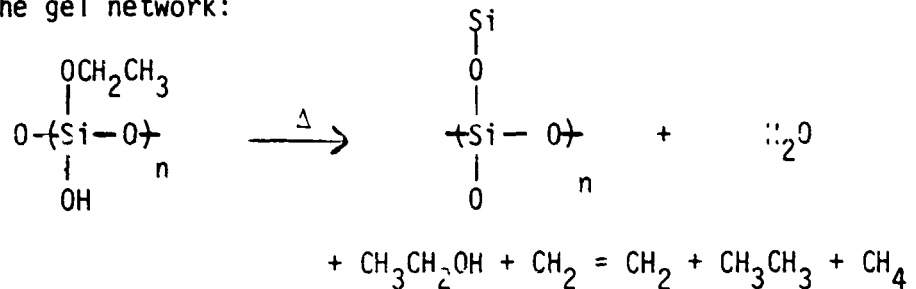
c) Samples 1 and 2 are two separate batches of gel synthesized and stored under dry air. Sample 3 was synthesized and stored under dry argon to exclude the CO<sub>2</sub> in air.

Figure 7  
PYROLYSIS - GC OF GEL POWDERS



metal-organic gel also include ethanol and its pyrolysates.

The source of the water consists of chemically bound species as well as molecular water adsorbed to the highly-active gel surface. Chemically bound water is present in the form of metal hydrates, silanol groups and metal-bicarbonates (see below). The organic gases and additional water arise from the pyrolysis of residual organic groups, such as silicon ethoxide in the gel network:



These gases serve as initial gel foaming (or expansion) agents even before oxidation occurs. Complete oxidation of the ethoxides (and the hydrocarbon pyrolysates) would further produce 2 moles of  $\text{CO}_2$  and 3 moles of water from every equivalent ethoxide. The oxidation of the organic pyrolysates (as they are evolved by the gel, not within the gel) is suggested by DTA analyses such as shown in Figure 8. Analyses using air as the ambient gas yielded exotherms at  $\sim 450^\circ\text{C}$  and at  $\sim 800^\circ\text{C}$ , whereas with nitrogen endotherms appear at these temperatures. These results attest to the evolution of oxidizable gases; however since elemental carbon is formed within the gel under these conditions, oxygen permeation of the gel must be minimal and any oxidation must be occurring external to the gel.

A correlation of TGA, DTA and PMS analyses of such an unhydrolyzed metal-organic gel, as in Figure 9, clearly shows the significant mass loss due to an initial loss of  $\text{H}_2\text{O}$ , ethanol, and  $\text{CO}_2$  and a rather sharp mass loss at approximately  $450^\circ$  due to the loss of the organic pyrolysates. This mass loss at  $450^\circ$  corresponds to the rather rapid formation of a closed-cell foam structure in the gel at  $400\text{-}500^\circ$ .

The pristine metal-organic gel, which is produced by a controlled partial hydrolysis of the precursor solution (in ethanol) of the appropriate metal-alkoxides, contains a significant number of ethoxide moieties in the dried gel. The moieties are expected to be water sensitive. While the dried gel has been shown to be stable when stored under anhydrous conditions, the gel does age when exposed to ambient humidity, with a consequent reduction in the

Figure 8  
DTA OF METAL - ORGANIC GEL

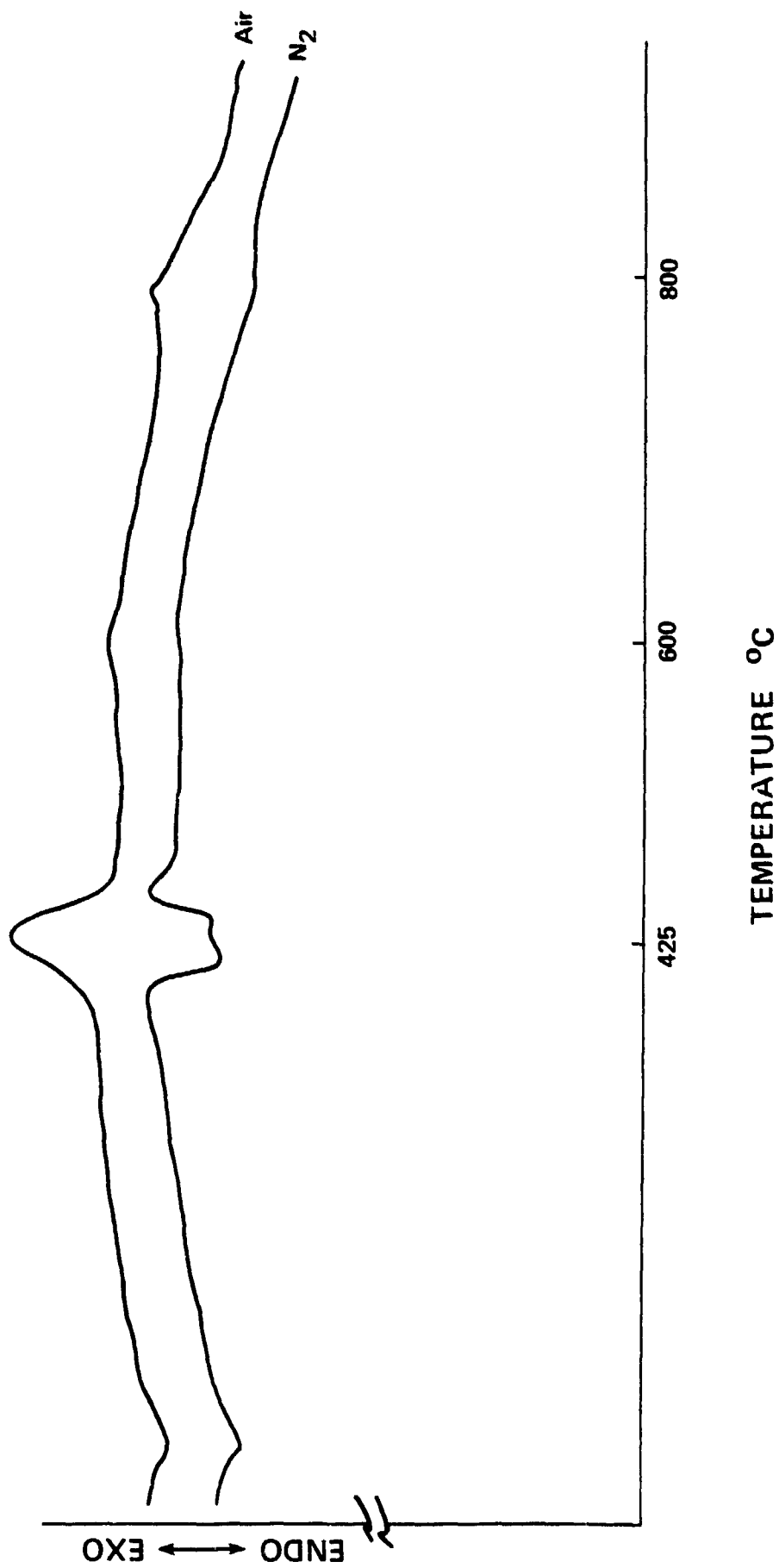
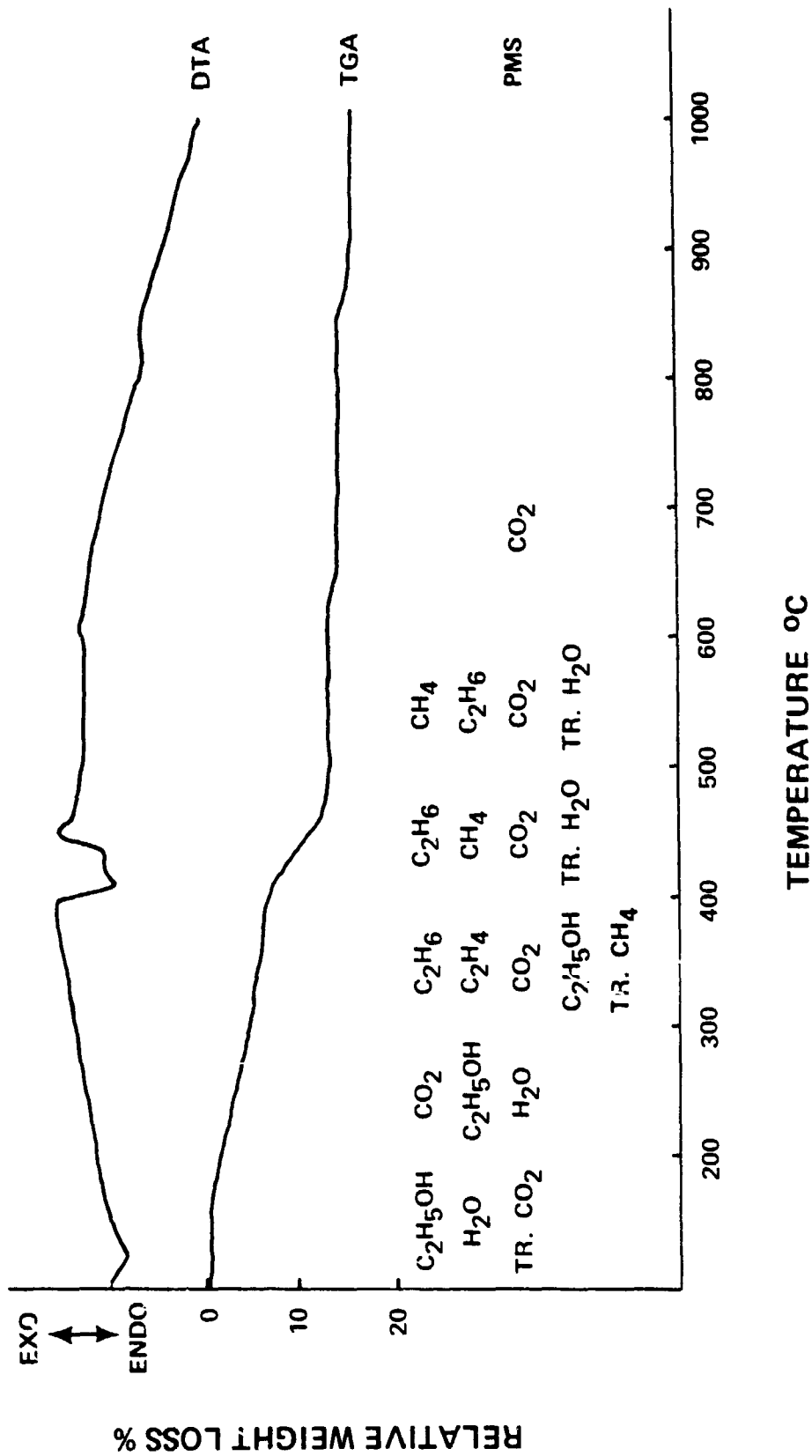


Figure 9

DTA - TGA - PMS CORRELATION FOR UNHYDROLYZED GEL



ethoxide content. In fact, removal of the bulk of the organic residues can be achieved by controlled hydrolysis of the gel through exposure of the gel to a constant high humidity environment. The extent of hydrolysis and the reduction of the organic constituents in the gel are reflected in the data of Table 5. While they show a decrease in organic pyrolysates, hydrolyzed gels also show an increase in evolved  $\text{CO}_2$  in PGC analysis. Since the gel is pyrolyzed in this analysis in an inert helium atmosphere, this suggests that the evolved  $\text{CO}_2$  is not organic in nature. This conclusion is substantiated by the considerable  $\text{CO}_2$  levels in PGC analyses of sodium silicate made from an inorganic, aqueous solution. A source of the evolved  $\text{CO}_2$  may be alkali carbonates or bicarbonates in the gel. Adsorbed or trapped air in the porous gel will not supply enough  $\text{CO}_2$  to blow shells since the natural level of  $\text{CO}_2$  in air is only 0.033 percent. A  $\text{CO}_2$  concentration mechanism is required, and can exist in the form of the reactive alkali (sodium) in the gel. Sodium bicarbonate,  $\text{NaHCO}_3$ , and sodium carbonate,  $\text{Na}_2\text{CO}_3$ , can form upon exposure of the moisture-sensitive metal-organic gel to the humidity and  $\text{CO}_2$  in the air. These reactions are thermally reversible, and should yielded  $\text{CO}_2$  in two distinct temperature regimes: a) below  $300^\circ\text{C}$ , by decomposition of  $\text{NaHCO}_3$  to  $\text{Na}_2\text{CO}_3$  and b) above  $900^\circ\text{C}$ , by decomposition of  $\text{Na}_2\text{CO}_3$  to  $\text{Na}_2\text{O}$ . When the gel was synthesized and handled under argon to prevent the formation of the carbonates due to exposure to ambient air, the PGC analysis showed a significant reduction of the  $\text{CO}_2$  levels in the gel pyrolysates (Table 5).

### 3. NATURE & SOURCE OF SHELL FORMING GASES

3.1 Residual Gases In Shells. The intermediate stage in the gel-to-glass shell transformation, a closed-cell foam structure, is formed by the gases generated and trapped in the pyrolyzed gel. These initial blowing gases are  $H_2O$ ,  $CO_2$  and the hydrocarbons methane, ethylene and ethane. The final stage, the fined hollow glass shell, is formed by the blowing gases that remain in the shell as residual gases. These gases were presumed to consist primarily of the descendents from the above pyrolysates and to originate from the organic species in the gel. The composition of these residual gases in the glass shells was analyzed by gas chromatography; the identification of the components was confirmed by mass spectrometry.

Carbon dioxide is the major gas constituent in the shells prepared from metal-organic gels. Oxygen and nitrogen are secondary, but together comprise 10 to 40 percent of the residual gases. Other possible permanent gases, such as carbon monoxide or nitro compounds, were not detected by either gas chromatography or mass spectrometry. The relative concentrations of these gases in four different shell samples, as determined by gas chromatography, are presented in Table 6. These data suggest a correlation between residual gas composition and glass composition but the information presently available is insufficient to establish this relationship. The pressure of the residual gases at room temperature is 0.17 to 0.20 atm for three of the samples; this is the expected range for shells initially at pressure equilibrium at the manufacturing temperature of 1200-1500°C and subsequently cooled to room temperature. The residual gas pressure in the calcium containing glass, however, is higher than would be expected from similar calculations based on the furnace temperature and glass surface tension considerations. This high residual pressure is not an artifact, having been observed in several calcium-containing glass samples.

Water was analyzed but does not appear in the gas analysis results presented in Table 6. Nevertheless, it is believed to be an important species in shell blowing, and, depending on its concentration in the gel and the furnace ambience, can influence several glass properties and shell characteristics. Indirect evidence for the existence of water vapor in the shell during the blowing process is the presence of "weathering" products detected on the interior surfaces of most shells by scanning electron

Table 6. Residual Gases in Shells of Several Compositions

Shell Glass System <sup>a)</sup>	Relative Concentration			Pressure (atm)
	Volume %, By GC			
	CO <sub>2</sub>	O <sub>2</sub>	N <sub>2</sub>	
Na, Si (Unhydrolyzed)	71	19	10	0.19
Na, Si (Hydrolyzed)	30	13	7	0.175
Na, K, B, Ca, Si (Unhydrolyzed)	63	16	21	0.23
Na, K, B, Si (Unhydrolyzed)	88	8	4	0.20

a) The metal oxide glasses were prepared from dried metal-organic gels which were either subsequently kept dry (unhydrolyzed) or exposed to 80% RH for about 5 days (hydrolyzed). Shells were blown in a dry air environment.

microscopy. These features are typically rich in alkali (such as sodium) and nearly identical in appearance to those found on the exterior of shells which are commonly associated with any alkali-rich glass surface exposed to water vapor. Water vapor, as high as 30% of residual gases, has indeed been detected as one of the residual gases when the shells were prepared in an environment enriched in water vapor (See Table 7) [9]. When glass shells are formed in furnace environments having low water-vapor content, water initially in the gel may participate in the blowing process, but subsequently it either diffuses through the shell walls and/or is totally consumed by the glass surface and it thus not found in residual gas analysis. This can also explain the low incidence of surface features on shells blown in dry air.

3.2 Source of the Gases. The pyrolysis of metal-organic gels generates up to 20% by weight (of the dry gel) of volatiles consisting of  $\text{CO}_2$ ,  $\text{H}_2\text{O}$ , and ethanol and its pyrolysates as noted above. All of these are potential shell-blowing agents.

An ample source of  $\text{CO}_2$  (and  $\text{H}_2\text{O}$ ) is the oxidation of the ethoxides, trapped ethanol and the pyrolysates of ethanol trapped in the gel. If the oxidation of these organic residues in the gel is the prime source of the  $\text{CO}_2$  blowing agent, then a reduction of these residues should affect shell formation. A reduction of organics was achieved by controlled hydrolysis of dried gel, which cleaved residual ethoxide groups from silicon and liberated ethanol. In addition, for comparison purposes, a gel sample was prepared from an aqueous sodium silicate; there were no organic materials used in the synthesis of the gel.

Subsequent shell-forming experiments using unhydrolyzed metal-organic gel, hydrolyzed metal-organic gel and inorganic gel produced shells of surprisingly good quality and yield for all three gels although the shells from the unhydrolyzed gel had higher aspect ratios (defined as the ratio of the shell diameter to wall thickness, OD/W). Likewise, gel pellets that were pyrolyzed at temperatures up to  $500^\circ\text{C}$  so that only low levels of elemental carbon and sodium carbonate remained, resulted in shell yields and quality similar to those produced by unpyrolyzed gel, as discussed above. These results are contrary to those expected from a comparison simply of the potential organic volatiles of these gels, as summarized in Table 5, and suggest that oxidation of organic species may not be the dominant source of  $\text{CO}_2$  for forming shells.

Table 7. Residual Gases in Shells Exposed to Water Vapor  
During Shell Blowing

Shell Sample	Glass System	Furnace Gas	Relative Concentration, Volume %, by GC			
			CO <sub>2</sub>	O <sub>2</sub>	N <sub>2</sub>	H <sub>2</sub> O
1	Na, K, B, Ca, Si	Dry Air	57.9	18.6	23.5	0
2	Na, K, B, Ca, Si	Water Vapor, Air	21.3	14.7	30.9	33.1
3	Na, K, B, Si	Dry Air	88.2	7.5	4.3	0
4	Repass of 3 through furnace	Water Vapor, Air	44.3	17.7	7.2	30.7
5	Na, K, B, Si	Water Vapor, Air	35.8	17.0	15.7	31.4
6	Repass of 5 through furnace	Dry Air	54.8	33.7	11.5	0

In addition, the PGC analyses of gels, in which the gel is pyrolyzed in a helium flow, show substantial levels of  $\text{CO}_2$  in the evolved gases and suggest a  $\text{CO}_2$  source in gels that is inorganic, e.g., alkali carbonates. Minimizing the carbonate formation by synthesizing, handling and hydrolyzing the gel under argon, free of  $\text{CO}_2$ , did decrease the available  $\text{CO}_2$ , but did not eliminate it. Such gel, i.e., with minimized carbonates and residual organic content, produced shells in yield, aspect ratio, and quality comparable to those shells from the three gels above. The results show essentially that minimizing the carbonates and residual organics in the gel has no significant effect on  $\text{CO}_2$  levels in the shells.

Other experiments performed in our laboratory have further substantiated our conclusion that residual levels of elemental carbon, formed by pyrolysis of the residual organics, and alkali carbonates generate sufficient  $\text{CO}_2$  to blow good shells [9]. Only gel pyrolyzed at  $900^\circ\text{C}$ , in air, suffers enough reduction in the elemental carbon and the alkali carbonate content to result in a significant decrease in the aspect ratio of the shells.

The source of the  $\text{O}_2$  and  $\text{N}_2$  in the residual blowing gases of the shells is probably the ambient furnace air, which permeates through the molten shell wall, driven by the partial pressure differential between the furnace ambience and the shell interior. Significantly, the oxygen is found in anomalously high levels compared to nitrogen; whereas in air  $\text{O}_2/\text{N}_2 \approx 0.27$ , in shells it is often  $\text{O}_2/\text{N}_2 > 1$ . This suggests that  $\text{O}_2$  and  $\text{N}_2$  enter the shells by permeating the molten shell wall, but at unequal rates, and are not the result of air encapsulation caused by gel sintering. A further though less convincing argument against encapsulation of ambient gases, such as air, in the gel during shell blowing is the observation that shells from gel made and stored under argon, but blown in an air-filled furnace, contained air, but not argon. The higher than expected  $\text{O}_2$  levels are not the result of  $\text{H}_2\text{O}$  thermolysis, as an increase of the water vapor pressure in the furnace decreases, rather than increases, the  $\text{O}_2/\text{N}_2$  ratio.

A further confirmation that permeation of ambient furnace gases can occur during shell formation was shown in a shell-blowing experiment using a partial backfill of argon in the furnace. A small amount of argon ( $\sim 5\%$ ) was found in the shells. Shells formed in air, when repassed through the furnace partially filled with argon, had similar argon levels as the above shells made in argon, and in this case argon could only be present by diffusion through the shell wall.

#### 4. FURNACE-TO-GEL HEAT TRANSFER MODEL

The gel powder, falling at terminal velocity through the hot furnace, is transformed into glass shells provided that sufficient heat is transferred to the particle during the time it resides in the furnace. If the powder particles are too massive and the total residence time of the powder is consequently too short, a product of diminished quality with respect to sphericity, uniformity, and gas bubble inclusions results. With our 3.9 m 1500°C furnace, the particle mass limit is of the order of 50  $\mu\text{gm}$ . The process is thereby currently limited to producing high quality shells with diameters that are less than 1 mm.

This limitation could be the result of several factors: a) very slow heat transfer from the furnace wall to the gel (poor heat conduction by the furnace gas), b) poor absorption of the radiant energy by the gel (or high reflectivity), c) slow rates for the chemical reactions that produce blowing gas and form molecular bonds in the glass, and d) slow rates of mass flow in the gel/glass (high viscosity and slow response to the stress created by the blowing gases). These will result in a very slow expansion of the particle, a correspondingly slow increase in particle buoyancy in the furnace gas, and relatively short and insufficient particle residence times in the furnace.

These possible limiting factors for shell production cannot be readily investigated and corroborated empirically in real time in the furnace, due to the hostile environment of the furnace, the small mass and dimensions of the sample, and the dynamic nature and short duration of the whole process. One of these factors, the possible limitation on shell size imposed by heat transfer to the gel, was approached with the aid of a forced-convection heat transfer model. This model was developed to calculate the temperature history of a gel particle falling through the furnace as a function of gel particle parameters and furnace parameters. Thus, for a given set of gel and furnace parameters, the model can predict whether the falling gel particle can reach the appropriate temperature for a pre-designated transformation, the rate at which that temperature is reached, and the residence time in the furnace. It does not address the question of whether a particular gel particle will form a hollow glass shell.

4.1 Mathematical Model. The heat transfer model has been written into a computer code, termed GELSHEL. It is a composite of two sub-models: a) a particle displacement model that calculates, as a function of time, the position of a gel particle in a drop-tower furnace, and b) a forced-convection heat transfer model that describes the rate of heat transfer from the furnace to the gel particle. The GELSHEL code thereby calculates the temperature of a gel particle (and the resulting shell) as a function of its drop time and vertical displacement in the furnace.

The particle displacement model is based on Newton's Second Law and Stokes' Law. The velocity of the particle is determined as a function of time from Newton's Second Law. Its displacement in the furnace is determined by integration of the velocity with respect to time. The displacement model that describes the particle position within the furnace as a function of the time of fall is summarized by:

$$\frac{dV}{dt} = g \left( 1 - \frac{\rho_f}{\rho} \right) - 12.5 \frac{\mu_f A}{\bar{D}m} V$$

$$\frac{dS}{dt} = V$$

where

V = particle velocity

S = particle displacement (distance of fall)

t = time

g = acceleration of gravity

$\rho_f$  = density of the furnace gas

$\mu_f$  = absolute viscosity of the furnace gas

$\rho$  = particle density

m = particle mass

A = frontal area of the particle

$\bar{D}$  = characteristic dimension in Reynolds' number; for the shell

$\bar{D}$  is the shell diameter; for the gel,  $\bar{D}$  is the arithmetic average of a gel pellet's diameter and length

The heat transfer model describes the rate of heating of the particle in the furnace as the sum of both convective and conductive heating by the hot furnace gas and radiative heating from the furnace tube walls.

The model is based on the fundamental heat transfer relationship (see Appendix I).

$$\frac{dT}{dt} = \frac{h A_s}{m C} (T_f - T) + \frac{\sigma E A_s}{m C} (T_f^4 - T^4)$$

where

- m = particle mass
- C = specific heat of the particle
- T = particle temperature
- T<sub>f</sub> = furnace temperature
- t = time
- A<sub>s</sub> = particle surface area exposed to the thermal environment
- h = convective heat transfer coefficient
- σ = Stefan-Boltzmann constant
- E = absorptance of the particle

The particle, as it drops through the furnace, changes in mass, size, geometry and specific heat. This evolution causes substantial changes in the heat transfer rate and particle velocity, as a consequence of the changing geometry, surface area and mass, and thus particle buoyancy and drag. To model these changes, this complex particle history is conceived as occurring in three discrete regimes on the basis of particle geometry, wherein the particle geometry is determined by the particle temperature. Particle characteristics are held constant within each regime, but can be changed from one regime to the next in a step-wise fashion. The temperature bounds (temperature switches) of the regimes and the particle characteristics within each regime are the variables that must be defined by the user. These regimes in their chronological order are:

- 1) cylindrical gel pellet regime; mass, dimensions, and specific heat may be changed at the end of this regime, but not the pellet geometry, which is a right circular cylinder.
- 2) pellet sintering regime; at the end of this regime, mass and geometry are changed (from a cylinder to a sphere), and specific heat and absorptance may be changed within this regime.
- 3) shell regime; absorptance may be changed within this regime, but mass, geometry and specific heat are constant for the glass shell.

The modelling approach is based on four simplifying assumptions: 1) gel pellet characteristics change in a step-wise and not a continuous fashion, 2) the geometry of the gel particle is a right cylinder, 3) the geometry change from pellet to shell is instantaneous and 4) the heat transfer from the surface to the bulk, of both pellet and shell, is instantaneous, so there is no temperature gradient within the particle.

The development of this model is described in detail in Appendix I, and the description of the GELSHEL code is given in Appendix II.

4.2 Model Predictions and Experimental Observations. Those parameters that can be controlled or determined empirically, or which are expected to have a profound influence on the history of the particle, were selectively varied in the code calculations. The particle temperatures, however, which served as gel regime switch points were determined from TGA and box-furnace test data, and were used as such, since variations on the order of 100°C did not have a significant effect on the calculated gel history.

Calculations using the GELSHEL code indicate the following:

- 1) An increase in mass significantly decreases the particle heating rate.
- 2) An increase in particle length, that is commensurate with an increase in particle mass, minimizes the terminal velocity, maximizes the heating and results in faster particle heating in comparison to a comparable increase in particle diameter.
- 3) Heat conduction from the furnace gas is the primary means of heat transfer, especially at temperatures lower than 1000°C. Not only does the heat conductivity of the gas determine its efficiency as a heat exchanger, but the gas viscosity and density affect the buoyancy and drag on the falling particle as well.
- 4) The initial specific heat of the gel has only a modest effect on the pellet temperature history.

GELSHEL code calculations indicate that an increase in the gel pellet mass results in a significant increase in the droptime and distance required by the gel geometry changes that accompany the mass increase. If the pellet diameter is doubled, commensurate with a four-fold increase in mass, and the length is held constant, the drop distance required by the pellet to reach 1000° is increased six-fold. If the pellet length is quadrupled to increase the mass four-fold, and the diameter is held constant, the drop distance is

only doubled. This behavior follows from the following considerations.

Since the rate of particle heating is given by:

$$\frac{dT}{dt} = \frac{A_s h (T_f - T)}{mC} + \frac{A_s \sigma E (T_f^4 - T^4)}{mC}$$

$$A_s = \frac{\pi D^2}{2} + \pi DL$$

$$m = V\rho = \frac{\pi D^2 L \rho}{4}$$

then the change in  $dT/dt$  for a change in  $L$  is given by:

$$\frac{\partial}{\partial L} \left( \frac{dT}{dt} \right) = \frac{-2a}{L^2}$$

$$\text{where } a = \frac{1}{\rho C} \left[ h (T_f - T) + \sigma E (T_f^4 - T^4) \right]$$

Similarly for a change in  $D$

$$\frac{\partial}{\partial D} \left( \frac{dT}{dt} \right) = \frac{-4a}{D^2}$$

Thus, as expected, any increase in dimensions in the pellet with constant density, will result in a decrease in the rate of temperature rise. Further, the rate of change in  $\frac{dT}{dt}$  will be the same for any change in  $D$  or  $L$  if the ratio of the pellet dimensions  $\frac{D}{L} = \sqrt{2}$

That is,

$$\frac{\left| \frac{\partial}{\partial L} \left( \frac{dT}{dt} \right) \right|}{\left| \frac{\partial}{\partial D} \left( \frac{dT}{dt} \right) \right|} = \frac{D^2}{2L^2} = 1 \quad \text{if } \frac{D}{L} = \sqrt{2}$$

if  $\frac{D}{L} > \sqrt{2}$ , then

$$\left| \frac{\partial}{\partial L} \left( \frac{dT}{dt} \right) \right| > \left| \frac{\partial}{\partial D} \left( \frac{dT}{dt} \right) \right|$$

Since the ratio of dimensions for the pellets that can be manufactured with our pellet press lies in the range

$$0.5 < \frac{D}{L} < 2$$

the above relationship and its inverse, i.e., if  $\frac{D}{L} < \sqrt{2}$ , and  $\left| \frac{\partial}{\partial L} \left( \frac{dT}{dt} \right) \right| < \left| \frac{\partial}{\partial D} \left( \frac{dT}{dt} \right) \right|$ , both apply for the range of pellets in use.

Further, the particle velocity is also affected by the pellet dimensions and mass because the buoyancy and drag terms in the particle acceleration equations are geometry-dependent. With proper definitions for the buoyancy and drag terms, the acceleration for the pellet is give by

$$\frac{dV}{dt} = g \left( 1 - \frac{\rho_f D^2 L}{4m} \right) - 12.5 \frac{\mu_f LV}{m}$$

Partial differentiation with respect to D and to L yields

$$\frac{\partial}{\partial D} \left( \frac{dV}{dt} \right) = - \frac{g \rho_f LD}{2m}$$

$$\frac{\partial}{\partial L} \left( \frac{dV}{dt} \right) = - \left( \frac{g \rho_f D^2}{4} + 12.5 \mu_f V \right)$$

Thus, for a given increase in pellet mass with a commensurate increase in diameter, the decrease in pellet acceleration is a function of the diameter and mass. For a commensurate increase in pellet length, the decrease in pellet acceleration is solely a function of the mass. Since the pellet mass and dimensions are interrelated variables, the above considerations significantly complicate an analysis of the effects of pellet mass on the thermal history of the pellet. The parameter of pellet mass in conjunction with pellet dimensions is nevertheless a sensitive probe for testing the heat transfer model.

Accordingly, a pellet series was fabricated with a nominal mass of 20, 40, 80, 160 and 200  $\mu\text{gm}$  and a density of  $\sim 1.4 \text{ gm/cm}^3$ . Because the pellet diameter is fixed by the press die dimension, it could not be continuously varied but was limited to two values - 250  $\mu\text{m}$  and 500  $\mu\text{m}$ . The pellet length was variable but in a relatively narrow range from  $0.5 D < L < 1.5 D$ .

Furnace experiments were conducted with several furnace profiles:  
 a) 1500°C, all units; b) 1300°C, all units; c) zoned, 1300°C top unit and remainder at 800°C; d) zoned, 1200°C top unit and remainder at 800°C; and e) zoned, 1000°C top unit and remainder at 800°C.

The results are best exemplified by a summary of the observed and

calculated results for experiments using furnace profile b, and are shown in Figure 10. The drop distances for the pellets were visually estimated at the point that the particle incandescence became indistinguishable from the ambient furnace radiation. Because of the speed of particle heating, the small size of the particle and the subjective nature of this determination of particle temperature equivalence, the particle temperature at this point is most likely in the range of 1000°-1300°C. Therefore, Figure 10 includes the calculated times and distances (by the GELSHEL code) that are required for the particle to reach the temperatures of 1000° and 1200°C respectively. The relatively minor differences between drop times and the corresponding particle drop distances for 1000°C and 1200°C illustrate the difficulty in estimating the point at which the particle is approximately equal to the furnace temperature in the visual tracking technique. Nevertheless, the calculated distances required for each pellet mass to reach 1200°C are in remarkably good agreement with the experimental observations.

From model calculations, the specific heat of the gel was expected to exert some influence, albeit a moderate one compared to gel mass and furnace gas, on the thermal history of the gel. The GELSHEL model predicts that a decrease in the specific heat should increase the pellet heating rate and result in a shorter drop distance (into the furnace) to bring the particle to its melting temperature. The thermal histories for gel pellet samples were calculated by the GELSHEL code, using the appropriate pellet mass and dimensions, for three different furnace temperature profiles: a) all furnace units at 800°C, b) top unit at 1000°C, and the remaining 5 at 800°C, c) top unit at 1200°C, and the remaining 5 at 800°C. In the profiles b and c, the hot zone (1000° and 1200° respectively) at the top of the furnace was 50 to 60 cm long; at 100 cm depth, the temperature had reached the 800°C baseline.

The effect of the lower specific heat of the heat-treated pellets is a faster heating rate. However, this effect is felt for only a short temperature range, since the specific heat rapidly decreases to that of glass as the gel is heated to 600°C and higher. This effect decreases with increasing furnace temperatures. The specific heat affects primarily the early portion of the pellet temperature history and to a lesser degree the maximum particle temperature, the total droptime, and distance required to attain it. These data are summarized in Table 8. These calculations are in good agreement with the drop distance of 30-50 cm observed for these in a furnace with temperature profiles b and c.

Figure 10  
 PELLET DROP DISTANCE AS A FUNCTION  
 OF PELLET MASS TO REACH  
 FURNACE TEMPERATURE

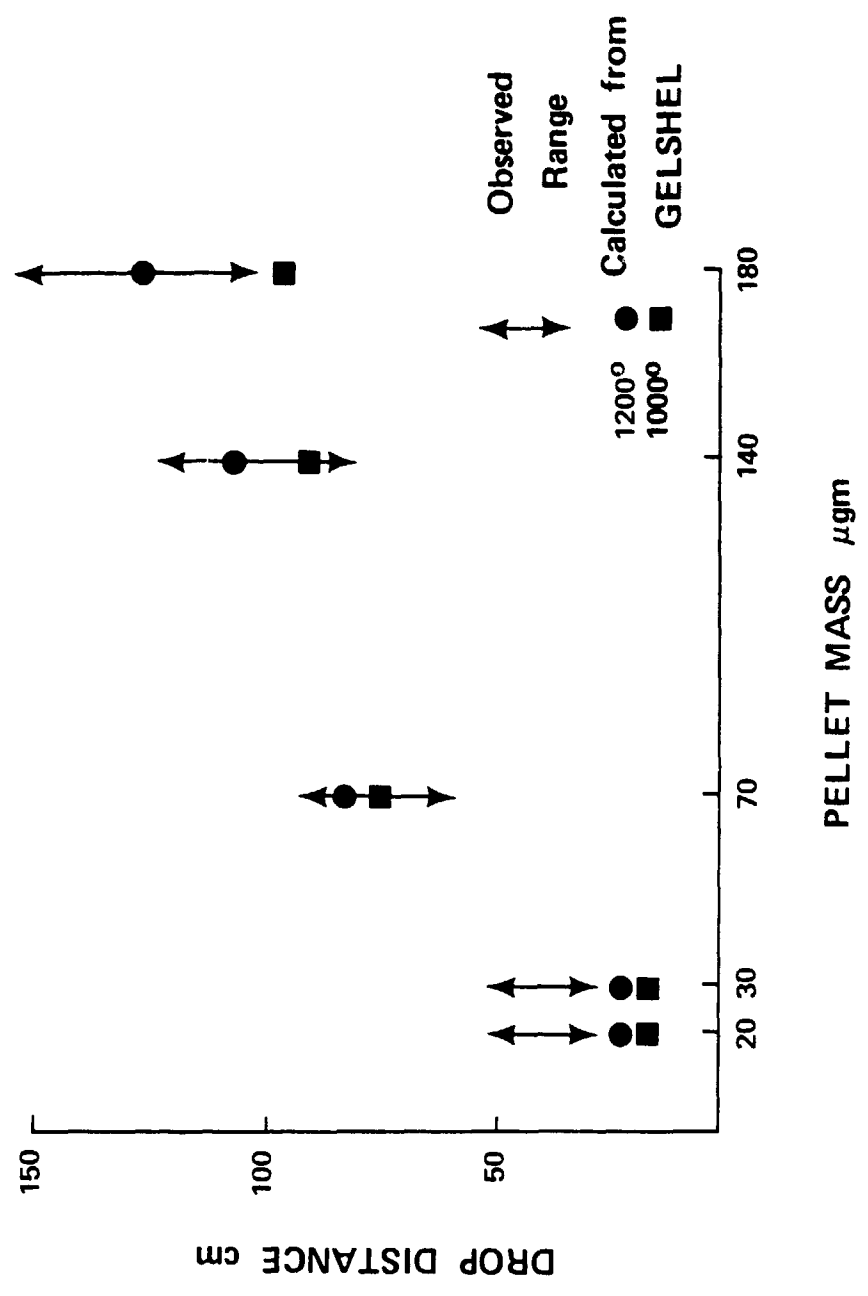


Table 8. Effect of Specific Heat on Pellet Heating

<u>Gel Treatment</u>	<u>Specific Heat (1)</u> j/gm°K	<u>Furnace Profile (2)</u>	<u>Peak Furnace Temp. °C</u>	<u>Peak Particle Temp. (3)</u>		
				<u>Temp. °C</u>	<u>Time, s</u>	<u>Distance, cm</u>
Untreated	5.44-0.85	a	1045	991	0.52	43.8
400°C/1 hr.	1.31-0.70	a	1045	1024	0.46	33.1
500°C/1 hr.	1.19-0.25	a	1045	1025	0.45	32.5
Untreated	5.44-0.85	b	1202	1161	0.43	27.7
400°C/1 hr.	1.31-0.70	b	1202	1179	0.42	27.7
500°C/1 hr.	1.19-0.25	b	1202	1180	0.42	28.2

(1) Range of values, measured between 100°C-600°C

(2) a) top unit set at 1000°C, lower 5 at 800°C  
 b) top unit set at 1200°C, lower 5 at 800°C

(3) Drop time (secs) and drop distance (cm) required by particle to reach the stated temperature based on calculations using GELSHEL code.

The third probe for testing the thermal model is the thermal conductivity of the furnace gas. The thermal conductivity, gas density and gas viscosity are expected to determine the rate at which thermal energy is transferred from the furnace wall to the pellet, as well as the velocity of the pellet through the heated zone. The GELSHEL code predicted that only helium was significantly more effective for heat transfer, and water vapor only moderately better than dry air. Because developing and maintaining a helium atmosphere in the open process tube of the furnace would require a fast gas flow, thus perturbing the particle trajectory, water vapor was chosen for the test. The experiments were performed with the heavier pellets to minimize any perturbation of the pellet trajectory by the updraft of water vapor and thus to generate a more valid comparison with the dry-air control experiment. These results are presented in Table 9. The effect of the higher heat conductivity of water vapor is to shorten the drop distance required to heat the gel, and is seen in both the GELSHEL calculations and the experimental observations. Further, the dry air and the water vapor experiment observations and corresponding calculations show a remarkable agreement between the model and the real particle behavior. In these experiments, any great disparities between the calculated and observed results probably reflect the inaccuracy inherent in the visual estimates of distance and particle temperature, especially in those cases wherein the particles plummet deep into the furnace before reaching the furnace temperature.

In all furnace experiments, to date, the pellets reached incandescence very rapidly corroborating the GELSHEL calculations, yet the final product from the more massive pellets did not have the surface characteristics expected for such a hot thermal history. The physical appearance of some of the larger (180  $\mu\text{gm}$ ) pellets, dropped through a zoned furnace, was equivalent to that of reference samples equilibrated at 500-800°C in a box furnace. Further experiments (in a box furnace and vertical furnace) wherein pellets were heated to 1000°C and 1200°C for short periods (< 5 secs), indicated that while the pellets reach incandescence rapidly, the mass flow is negligible. There are two explanations for these observations:

- 1) While the thermal response of the pellet to the furnace environment is rapid, the viscous response of the gel to its internal stresses is much slower in comparison.

Table 9. Effect of Furnace Gas<sup>(1)</sup>

Pellet Batch	GELSHEL Calculations <sup>(2)</sup>						Experimental Observation <sup>(3)</sup>	
	Mass, $\mu\text{gm}$	Dry Air Time, s	Dry Air Dist., cm	Time, s	H <sub>2</sub> O Dist., cm	Dry Air Dist., cm	H <sub>2</sub> O Dist., cm	
9	74	.57	84	.41	53	60-100	30-50	
10	143	.75	136	.52	80	80-100	50-100	
11	181	.82	162	.56	93	100-140	50-100	

(1) All six furnace units at 1500°C.

(2) Calculated time and distance for the particle to reach 1400°C.

(3) Observed drop distance (into furnace) at which pellet radiation became indistinguishable from furnace radiation.

- 2) The pellet, because of limited heat conductivity, may develop a significant temperature gradient resulting in an incandescent surface and a substantially cooler bulk.

This latter point questions the validity of a basic assumption in the GELSHEL model. Namely, because of the small pellet mass, the heat transfer in the pellet bulk is assumed to be instantaneous; no significant temperature gradient develops in the pellet. The radial temperature gradient was therefore calculated for a typical pellet with a 20  $\mu\text{gm}$  mass and a 300  $\mu\text{m}$  diameter, having the thermal properties of glass (specific heat of 0.9-1.3  $\text{j/cm K}$ ; heat conductivity of  $10^{-2}$   $\text{w/cmK}$ ) as discussed in Appendix III. The heat flux to the pellet, due to convection and radiation, was calculated from the heat transfer equation. For a pellet injected into a furnace having ideally a constant temperature profile of 1500°C, the maximum radial temperature gradient of 75°C developed within 4 msec droptime. This gradient rapidly decreased beyond that time, to 50°C after 20 msec, corresponding to a pellet displacement of only 2 mm into the 1500°C furnace. Since in reality the mouth of a 1500°C furnace is only 750°C, a pellet that has descended 2 mm into the furnace sees a 750°C environment. A recalculation of the radial temperature gradient for such conditions resulted in a 22° gradient that decreased to 12 after 20 msec (see Appendix III). Similarly, a 180  $\mu\text{gm}$  pellet develops a maximum radial temperature gradient of 105°C within 20 msec after injection into a 1500° environment, and 25°C within 20 msec after injection into a 750° environment. These radial temperature gradients are indeed not significant in view of the fact that they maximize within a very short time after injection, and rapidly decrease to lesser values.

To differentiate empirically between a temperature gradient or viscous inertia in the pellet requires a model material with a specific heat similar to glass, but with a high surface tension, a sharp melting point, and very low viscosity (for the molten mass) to drive the rapid spheridization of the molten mass. Thus, such a material would heat like glass but spheridize rapidly at its melting point. Except for their high heat of fusion, inorganic salts, with a melt viscosity near 1 centipoise, seemed suitable. Accordingly, NaCl and Na<sub>2</sub>SO<sub>4</sub> crystals of 212-250  $\mu\text{m}$  sieve range and 20-25  $\mu\text{gm}$  mass, were injected in the furnace in the usual manner. With the top unit of the furnace at 1000°C and the remaining units at 750°C, NaCl crystals (m.p. 801°C,

$\Delta H_f = 6.73 \pm 0.04$  kcal/mole) became incandescent within 30 cm drop; the product consisted largely of solid spheres, with some unaffected crystals. With the top unit at 900°C, NaCl did not spheridize even though incandescence was reached and maintained for 1 m drop. This failure to spheridize, even with exposure to at least 65 cm of travel through a furnace zone above 800°C, reflects the high heat of fusion of NaCl (6.73 kcal/mole) and the short residence time, rather than a significantly large  $\Delta T$  in the particle. Had the product experienced a large temperature gradient within the particle, a substantial number of partially-melted crystals should have resulted, whereas the products were sharply divided into spheres and unaltered crystals. Similar results were obtained for  $\text{Na}_2\text{SO}_4$  (m.p. 884°C) fired at 1200° and 1000°C.

The qualitative agreement of the experimental results with the calculations from the model verifies that the model can satisfactorily describe the temperature history of the gel in the furnace. Thus, a gel particle with a mass of 20  $\mu\text{gm}$  and a diameter and length of 250  $\mu\text{m}$  is heated rapidly to the temperature of the furnace, typically at a rate of 3000°/sec. In fact, a gel pellet of such mass and dimensions forms a thick-walled sphere 356  $\mu\text{m}$  diameter whose walls are opaque with carbon inclusions after dropping through one furnace unit (60 cm long) at 1300°C. A significant number of these spheres will have multiple voids, or have single voids with remnants of the intercellular membranes (such as shown in Figure 2), indicating that the glass was molten but had insufficient time (1 sec) to form a uniform hollow sphere (or a smooth internal surface).

Increasing the heating time of the shell by the sequential addition of 60 cm long furnace units at 1300° resulted in shells with decreased carbon inclusions and increasing diameter. With all six furnace units at 1300°, forming a 3.9 m long hot zone, the heating time for the shell was increased to 6.1 secs; the shells formed from gel in the 3.9 m hot zone were relatively free of carbon inclusions. Furthermore, the average diameter of these shells was 407  $\mu\text{m}$ , representing a 50% increase in shell volume as a consequence of the increased time of heating. This is summarized in Table 10. These experiments suggest that the gel-to-shell transformation is indeed rapid, forming a crude shell in the time (approximately 1 sec) it takes the gel pellet to drop approximately 0.6 m. They suggest as well that the process is not limited by the heat transfer rate, that the gel is indeed being heated

Table 10. Effects of Hot Zone Length on Shell Characteristics

Shell Run (1)	Number of Hot Zones (2)	Total Residence time above 1000°C, sec	Shell Characteristics			$\Delta V$ (3)
			$\bar{m}$ , $\mu\text{gm}$	$\bar{\text{OD}}$ , $\mu\text{m}$	Gross Volume, ml	
1	1	0.9	12.6 $\pm$ 1.1	356 $\pm$ 14	2.36 $\times 10^{-5}$	-1.7%
2	2	1.7	13.4 $\pm$ 1.1	354 $\pm$ 27	2.32 $\times 10^{-5}$	4.3%
3	3	2.7	13.2 $\pm$ 1.1	361 $\pm$ 23	2.46 $\times 10^{-5}$	8.7%
4	4	3.9	12.4 $\pm$ 0.8	366 $\pm$ 26	2.57 $\times 10^{-5}$	22.6%
5	5	4.9	13.5 $\pm$ 0.9	381 $\pm$ 34	2.90 $\times 10^{-5}$	49.4%
6	6	5.9	13.1 $\pm$ 1.0	407 $\pm$ 49	3.53 $\times 10^{-5}$	

1) Pellet Characteristics

$$D = 260 \quad L = 250 \quad M = 17.6 \pm 1.5 \mu\text{gm}$$

2) T = 1300° for hot zones

T = 900° for the baseline units (cool units)

$$3) \Delta V, \% = \frac{V - 2.36 \times 10^{-5}}{2.36 \times 10^{-5}} \times 100$$

very rapidly to a fluid state. It is apparent that for gel mass as large as 20  $\mu\text{m}$  the rate of mass transport is relatively rapid in the gel-to-shell transformation, and that the rate of glass fining is the limiting factor in the production of quality shells.

Further, the rate of heat transfer by the furnace gas is sufficient to melt gel particles as massive as 200  $\mu\text{m}$  and is not the rate-limiting mechanism of the gel-to-glass transformation. Rather, experimental observations indicate the gel particles as large as 200  $\mu\text{m}$  simply do not develop sufficient drag and buoyancy that would otherwise decrease the terminal velocity and thus increase the residence time of the gel particle. This suggests that for such large particles, the shell formation is limited by the large mass and the "viscous" inertia of the gel.

The feasibility of describing and modeling the fluid dynamics of the transformation, which is central to the development of a complete and general gel-to-shell transformation model, was examined. However, the complexity of the process was too formidable to model with our limited time and resources. Thus, rather than addressing the question of whether process conditions were insufficient to develop good shell uniformity, we chose to address the question of possible mechanisms that would affect the uniformity of such shells already formed.

## 5. EFFECT OF GRAVITY ON SHELL CONCENTRICITY

5.1 Shell-Decentering Model. A consideration in the manufacture of highly-uniform glass shells is the effect of gravity on the uniformity of the product. The force of gravity can produce decentering of the interior and the exterior surfaces of a molten shell that is initially concentric by causing the molten glass to flow while the shell is falling. This motion of the interior surface can be viewed as the motion of a buoyant gas bubble which rises within the fluid glass shell at a rate governed by the buoyant force and the glass viscosity. A decentering model was developed which predicts the extent of this decentering of the surfaces of an initially-concentric shell as a function of time and the applied force.

The motion of a small buoyant gas bubble in an infinite glass pool is adequately described by Stokes Law. This description is not adequate for molten glass shells with a thin but finite wall, wherein the "wall effects" must be considered, since glass flow is constrained between two spherical surfaces. This configuration is crudely modelled, at best, by the classical case of a buoyant gas bubble in a cylinder of fluid of comparable dimensions, such as Francis' modification of the Stokes equation [11]. Wang has suggested the use of the Stefan-Reynolds equation to model the effects of buoyant forces in molten glass shells. This treatment may be more satisfactory but details of the analysis have not, to our knowledge, been published [12]. The paucity of satisfactory models has prompted us to initiate our own investigation of this question. Consequently, we have developed a model quantitatively describing the development of wall-nonuniformity in a molten shell, by gravity-driven decentering of the inner and outer surfaces. The model assumes that the shell initially has perfect wall uniformity. The decentering process is described as a function of time as well as glass characteristics.

The model is based on the following conditions and assumptions:

- 1) Two types of forces control the dynamic behavior of the fluid shell:
  - a) forces due to the constant acceleration field of gravity
  - b) forces caused by the viscosity of the glass fluid.
- 2) The fluid shell has initially two concentric, spherical surfaces stabilized by the surface tension of the glass

- 3) The density of the gas in the internal void is negligible compared to the glass density.
- 4) The molten glass is a Newtonian fluid of constant viscosity.
- 5) All stresses, other than those due to viscous forces, are negligible.
- 6) Transient velocity distributions are negligible.
- 7) The shell is thin.

The wall nonuniformity (WNU) at time,  $t$ , is defined as:

$$WNU = \frac{\delta_{\pi} - \delta_0}{\delta_0} = \frac{\delta_{\pi}}{\delta_0} - 1 .$$

where

$\delta_{\pi}$  is the maximum thickness of the shell at time,  $t$ , and

$\delta_0$  is the minimum thickness of the shell at time,  $t$ .

Since the shell is initially uniform,  $WNU = 0$  when  $t = 0$ . The mathematical expression of WNU developed in the model is

$$WNU = \left( \frac{1 + \tau}{1 - \tau} \right)^{1/2} - 1 \quad (1)$$

where

$$\tau = \frac{8\rho a D t}{3\mu(AR)^2} ; \quad \text{where } \rho \text{ is the density of the molten}$$

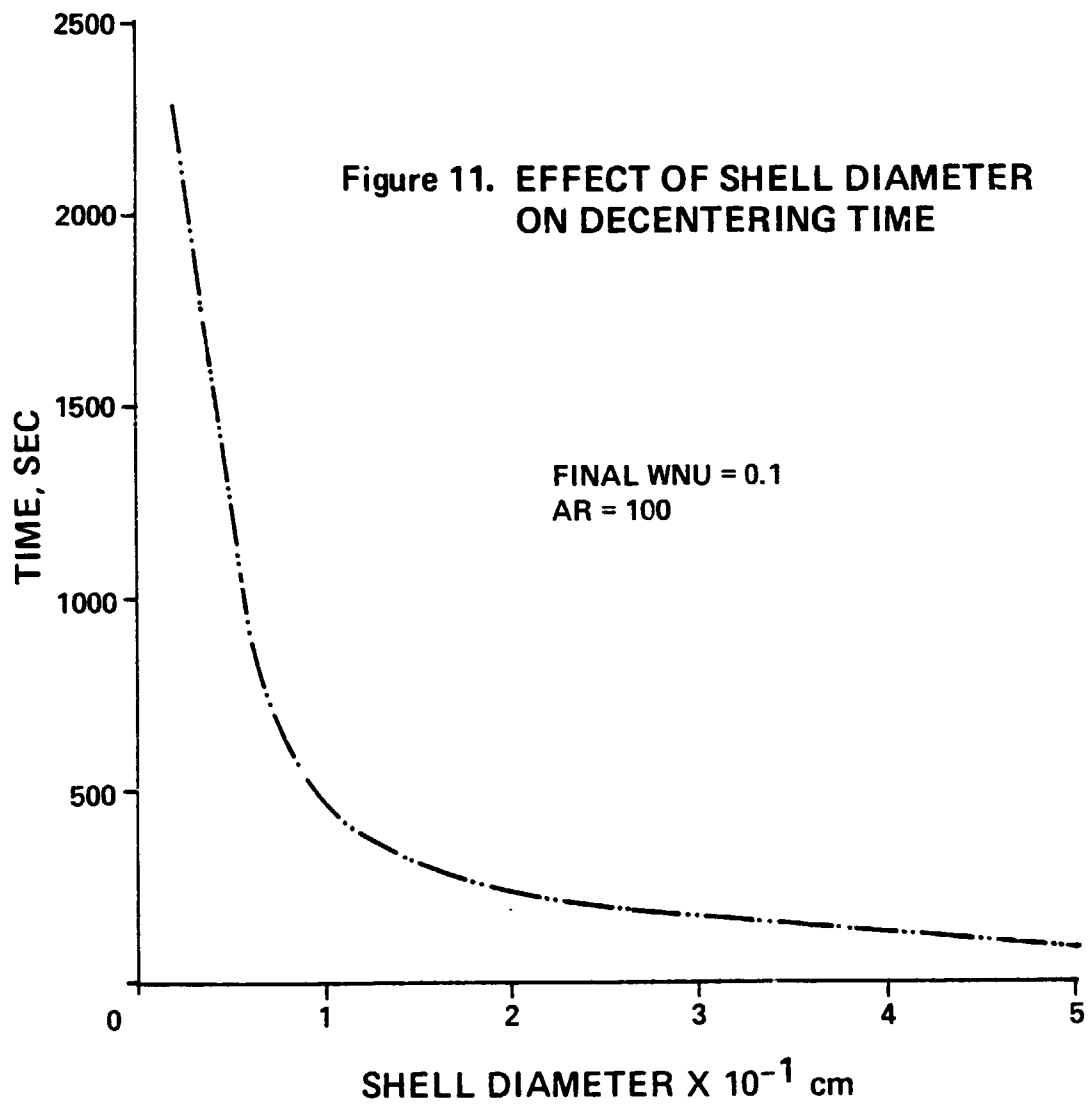
glass,  $a$  is the acceleration, which for our case is  $g$ , the acceleration due to gravity;  $D$  is the outside diameter of the shell;  $\mu$  is the absolute viscosity of the molten glass;  $(AR)$  is the aspect ratio of the shell; the ratio of the outside diameter of the shell to the mean wall thickness;  $t$  is time. The development of this model is discussed in detail in Appendix IV. As an example of the model's application consider the following molten glass shell and environment:  $D = 200 \mu\text{m}$ ,  $(AR) = 100$ ,  $\mu = 300 \text{ gm/cm/sec}$ ,  $\rho = 2.4 \text{ gm/cc}$ , and  $a = g = 980 \text{ cm/sec}^2$ . Using equations 1 and 2 the time interval,  $t$ , required to develop a WNU of 0.1 is found to be 2300 sec. This time interval is probably 2 orders of magnitude greater than the interval during which the shell will be molten in its fall through a 4 m tower furnace. The time required to develop 1% nonuniformity ( $WNU = 0.01$ ) is 260 secs. Thus, it is improbable that gravity effects will cause even a 1% nonuniformity in this shell.

In general all three models, (KMSF, Stefan-Reynolds equation, and Stokes-Francis equation) indicate that gravitational decentering of shells is negligible for shells less than 2 mm in diameter. For our model, the decentering time as a function of shell diameter is shown in Figure 11; shell parameters are the same as above. Thus a 2 mm diameter shell will develop a wall-nonuniformity of 0.1 in 200 seconds, which is a long time interval compared to a normal residence time of  $\sim 5$  secs in a vertical, 4-meter long furnace. For a 2 mm shell, the decentering time is comparable to furnace residence times only for thick-walled, low aspect ratio shells. A 2 mm shell with 80  $\mu\text{m}$  walls decenters in approximately 15 secs to a wall-nonuniformity of 0.1. Thus gravity will significantly decenter only those shells having a large diameter, a long residence time in the furnace, a low aspect ratio, or a very low viscosity. For materials such as liquid metals with a viscosity near 0.01 gm/cm sec, the shell in the example (200  $\mu\text{m}$  OD) would develop a wall-nonuniformity of 0.1 in  $\sim 0.07$  seconds. The resistance of a glass shell to gravity decentering is essentially a consequence of its relatively large viscosity.

We are concerned however that the model may have a serious weakness resulting from one of the boundary conditions employed in its development. Specifically, in an evaluation of the development of this model, R. S. Subramanian [13] has suggested replacing our assumption of no slip at the exterior shell surface by a condition of zero tangential stress. We agree with this recommendation; however, the incorporation of the zero-stress condition into the model will produce a much more complex model which probably cannot be solved in closed form.

5.2 Preliminary Model Testing Experiments. As discussed above, the model for gravity-driven shell decentering predicts very low rates of decentering for glass shells of the small dimensions and compositions currently produced because the shells experience only relatively short residence times in the furnace.

Testing of the model requires heating shells for much longer time periods than those elapsing during shell formation. One method of increasing heating time is to repass shells through the furnace. However, our past experience has shown that multiple passes of glass shells through a vertical furnace is rather ineffective for remelting and reforming the shell; even though the sample surface is uniformly heated, the particle's



residence time and temperature history cannot be controlled easily. Further, air turbulence at the top of the furnace results in the loss of many shells to the wall of the furnace during shell injection. In addition, a continuous rather than cumulative re-heating of shells is preferred, to avoid questions concerning the effects on the shells of repeated remelting and solidification.

A controlled gas-jet which levitates the shell in a furnace, rather than repeated passes through the furnace, is a more satisfactory method to increase shell residence time at its forming temperature.

A levitator/furnace system, with a collimated hole structure (CHS) levitation jet and an elliptically-focused infrared heater, was made available to us by Edwin Ethridge of Marshall Space Flight Center (MSFC) [8]. It had been designed and built by S. Dunn (Bjorksten Laboratories) and E. Ethridge (MSFC). We conducted a series of levitation/heating experiments jointly with E. Ethridge at MSFC using a batch of shells prepared at KMSF. The shells ranged in diameter from 500 to 1000  $\mu\text{m}$  and were prepared from a gel of nominal composition 73%  $\text{SiO}_2$ , 12%  $\text{K}_2\text{O}$ , 8%  $\text{Na}_2\text{O}$ , and 7%  $\text{B}_2\text{O}_3$  (weight percent). The shells were not analyzed for composition, but on the basis of similar experiments, are expected to have considerably less alkali and boron than found in the gel.

In general, the very large shells ( $\sim 1$  mm) levitated easily and stably, requiring only a minimum of gas flow adjustments during the heating sequence. However, poor uniformity of sample illumination (heating), poor levitation stability during temperature programming and slow heating rates ( $\sim 300^\circ\text{C}/\text{min}$ ) were significant problems encountered for heating large shells with this type of system.

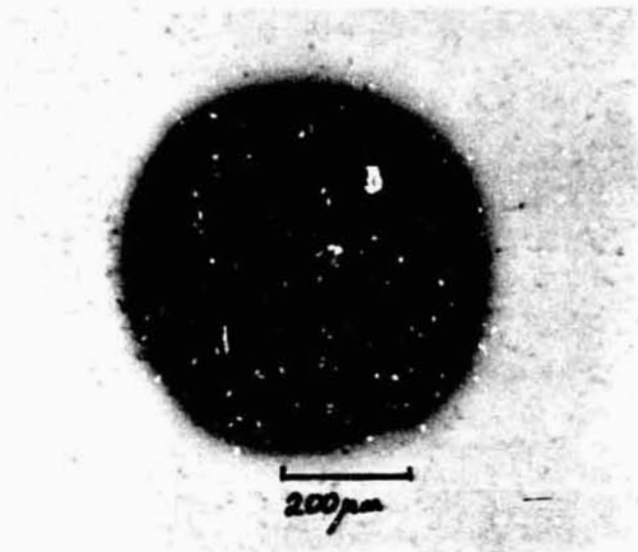
At  $700^\circ\text{C}$ , the shells generally dimpled and wrinkled in the hemisphere of the shell opposite the impinging gas stream, and this deformation became progressively worse with increasing temperature. This uneven heating and collapse is due to the system configuration. The shell is shielded from reflected radiation from below by the jet body, and partially from above by the thermocouple bead. Complete collapse of the shell did not occur. A few shells, upon reaching  $\sim 900$ - $1000^\circ\text{C}$ , turned opaque ("frosted"), presumably due to phase separation. The shells that remained stable during the partial collapse did reform into spherical shells above  $1050^\circ\text{C}$ , but with smaller diameters. In these shells gross changes were observed in the shell dimensions and surface finish.

The recovered shells were examined by optical and SEM microscopy at KMSF. Shells that were heated at 900°C or more for any length of time had become translucent or opaque. Optical microscopy showed a "wormy" optical texture in the glass of the shells, indicative of phase separation, as well as large cracks and gross surface deformations. SEM microscopy revealed surfaces riddled with deep pitting and craters (20 to 50  $\mu\text{m}$  in diameter), and numerous large cracks as shown in Figure 12. Whereas the glass surface of the unheated shells was smooth with roughness  $< 0.05 \mu\text{m}$  (except for a moderate incidence of 0.1-0.5  $\mu\text{m}$  weathering bumps), the remelted surface had a uniformly coarse and grainy texture ( $\sim 0.5 \mu\text{m}$ ), appearing almost porous, as in Figure 13.

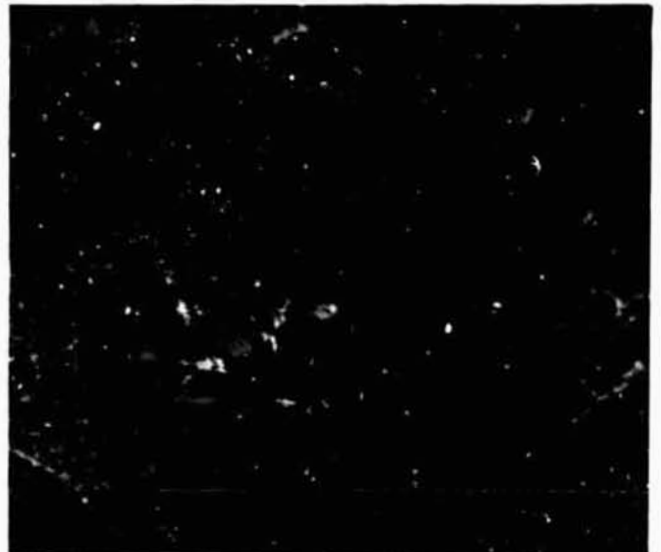
Shells heated to less than 900°C, while optically clear, showed surfaces that were coarse and dimpled with very shallow flat-bottomed craters (10 to 20  $\mu\text{m}$  in diameter). These craters invariably had fine diametric cracks, as in Figure 14. Because of the crater frequency, these shells resembled golf balls. The Energy Dispersive X-Ray Spectroscopy (EDXS) data indicated that the bottoms of the craters were depleted in alkali, with an alkali (Na and K) composition less than half that of the surrounding glass matrix. The alkali loss was localized to cratered areas; the composition of the surrounding matrix was similar to that of unheated glass shells shown in Table 11.

The observed change in composition and degradation in shell quality, resulting even from mild ( $\sim 900^\circ\text{C}$ ) heating, underscores the difficulty of remelting glass shells either to improve them [14] or to determine the effects of gravity on shell WNU. These problems may be solely a function of glass composition; the composition may be particularly susceptible to phase separation and alkali loss. Other compositions may be substantially more stable but our experience with glass indicates a significant volatilization rate for alkali and boric oxide components in most glasses, when in the form of small shells. Thus the glass-melts continually change in composition when held at temperature for a long time, resulting in a corresponding increase in viscosity. Since glass viscosity is a parameter of the model which must be held constant (and since increasing viscosity will decrease the rate of gravity-induced glass flow) the model is quite difficult to test unless the glass composition is held constant. The change in composition with time may also promote phase separation, but equally conducive for phase separation is the relatively slow heating and cooling

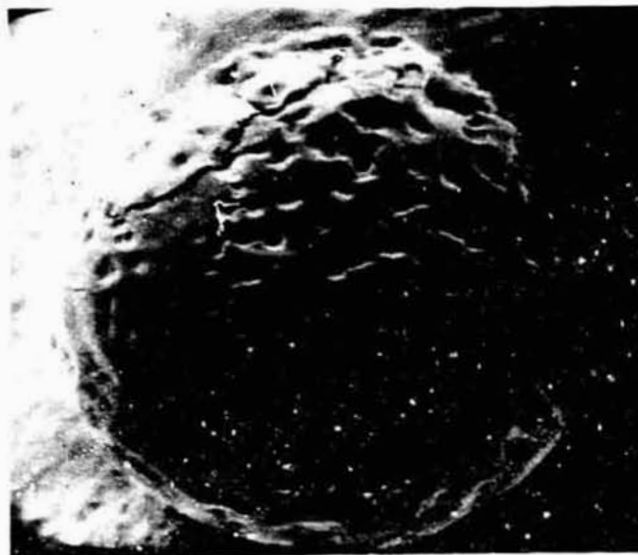
ORIGINAL PAGE  
BLACK AND WHITE PHOTOGRAPH



A) Optical Photomicrograph of Shell



B) Optical Magnification of A



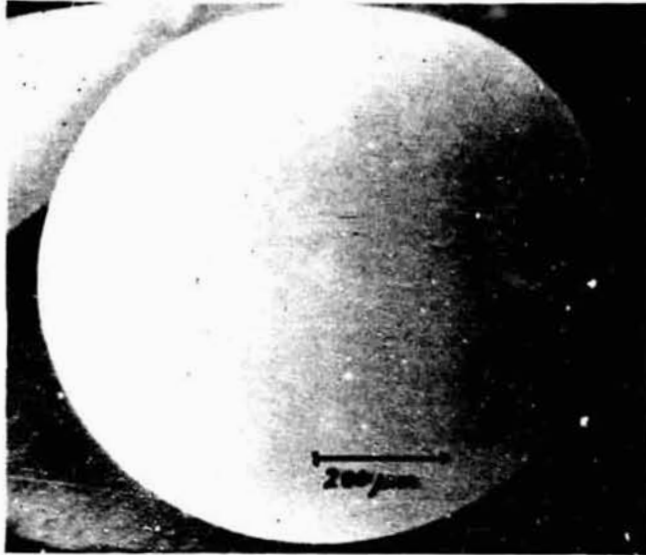
C) SEM Photomicrograph of Shell Surface



D) SEM Magnification of Surface Crater

Figure 12. Photomicrographs—Phase Separation in Shells Reheated at 1300° C.

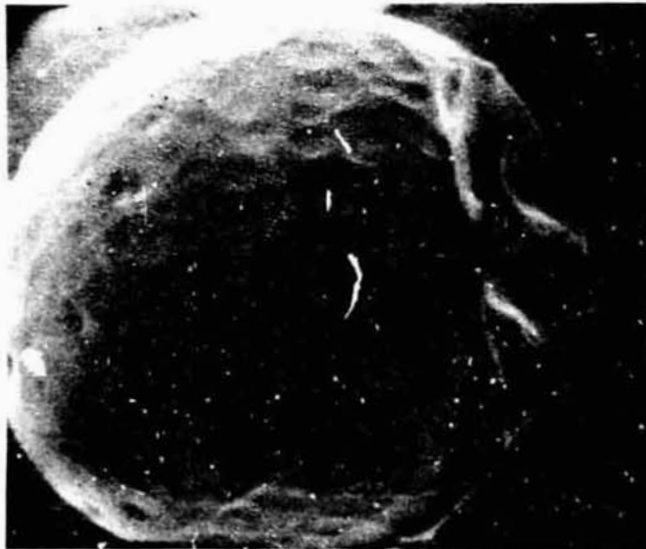
ORIGINAL PAGE  
BLACK AND WHITE PHOTOGRAPH



A) Control Shell



B) Surface Detail of Control Shell



C) Shell Reheated to 900°C



D) Surface Detail of Reheated Shell

Figure 13. Change in Surface Texture Upon Reheating Shells to 900° C.

ORIGINAL PAGE  
BLACK AND WHITE PHOTOGRAPH

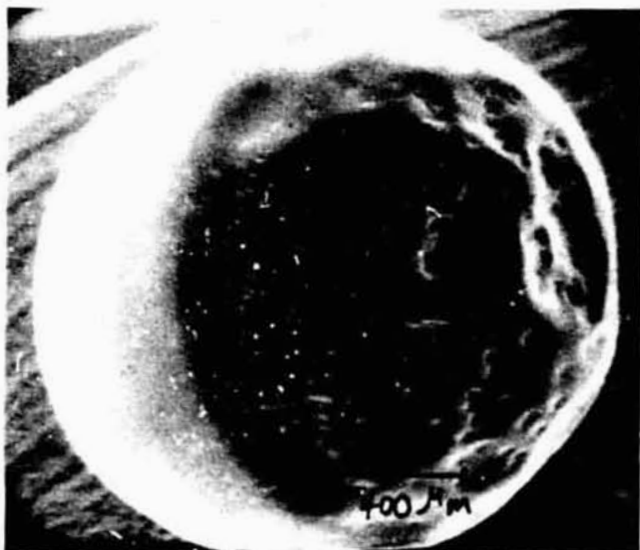
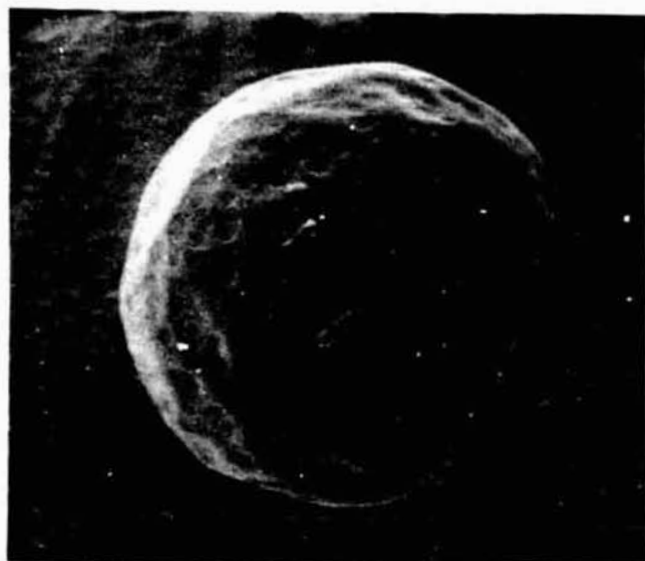


Figure 14. Phase Separation in Shells Reheated to 800–900° C.

Table 11. EDXS Elemental Analysis of Remelted Glass Shells

<u>Sample</u>	<u>Treatment History</u>	<u>Sampling</u>	<u>EDXS Analysis</u>	
			<u>Na/Si</u>	<u>K/Si</u>
Control	not heated	averaged- whole surface	0.017 ± .008	0.029 ± 0.015
1	900°C	whole surface	0.019 ± .004	0.030 ± .016
2	900°C	crater bottom <sup>1</sup>	0.008 ± .004	0.008 ± 0.004
		matrix	0.016 ± .002	0.021 ± 0.002
3	1300°C	whole surface	0.009 <sup>2</sup>	0.001 <sup>2</sup>

1 Data for 5 crater and 5 matrix readings on one shell.

2 Shell melted and reformed at 1300°C; the sole shell recovered from this treatment.

rates used in the experiments. The solution to this difficulty may be a) to minimize the total heating time by increasing the efficiency of melting the shells, e.g., with a CO<sub>2</sub> laser beam [15], or b) to employ non-volatile glass systems with very low and stable viscosity. Germania, a single-component glass, would be an ideal candidate on the basis of these criteria, except for its relatively high viscosity in the liquidus. Although lower than the silica liquidus ( $\sim 10^8$  poise), it is still higher than found for many alkali borosilicate and soda-lime glasses which range from 10 to 10<sup>4</sup> poise. In testing for the effect of gravity on molten shells, such viscosities would require unacceptably long sample residence times in a vertical furnace, or higher temperatures than are currently possible with the CHS levitator and radiant furnace described above.

Since the viscosity of pure germania glass is considerably higher than desired for reheating experiments, binary glasses in the silica and germania glass systems were investigated. Phase diagram data eliminated the alkaline earth silicates as candidates. Even though this system has the advantage of a stable composition due to the non-volatility of the alkaline earth oxide glass modifier, it has the problems of a) phase separation in the liquid state due to immiscibility over a large concentration range, and b) an excessively high eutectic temperature ( $> 1400^\circ$ ) [16]. Alkali silicates were undesirable since high concentrations of alkali ( $\sim 15$ -25 mol percent) are required to significantly reduce the liquidus temperature (to 1000-1200°C) [16]. Such high concentrations of alkali render the glass susceptible to alkali volatilization and the consequent composition and viscosity changes upon reheating.

The binary germania system has an inherent advantage. The liquidus temperature of pure germania is already in the desired range. The addition of moderate amounts of alkali oxides, e.g.  $\sim 5$  mole percent, will bring it well within the desired range, from 1150°C to 900-1000°C; the eutectics occur at 4-10 mol percent M<sub>2</sub>O [17]. The alkali are desired solely for viscosity modification, and in the germania system, small amounts of alkali oxide, such as Na<sub>2</sub>O, very sharply reduce the viscosity. For example, the addition of 1.2 mole percent Na<sub>2</sub>O to pure Ge<sub>2</sub>O reduces it to 20 poise [17,18]. The addition of lithium and potassium oxides yield similar results. While high alkali oxide ( $\sim 5$ -7 mol percent) germania glasses are expected to be moderately volatile and compositionally varying at the liquidus temperature, the correspondingly low glass viscosity should require

a very short sample residence time in the furnace (during experiments testing for gravity effects on the molten shell). Because of the low operating temperatures and the initially low concentration of alkali, low-alkali oxide germania glasses (< 1 percent) are expected to have only negligible alkali loss rates during the course of the reheating experiments, and the composition and viscosity should remain constant in time. Thus a series of glasses, with a wide range in viscosities, may be possible for testing the gravity-driven decentering model.

Although of poor quality (wall uniformity) germania shells were made by the metal-organic gel method several years ago at KMSF using precipitated powder from the hydrolysis of germanium ethoxide. More recently, the synthesis of homogeneous germania gels was attempted by hydrolysis of ethanolic solutions of a) germanium tetrachloride, b) germanium tetrachloride acidified with oxalic acid [19], and c) germanium tetraethoxide [20,21]. However, these reactions yielded either crystalline or gelatinous precipitates which dried to a fine, chalky powder rather than a glassy friable gel. These gels were also devoid of residual organics, as confirmed by TGA and PGC.

Superior homogeneous gels of germania and the more reactive sodium germanate (5 mol %  $\text{Na}_2\text{O}$ ) were synthesized by controlled partial hydrolysis of alcohol solutions of germanium and germanium/sodium alkoxide mixture (80% of stoichiometric amounts of  $\text{H}_2\text{O}$ ) at  $-50^\circ\text{C}$ . These reactions yielded homogeneous, translucent gels which, when dry, were glassy and friable. Sodium germanate shells as large as  $600\ \mu\text{m}$  have been produced at  $1300^\circ\text{C}$  from the freshly-prepared corresponding gel. These gels are very sensitive to atmospheric moisture. They hydrolyze readily and completely, with consequent loss of all the residual organics and a concomitant reduction of the high surface area (from  $460\ \text{m}^2/\text{gm}$  to less than  $10\ \text{m}^2/\text{gm}$ ). Unlike the silicate gels, this hydrolyzed sodium germanate gel produced only small thick-walled shells of very poor uniformity.

A possible approach to get around this problem is the incorporation into the gel of an auxiliary blowing agent which is immune to hydrolysis. Urea, a compound used in blowing of silicate based glass shells, was successfully incorporated into the germania gel in an apparently homogeneous manner, but shell blowing experiments could not be done before the expiration of this contract.

## 6. CONCLUSIONS

The purpose of this work has been to study and model the mechanisms that produce glass shells from metal-organic gels, and thereby to provide a basis for an assessment of the benefits of manufacturing shells in space. The objectives have been to determine: 1) the effects of gel pyrolysis, and thus the nature of the gel-to-shell transformation, 2) the effective heating rate of a gel particle falling through a vertical furnace, and 3) the effect of gravity on the shell concentricity (i.e., shell-wall uniformity) as the molten shell drops through the furnace.

A gel particle falling through a vertical furnace is rapidly pyrolyzed and transformed to a hollow shell. For the size of gel currently used ( $\sim 20 \mu\text{m}$ ), that transformation occurs within one second ( $@ 1300^\circ\text{C}$ ) and is rapid with respect to the time needed for complete firing of the glass in the shell. The transformation to a shell is comprised of several distinct processes: a) surface closure of the porous structure of the gel, either by low-temperature ( $< 400^\circ\text{C}$ ) sintering or else by hydrolysis, b) formation of a closed-cell foam structure ( $\sim 400^\circ\text{C}$ ), c) expansion and spheridization of the particle ( $\sim 600\text{--}800^\circ\text{C}$ ), d) coalescence of the foam to form a single-void shell ( $\sim 800\text{--}1000^\circ\text{C}$ ), and e) firing of the glass walls of the shell. These processes have been observed during gel pyrolysis by hot stage microscopy, or have been inferred from pyrolyzed-gel intermediates recovered from shell-forming experiments. The driving force for the formation of the initial closed-cell foam structure in the gel is supplied by the gaseous pyrolysates generated from the gel. These gases are typically comprised of  $\text{H}_2\text{O}$ ,  $\text{CO}_2$ , ethylene, ethane, and methane, and are generated from the metal alkoxides, the silanols and the bicarbonates in the gel at fairly low temperatures. The pyrolysis decomposition of the metal-alkoxides also produces elemental carbon, resulting in a characteristic black appearance to the gel. The oxidation of this carbon, as well as the decomposition of metal carbonates in the gel, produces the  $\text{CO}_2$  that drives the further expansion of the foamed spheroid and the final shell. Undoubtedly, most of the pyrolysates are rapidly lost and may be ineffective in shell-blowing, except to separate a charge of gel powder into a well-dispersed plume upon injection into the furnace. The average metal-organic gel loses more than 20% of its mass as gas, while much less than 1% remains to form the final shell. These two

conclusions are supported by two observations. Gels that were pyrolyzed to remove all of the gaseous pyrolysates ( $\sim 26\%$  of the initial gel mass) formed shells in yield and quality similar to those made from unpyrolyzed gel. In addition, metal-organic gels that were hydrolyzed (under argon or in air) to remove all of the organic species (except for trace levels) produced shells of similar yield and quality as those from unhydrolyzed gels. In the latter case, the blowing gas,  $\text{CO}_2$ , is derived primarily from carbonates in the gel, and comprises  $\sim 1\%$  of the total gel mass; yet only  $\sim .01\%$  ends up among the final blowing gases in the shell. (The other constituents of the residual gases in the shells are  $\text{O}_2$ ,  $\text{N}_2$  and sometimes  $\text{H}_2\text{O}$ . The  $\text{O}_2$  and  $\text{N}_2$  permeates the shell from the furnace ambience.)

The various desorption and decomposition reactions that occur during gel pyrolysis constitute a thermal inertia, or latent heat, in the gel, and increase the specific heat of the gel over that of the corresponding glass. However, the oxidation of the organic pyrolysates and the reduction in surface free energy (due to sintering) are exothermic and partially compensate for the endothermic reactions. The average specific heat for unhydrolyzed metal-organic gel is less than twice ( $\sim 1.5\text{-}2 \text{ j/gm K}$ ) that for glass. In any event, this latent heat has no effect on shell production, as was evidenced by the shells produced from pyrolyzed gels.

The results of the heat-transfer modeling and the experiments in support of this modeling indicate that gel particles as large as  $20 \mu\text{m}$ , which yield  $400\text{-}600 \mu\text{m}$  shells (depending on furnace conditions), are heated very rapidly, at a rate of approximately  $3000^\circ\text{C}/\text{sec}$ . The gel-to-glass shell transformation is completed in  $\sim 1 \text{ sec}$ . The final fining of the glass, to remove the remaining carbon and gas inclusions in the wall, takes considerably longer depending on the furnace gas and temperature (e.g.,  $>5 \text{ secs}$  at  $1300^\circ\text{C}$ , in air). Gel particles as large as  $200 \mu\text{m}$  are also heated rapidly to the temperature of the furnace ambience, at a rate of approximately  $\sim 2000^\circ/\text{sec}$ . However these massive particles develop a high terminal velocity and fall deeply into the furnace ( $\gtrsim 1 \text{ m}$ ) before reaching that temperature. Because of the larger mass, the gel transformation is significantly slower, and the particles do not expand rapidly enough to generate sufficient buoyancy and drag to decrease the terminal velocity of the particles. Consequently such massive gel particles have a very short residence time ( $< 2 \text{ secs}$ ) and cannot transform completely into shells. The crux of this problem is the high terminal velocity.

of the particles. Thus the problem can be solved only by increasing the furnace length, by reducing the terminal velocity with counter-flowing gas (or gas-jet levitation); or by reducing the gravitational acceleration on the particle.

The model for gravity-induced decentering of shells predicts significant decentering rates for molten glass shells less than 2 mm in diameter. There is a real concern that the model has improper boundary conditions for the external shell surface. With the apparently appropriate boundary conditions extremely rapid and extensive decentering of the internal and external shell surfaces are suggested. However, such extensive decentering has not been observed in current shell manufacture. These observations suggest that either these boundary conditions are not correct, or an active centering mechanism exists to counteract the effect of gravity. The latter appears to be the more likely answer.

Efforts to test the validity of the decentering model have been hampered by problems related to uniform and controlled shell heating, stable levitation, and stability of the glass compositions. Consequently these empirical studies have not yet been completed.

## 7. RECOMMENDATIONS

We believe that a significant advance in the understanding of the processes involved in glass shell synthesis from metal-organic gels has been achieved from work done under this contract. On the basis of this knowledge, plus the additional understanding which has accrued from related work under our Department of Energy contract over the past three years, we can identify incomplete and unstudied areas for further research. We have been motivated in our research by the ultimate goals of 1) understanding the mechanisms which control the formation of highly uniform glass shells suitable for inertial fusion energy research and 2) preparing for the potential necessity of making in space large shells which may not be obtainable in a terrestrial laboratory. These goals also motivate our suggestions and recommendations for future work. These recommendations can perhaps best be made in the context of further mechanistic studies required for three processes that affect the formation of uniform glass shells from gel. Each part of any future research should contain both a mathematical and an experimental component.

### 7.1 Mass Transport Study

**Mathematical Model.** Develop a second generation heat transfer/particle trajectory/fluid mechanical model for gel particles forming a shell in a vertical furnace. This model should be able to handle inhomogeneities in physical and chemical properties for the gel and shell during the shell forming process.

**Experimental Program.** Conduct experiments to collect thermodynamic and chemical kinetic data required for mathematical modeling.

A successful model would predict the time and temperature required to form a complete bubble-free shell from a given size gel particle of known composition.

### 7.2 Shell Concentricity Study

**Mathematical Model.** Experimental evidence from shell-forming and gel pyrolysis studies suggest the existence of an active centering mechanism(s), that produces shells with uniform walls from asymmetric spheroids. Among the concepts that have been suggested and/or partly investigated we propose that the following centering forces be studied in more detail:  
a) the tumbling action of the shell, b) surface tension gradients in the shell

surface caused by compositional gradients resulting from differential vaporization of alkali and boron oxides, c) viscosity gradients resulting from the composition (or temperature) gradients, or d) expansion-contraction cycles caused by applied force or by heating and cooling cycles due to small, localized temperature gradients in the furnace.

Experimental Model. Conduct experiments to test the validity of models as they are developed. The role of composition gradients (b and c above) should be examined by comparing shell blowing experiments using gel starting materials with a wide range of volatile components and variations in chemical homogeneity.

### 7.3 Shell Decentering Study

Mathematical Model. The current gravity-induced decentering model (of an initially concentric shell) may have serious weaknesses due to the boundary conditions employed. We propose the development of a model based rigorously on the principles of Low Reynold's Number Hydrodynamics with appropriate use of computers to achieve numerical solutions.

Experimental Model. Considerable effort has been expended in preliminary experiments concerning the effect of gravity on the concentricity of the inner and outer shell surfaces. The progress of this work has been hampered by problems of a) compositional instability of the molten glass shells and b) inadequate methods for containerless reheating of characterized shells. These problems completely mask the more subtle effects of gravity. We recommend the continuation of this line of research, with emphasis on the development and use of a) glass shells having a suitably low viscosity, a stable composition, and resistance to phase separation and devitrification, b) a containerless method for uniform, controlled heating of the shell surface, such as an acoustic or air-jet levitation with a CO<sub>2</sub>-laser heating system, and c) shell-forming and shell-reheating experiments aboard KC-135 flights. In this manner, the uniformity of the shell walls could be investigated as a function of gravity and heating time.

## ACKNOWLEDGEMENTS

We wish to acknowledge the financial support of this work by the National Aeronautics and Space Administration through a 3-year research contract, NAS8-33103 (1978-1981). We gratefully acknowledge the following support: R. B. Jacobs (of R. B. Jacobs Associates), for his work in mathematical modeling and his helpful discussions, criticisms and suggestions; R. J. Simms, for his work in developing the computer programs for the heat transfer problems; B. D. Homyk, for help with gel and shell analyses; J. J. Rolen, for Scanning Electron Microscopy; W. J. Miller, for help with the initial synthesis of gels; L. Scott, for elemental analyses; and T. M. Henderson, M. Mikeska, K. Horn and M. Harper for help in assembling this report. We also wish to thank Edwin Ethridge of MSFC for helpful discussions, for supplying equipment and expertise for air-jet levitation/reheating of glass shells, and for sharing his filmed sequences of air-jet levitation and heating of gel particles.

## REFERENCES

1. F. Veatch, H. E. Alford and R. D. Croft, to The Standard Oil Co., Hollow glass particles and method of producing same. U.S. Patent No. 3,030,215, April 17, 1962.
2. W. R. Beck and D. L. O'Brien, to Minnesota Mining and Manufacturing Co., Glass bubbles prepared by reheating solid glass particles. U.S. Patent No. 3,365,315, April 23, 1968.
3. C. D. Hendricks, to The United States of America as represented by the United States Department of Energy. Method and apparatus for producing small hollow spheres. U.S. Patent No. 4,163,637, August 7, 1979.
4. R. G. Budrick, F. T. King, R. L. Nolen, and D. E. Solomon, to KMS Fusion Inc., Method for manufacturing glass frit. U.S. Patent No. 4,021,253, May 3, 1977.
5. R. L. Nolen, R. L. Downs, W. J. Miller, M. A. Ebner, N. E. Doletzky and D. E. Solomon in Digest of Topical Meeting on Inertial Confinement Fusion. (Opt. Soc. Am., Washington, D.C., 1978) paper TuE-1.
6. R. G. Budrick, F. T. King, A. J. Martin, R. L. Nolen and D. E. Solomon, to KMS Fusion, Inc., Method and apparatus for making uniform pellets for fusion reactors. U.S. Patent No. 4,017,290, April 12, 1977.
7. T. P. O'Holleran, R. L. Nolen, R. L. Downs, D. A. Steinman and R. L. Crawley, J. Vac. Sci. and Tech., 18(3), 1242-1243 (1981).
8. E. Ethridge and S. Dunn, Proceedings of the Materials Research Society, November 16-18, 1981, Boston, MA, in press.
9. R. L. Downs, M. A. Ebner, B. D. Homyk and R. L. Nolen, J. Vac. Sci. and Tech., 18(3), 1272-1275 (1981).
10. T. P. O'Holleran, R. L. Downs, M. A. Ebner and R. L. Nolen, "Shells from Compacted Powder," KMS Fusion Annual Technical Report, 1980, I.55-I.58. Also, P. J. Evans, unpublished results.
11. A. W. Francis, Physics, 4 (Nov), 403-406 (1933). (Now - Journal of Physics.)
12. T. G. Wang, "Gravitation Effects on Target Fabrication", Digest of Topical Meeting on Inertial Confinement Fusion (Optical Society of America), Washington, D.C., (1980). Also, NASA Contact Review Meeting, March 1980.
13. R. S. Subramanian, Clarkson College of Technology, Potsdam, NY, private communication.

14. Stanley A. Dunn, Final Report: Concentring of Glass Microballons, prepared for University of California, Los Alamos Scientific Laboratory, Contract No. LP6-62129-1.
15. Paul C. Nordine, personal communication; and D. W. Winborne, P. C. Nordine, D. E. Rosner, and N. F. Marley, Metallurgical Transactions B, 7 B, 711-713 (1976).
16. E. M. Levin, C. R. Robbins, and H. F. McMurdie, Phase Diagrams for Ceramists. (The American Ceramic Society, Columbus, Ohio, 1964), pp. 66, 87, 91, 93, 94, 97, and 104.
17. E. F. Riebling, Journal of Chemical Physics, 39(7), 1889-1895 (1963).
18. C. R. Kurjian and R. W. Douglas, Physics and Chemistry of Glasses, 1(1), 19-25 (1960).
19. Edward Gorlich, et al., Roczniki Chemii (Ann. Soc. Chem. Polonorum), 50, 1673-79 (1976).
20. A. W. Laubengayer and P. L. Brandt, J. Am. Chem. Soc., 54, 549 (1932).
21. D. C. Bradley, L. J. Kay, and W. Wardlaw, J. Chem. Soc., 4916-26 (1956).

## APPENDIX I

### Heat Transfer/Thermodynamic/Fluid Mechanical Model of Processes Occurring During the Manufacture of Glass Shells in Vertical Furnaces\*

The purpose of this appendix is to outline the development of a first-generation model of the processes occurring during the manufacture of glass shells in vertical furnaces. The purposes of the model are:

1. To investigate the heat transfer and fluid mechanical phenomena associated with the manufacture of glass shells in vertical furnaces.
2. To delineate the furnace parameters that are important to the manufacture of high-quality glass shells, and their quantitative influence on the quality of the product.
3. To predict the largest shells of acceptable quality that can be manufactured in a 1 g environment with existing equipment.
4. To specify furnace equipment that will be required to manufacture glass shells for future requirements, which will have more stringent specifications.

This type of model is primarily the embodiment of some of the fundamental principles of classical physics. Effective use of the model requires the availability of additional information, such as materials property data, and insight to the processes resulting from specific empirical investigations.

This first generation model was developed at the beginning of the program when little information was available on the details of the processes occurring in the shells and their precursors. One consequence is the assumption that, at every instant, the shells and their precursors are homogeneous. During the course of the program significant insight has been gained regarding the temperature ranges in which specific physical and chemical processes occur, and relevant quantitative materials properties. Consequently, a second generation model is currently being developed in which the shells and their precursors are not assumed to be homogeneous.

The furnaces with which we are concerned have interior heated regions whose walls are vertical circular cylinders. The cylinder diameters are about 3 inches, and the lengths of the heated sections have varied from

\*Appendix I was authored by R. B. Jacobs of R. B. Jacobs Associates, consultant to current contract.

2 to 12 feet; about 2 feet of unheated region are at the bottom end. The furnaces are heated by electrical resistance heaters, usually wired so that several axial sections can be heated and their temperature controlled independently. In existing equipment, the operating temperatures are varied from 800°C to 1500° C. The heated region is usually filled with static, atmospheric air; the only flows are those due to natural convection and those that may be caused by the presence of material associated with the manufacture of the glass shells. The species of gas within the furnaces can be changed, and generally axial flows can be imposed upon the gas.

The raw materials from which the glass shells are made are classified as gel powders and pellets. (For convenience in the following discussions, the raw material will be called "frit"; it need not be frit, but may just as well be cast, extruded, etc.) The frit is introduced, at room temperature, into the upper end of the furnace, and falls vertically downward (except for possible effects of radial and tangential components of the gas velocity, and of the method for introducing frit). As it falls, the frit and its descendents are heated by the furnace walls and the furnace gas. Heat transfer involves both radiation and convection, the latter including gas conduction. Additionally, the frit and its descendents interact mechanically with the furnace gas; this interaction, along with the effects of gravity, determines the motion of the particles. As a result of the heating, the constituents of the frit begin to react to form glass and a blowing gas. Under proper conditions, the physical and chemical processes produce high-quality, thin-walled glass shells. The products of these processes are collected at the lower end of the furnace.

It is postulated here, and can be inferred from experience, that the manufacture of high-quality glass shells requires that the gel material be heated to a sufficiently high temperature and maintained there for a sufficiently long time interval. We may therefore conclude that the rates of heat transfer from the furnace to the materials therein, and the residence times of the materials within the furnace are of primary importance. Therefore, our primary objectives here are to investigate the phenomena and variables that influence the heat transfer and residence times, and to relate these to characteristics and properties of the gel and glass shells, and to design and operating parameters of the furnaces.

The remainder of this development therefore consists of two sections:

1. Heat transfer considerations which embody the requirements of the First Law of Thermodynamics.
2. Particle motion considerations which embody the requirements of Newton's Second Law.

The model is expressed here in differential form and has also been expressed in finite difference form for programming for parametric studies.

### HEAT TRANSFER

The heat transfer from the furnace (walls and gas) to a particle therein (gel particle or shell) is described by:

$$\frac{mC}{A_s} \frac{dT}{dt} = h (T_g - T) + \sigma E(T_g^4 - T^4). \quad (1)$$

The left-hand term is the rate of increase of energy of the particle being heated. The middle term describes the rate of convection heat transfer (including gas conduction) from the furnace gas to the particle. The right-hand term describes the rate of radiant heat transfer from the furnace walls and gas to the particle; we assume that the walls and gas are effectively at the same temperature.

Equation 1 is applied to individual particles from the time that they are introduced as frit to the time that they exist as shells. We ignore mechanical and thermal interactions between the particles themselves, and mechanical interaction between the particles and the walls. It has also been assumed, in the derivation of equation 1, that the temperature of the particle is always uniform. This assumption, together with the assumption of material homogeneity, give rise to the most severe limitations of this first generation model. It is justified, from a thermal history viewpoint, by the fact that the time intervals required to equilibrate temperature differences within the particles are short relative to the time intervals associated with the heating of the particles. The elimination of the temperature-uniformity and material homogeneity assumption is the basis of the second-generation model mentioned above.

The variables and parameters in equation 1 are:

$m$  is the mass of the particle. As the manufacturing process proceeds,  $m$  changes. If these changes were known as a function of temperature,

they could be readily managed in the development of solutions to equation 1; however, this was not the case. We did know that a significant mass (of the order of 15%) was lost below 600°C as the result of the loss of blowing gas. Therefore, in this model it is assumed that there is a single, instantaneous loss of mass. This loss occurs when the particle attains the temperature  $T_1$ ; the fraction of the initial mass which is lost is  $(1 - \Gamma)$ .  $T_1$  and  $\Gamma$  can be treated as parameters whose values are determined by efforts to obtain agreement between the model and empirical information. On the basis of early experiments, initial values for these parameters can be  $T_1 = 500^\circ\text{C}$  and  $\Gamma = 0.85$ .

$C$  is the effective specific heat of the particle being heated. It should account for the various latent heats associated with the manufacturing process; e.g., heats of chemical reaction and phase transitions. There was also a dearth of information in this area.

$A_s$  is the surface area, of the particle, that is exposed to the heating environment. It varies with time, and may be correlatable with temperature. However, it is not now possible to express  $A_s$  as a function of time or temperature. In this model, we specify a geometry for the initial frit particle: a right circular cylinder of diameter  $D_f$  and length  $(2 D_f)$ . This limitation can be eliminated as discussed below. We assume that at a specified temperature ( $T_2$ ), the frit particle instantaneously transforms to a sphere of diameter,  $D$ , the final diameter of the shell. As will be discussed below,  $D_f$  and  $D$  will be related by a parameter which, along with  $T_2$  might be determined by correlating empirical information to fit the model.

$T$  is the absolute temperature of the particle being heated.

$t$  is time.

$h$  is a heat transfer coefficient that characterizes the convective (and gas conductive) heat transfer from the furnace gas to the particle being heated. It depends upon the geometry of the particle, properties of the furnace gas, and the flow field of the furnace gas relative to the particle. For this model, we express it in terms of fairly reliable steady-state theoretical formulations and empirical correlations. This

is partially justified because the time intervals required to develop steady-state flow fields are short relative to the residence times in the furnaces. The major uncertainties stem from lack of information regarding the geometries of the particles as they pass through the furnace. The same assumptions are used to assist in the calculation of  $h$  as were discussed in connection with  $A_s$ .

As we shall see later, in our discussion of residence times of particles in the furnace, the Reynold's numbers associated with the particles in the furnace are small. From McAdams<sup>1</sup> we find that we shall be somewhat conservative (i.e., predicted temperature changes are too small) if we use:

$$h = 2 \frac{k_g}{L}, \quad \text{where} \quad (2)$$

$k_g$  is the thermal conductivity of the furnace gas, and

$L$  is a characteristic dimension of the particle.

For the frit particle,  $L$  is assumed to be the arithmetic average of the length and diameter; for the shell,  $L$  is its diameter,  $D$ .

$T_g$  is the absolute temperature of the furnace gas (and walls). In general,  $T_g$  is a function of position in the furnace, and therefore, in equation 1, a function of  $t$ . In our experiments, this function is known and is therefore used in developing solutions to our model.

$\sigma$  is the Stefan-Boltzmann constant, and is approximately  $5.67 \times 10^{-12}$  watt/cm<sup>2</sup>K<sup>4</sup>.

$E$  is the effective absorptance of the particle to the radiation emitted by the furnace walls and gas. It is a function of the geometries of the furnace and particle, and of properties of the furnace walls, furnace gas, and particle. Because the object being heated is tiny relative to the size of the furnace,  $E$  is effectively equal to the absorptivity of the particle to the radiation emitted by the furnace. It is probable that the frit absorbs essentially all of the radiation incident upon it, and that the clear glassy material will absorb a negligible amount of the radiation incident upon it. We assume, therefore, in this model that  $E = 1$  until the temperature of the particle becomes  $T_3$ ; at this time the value of  $E$  instantaneously becomes zero ( $E = 0$ ). As indicated with  $T_1$  and  $T_2$ ,  $T_3$  can also be used as a correlating number.

We are now in a position to formulate the preceding discussion into relations that can be substituted into equation 1. The results are:

For  $T \leq T_1$ ,

$$\begin{aligned} \frac{\rho_{gl} C_f}{2.5 \Gamma} \Delta^{2/3} \eta \frac{dT}{dt} &= \\ &= \frac{4}{3} \frac{k_g}{D} \Delta^{1/3} (T_g - T) + \sigma(T_g^4 - T^4). \end{aligned} \quad (3a)$$

For  $T_1 < T \leq T_2$ ,

$$\begin{aligned} \frac{\rho_{gl} C_f}{2.5} \Delta^{2/3} \eta \frac{dT}{dt} &= \\ &= \frac{4}{3} \frac{k_g}{D} \Delta^{1/3} (T_g - T) + \sigma(T_g^4 - T^4). \end{aligned} \quad (3b)$$

For  $T_2 < T \leq T_3$ ,

$$\rho_{gl} C_{gl} \eta \frac{dT}{dt} = 2 \frac{k_g}{D} (T_g - T) + \sigma(T_g^4 - T^4). \quad (3c)$$

For  $T > T_3$ ,

$$\rho_{gl} C_{gl} \eta \frac{dT}{dt} = 2 \frac{k_g}{D} (T_g - T). \quad (3d)$$

Equations 3a, 3b, 3c, and 3d (i.e., equations 3) are the final embodiments, in differential form, of our energy equation for the temperature ranges of interest. The new symbols which have not yet been defined are:

$\rho_{gl}$  = is the mass density of the glass in the shell.

$C_f$  = is the effective specific heat of the frit material.

$$\Delta \equiv \left( \frac{\rho_f}{\rho_{gl}} \frac{\Gamma}{2} \frac{D}{\eta} \right) = \left( \frac{D}{D_f} \right)^3.$$

$\rho_f$  = is the mass density of the frit material.

$\eta$  = is the thickness of the shell wall.

$C_{gl}$  = is the effective specific heat of the glass in the shell wall.

It is reasonable to assume that, for a specific shell manufacturing process,  $\rho_f$ ,  $\rho_{gl}$ , and  $\Gamma$  should be fixed. Thus, from the above definition

of  $\Delta$ , there should be a unique linear relation between  $(D/D_f)^3$  and  $(D/\eta)$ .

In order to become numerically oriented, we have used some of our data to calculate  $\left(\frac{\rho_f}{\rho_g} - \frac{\Gamma}{2}\right)$ . We obtained that  $\frac{D}{D_f} = \left(.16 \frac{D}{\eta}\right)^{1/3}$ .

There is no reason we believe that this relation is valid for any situation except for the one from which it was derived.

### PARTICLE POSITION

The purpose of this development is to derive relations that will allow us to predict the position of a particle, as a function of time, as it falls through the furnace. By using these relations, in conjunction with equations 3, we can predict the temperature of the particle as a function of its position in the furnace.

The position of the particle, as a function of time, is computed by integrating its velocity with respect to time. The velocity of the particle is obtained by applying Newton's Second Law to the particle falling through the furnace gas under the action of gravity. The effect of the gas upon the velocity of the particle is manifested through the "drag" force exerted by the gas on the particle. As this depends upon the geometry of the particle, and as the mass of the particle enters directly into Newton's Second Law, the computation of particle position is divided into four temperature regimes, as was the computation of the particle temperature.

There are three forces acting on the particle as it falls through the furnace: drag, buoyancy, and gravity. The drag force may be represented satisfactorily by Stokes' Law. The resultant differential equations for the velocity ( $U$ ) and the displacement ( $S$ ) of the particle are:

$$\frac{dU}{dt} = (\gamma + \delta U), \quad (4)$$

and

$$\frac{dS}{dt} = U \quad (5)$$

$$\gamma = g \left(1 - \frac{V \rho_g}{m}\right), \quad (6)$$

and

$$\delta = - \frac{12.5 \mu_g A}{\bar{D} m} \quad (7)$$

$g$  = acceleration of gravity.

$V$  = volume of particle.

$\rho_g$  = density of the furnace gas.

$m$  = mass of particle.

$\mu_g$  = absolute viscosity of furnace gas.

$A$  = frontal area of particle.

$\bar{D}$  = characteristic dimension in Reynolds' number.

The detailed formulations of the parameters in equations 6 and 7 depend upon the temperature ranges discussed previously. For each temperature,  $\gamma$  and  $\delta$  can be taken as constant (if average values be used for  $\rho_g$  and  $\mu_g$ ). Then, equations 4 and 5 can be easily solved for  $U$  and  $S$ :

$$(\gamma + \delta U) = (\gamma + \delta U_0) e^{\delta(t - t_0)} \quad (8)$$

$$S = \left[ U + \frac{1}{\delta} \left( \frac{\gamma}{\delta} + U_0 \right) e^{\delta(t - t_0)} - \frac{\gamma}{\delta} (t - t_0) \right]; \quad (9)$$

$$U = U_0 \text{ and } S = S_0 \text{ when } t = t_0.$$

Because of the non-linearity of equations 3, and because of the variable properties therein, equations 7 are solved numerically by means of computers. It is therefore convenient to solve the particle position relations numerically also. As a result, our working model uses equations 4 and 5, rather than equations 8 and 9.

Introducing our previously discussed concepts into equations 6 and 7, we develop our expressions for  $\gamma$  and  $\delta$  for our various temperature regimes.

For  $T \leq T_1$ ,

$$\gamma = g \left\{ 1 - \left[ \frac{\rho_g}{\rho_{g1}} \frac{\Gamma(AR)}{\Delta} \right] \right\} \quad (6a)$$

$$\delta = - \frac{25(2 + \frac{\pi}{4})}{3\pi} \left( \frac{\mu_g}{\rho_{g1}} \right) \left[ \frac{\Gamma(AR)}{\Delta} \right] \frac{1}{D^2} \Delta^{2/3} \quad (7a)$$

For  $T_1 < T \leq T_2$

$$\gamma = g \left\{ 1 - \left[ \frac{\rho_g}{\rho_{g1}} \right] \left[ \frac{(AR)}{\Delta} \right] \right\} \quad (6b)$$

$$\delta = - \frac{25(2 + \frac{\pi}{4})}{3\pi} \left( \frac{\mu_g}{\rho_{g1}} \right) \left[ \frac{(AR)}{\Delta} \right] \frac{1}{D^2} \Delta^{2/3} \quad (7b)$$

For  $T > T_2$  (contains  $T_2 < T \leq T_3$  and  $T > T_3$ ),

$$\gamma = g \left\{ 1 - \frac{(AR)}{6} \left( \frac{\rho_g}{\rho_{g1}} \right) \right\} \quad (6c)$$

$$\delta = \frac{-12.5}{4} \left( \frac{\mu_g}{\rho_{g1}} \right) \frac{1}{D^2} (AR). \quad (7c)$$

AR (the aspect ratio) is the ratio of the diameter of the shell to its average wall thickness. It should be noted that the foregoing model is expressed in terms of furnace characteristics, properties of the materials involved in the manufacturing process, and geometrical characteristics of the shell. Summarizing, our model is described by:

1. Equations 3a, 4, 5, 6a and 7a prior to the mass loss, and characterized by the parameter  $(1 - \Gamma)$ .
2. After the mass loss, but prior to the transformation from frit to shell, equations 3b, 4, 5, 6b and 7b.
3. After the transformation from frit to shell, but prior to becoming transparent to radiation, equations 3c, 4, 5, 6c and 7c.
4. After becoming transparent to radiation, equations 3d, 4, 5, 6c, and 7c.

It should be noted, that the foregoing equations were developed so that the geometry of only the shell appears explicitly; the geometry of the gel particle does not appear. This was accomplished by assuming that all gel particles are geometrically similar; namely, the length of the particles is twice their diameters. This is, of course, usually not the case. The equations can be modified in the following ways to eliminate this limitation so that the rate of heating is explicitly a function of the pellet dimensions of diameter (D) and length (L), each of which in this case is an independent parameter.

Thus, equation (3a) is changed to:

$$\frac{D_{f1} L_{f1} \rho_{f1} C_{f1}}{4\left(\frac{D_{f1}}{2} + L_{f1}\right)} \frac{dT}{dt} = \frac{4 k_g}{(D_{f1} + L_{f1})} (T_g - T) + \sigma(T_g^4 - T_4^4). \quad (3a^1)$$

Equation (3b) is changed to:

$$\frac{D_{f2} L_{f2} \rho_{f2} C_{f2}}{4\left(\frac{D_{f2}}{2} + L_{f2}\right)} \frac{dT}{dt} = \frac{4 k_g}{(D_{f2} + L_{f2})} (T_g - T) + \sigma(T_g^4 - T_4^4). \quad (3b^1)$$

Equation (3c) and (3d) are unchanged.

Subscript f refers to frit (or gel) particle.

Subscript 1 refers to particles when  $T \leq T_1$ .

Subscript 2 refers to particle when  $T_1 < T \leq T_2$ .

D is particle diameter.

L is particle length.

Equation (6a) is changed to:

$$\gamma = g\left(1 - \frac{\rho_g}{\rho_{f1}}\right). \quad (6a^1)$$

Equation (6b) is changed to:

$$\gamma = g\left(1 - \frac{\rho_g}{\rho_{f2}}\right). \quad (6b^1)$$

Equation (6c) is unchanged.

Equation (7a) becomes

$$\delta = -\frac{50}{\pi} \mu_g \frac{\frac{\pi}{4} D_{f1} + L_{f1}}{(D_{f1} + L_{f1}) D_{f1} L_{f1} \rho_{f1}}. \quad (7a^1)$$

Equation (7b) becomes

$$\delta = -\frac{50}{\pi} \mu_g \frac{\frac{\pi}{4} D_{f2} + L_{f2}}{(D_{f2} + L_{f2}) D_{f2} L_{f2} \rho_{f2}}. \quad (7b^1)$$

Equation (7c) is unchanged.

$\mu_g$  is absolute viscosity of furnace gas.

$\rho$  is mass density.

References:

1. McAdams, W. H. Heat Transmission. New York: McGraw Hill, 1954.

## APPENDIX II\*

### GELSHEL Program

A program (GELSHEL) has been developed to calculate the position, thermal characteristics and the temperature history of a particle dropped through a vertical furnace. The governing differential equations are discussed in Appendix I and will not be repeated here. The program utilizes the forward finite difference of approximation to the differential equations.

The program keeps track of the particle as it undergoes four temperature-dependent transformations shown in Figure 1. The particle is dropped from rest into the top of the furnace. Initially, the input particle is at room temperature, its mass and IR absorptance are  $m_1$  and  $\alpha_1$ , its geometry is that of a right circular cylinder of diameter and length  $D_1$ ,  $L_2$  and its specific heat is  $(1 + X_1)C_p$ . The additional  $X$  is used to approximate endothermic reactions that take place in the particle.

Upon reaching  $T_1$  the particle undergoes changes in mass ( $m_1 \rightarrow m_2$ ), dimensions ( $D_1 \rightarrow D_2$ ,  $L_1 \rightarrow L_2$ ) and specific heat ( $X_1 \rightarrow X_2$ ). At  $T_3$ , the endothermic reactions are deemed complete and the particle's specific heat reverts to  $C_p$ , the specific heat of glass at  $T_2$ , the geometry changes from that of a right circular cylinder to that of a spherical shell. The final transformation occurs when the particle temperature reaches  $T_4$ . At this temperature, the IR absorptance changes from  $\alpha_1$  to  $\alpha_2$ . The execution of the program is terminated when the particle exits the furnace ( $S = 370$  cm).

The program accepts the following input data:

$M_1$ ,  $M_2$  and  $M_3$  of particle

$D_1$ ,  $D_2$ ,  $D_3$ ,  $L_1$  and  $L_2$  of particle

$\rho_{\text{glass}}$ ,  $X_1$ ,  $X_2$ ,  $\alpha_1$ ,  $\alpha_2$

$T_1$ ,  $T_2$ ,  $T_3$ ,  $T_4$

Furnace Temperature Profile ( $T_f$  vs.  $S$ )

Furnace Gas Code (1,2,3,4,5,6,7)

Typical values for an input data set might be as follows:

$m_1$ ,  $M_2$ ,  $M_3$ (g): 19.2E-6, 13.8E-6, 13.8E-6

$D_1$ ,  $D_2$ ,  $D_3$ (cm): 266E-4, 333E-4, 396E-4

$L_1$ ,  $L_2$ (cm): 252E-4, 365E-4

\*Appendix II was authored by R. J. Simms of KfS Fusion, Inc.

$\rho_{\text{glass}}$  (g/cc): 2.4  
 $X_1, X_2$ : 1.0, 0.0  
 $\alpha_1, \alpha_2$ : 1.0, 0.0  
 $T_1, T_2, T_3, T_4$  (C): 500, 1000, 850, 1250  
 $S$  (cm): 0, 4, 7, 10.5, 18, 21  
 $T_f$  (C): 750, 1000, 1200, 1300, 1400, 1425  
 $S$  (cm): 25, 31.5, 46.5, 54, 370  
 $T_f$  (C): 1450, 1475, 1500, 1510, 1510  
 Furnace Gas : 1 (air)

The specific heat ( $C_p$ ) of the particle is assumed to be that of glass which is temperature dependent. A table of the specific heat of glass vs. temperature is contained in arrays within a subroutine. Linear interpolation between table values is used to update the specific heat of the particle at each interaction.

Also contained in arrays are the pertinent temperature-dependent properties (viscosity, conductivity and density) of seven furnace gases: air, argon, carbon dioxide, nitrogen, oxygen, steam and helium. Once the furnace gas is selected, the program writes a working table of the temperature dependent properties. Again, linear interpolation is used to update the viscosity ( $\mu_f$ ), thermal conductivity ( $k_f$ ) and density ( $\rho_f$ ) of the furnace gas at each interaction.

At the start, the temperature of the particle ( $T_p$ ) is 20°C and its displacement ( $S$ ) from the top of the furnace and its velocity are zero. Using the value of  $S$ , the program determines the temperature ( $T_f$ ) of the furnace gas from the temperature profile table with the value of  $T_f$ , the program then determines the furnace gas viscosity ( $\mu_f$ ), thermal conductivity ( $k_f$ ) and density ( $\rho_f$ ). Using  $T_p$ ,  $k_f$ , and  $T_f$  the program calculates the temperature rise of the particle from its thermal capacitance, the rates of heat transfer to the particle by convection and radiation and the time-step. It then uses the mass and dimensions of the particle and the values of  $\mu_f$  and  $\rho_f$  to calculate the "new" displacement of the particle. This process is repeated until the particle exits the furnace.

The output of the program, in addition to the input data, consists of the following:

1. Working tables of temperature-dependent properties.
2. Temperatures, times and displacements at which the particle transformations occurred.
3. Particle temperature, displacement, velocity and specific heat histories.
4. Values of selected expressions used in the calculations of (3) above.
5. Plot of the particle temperature history.

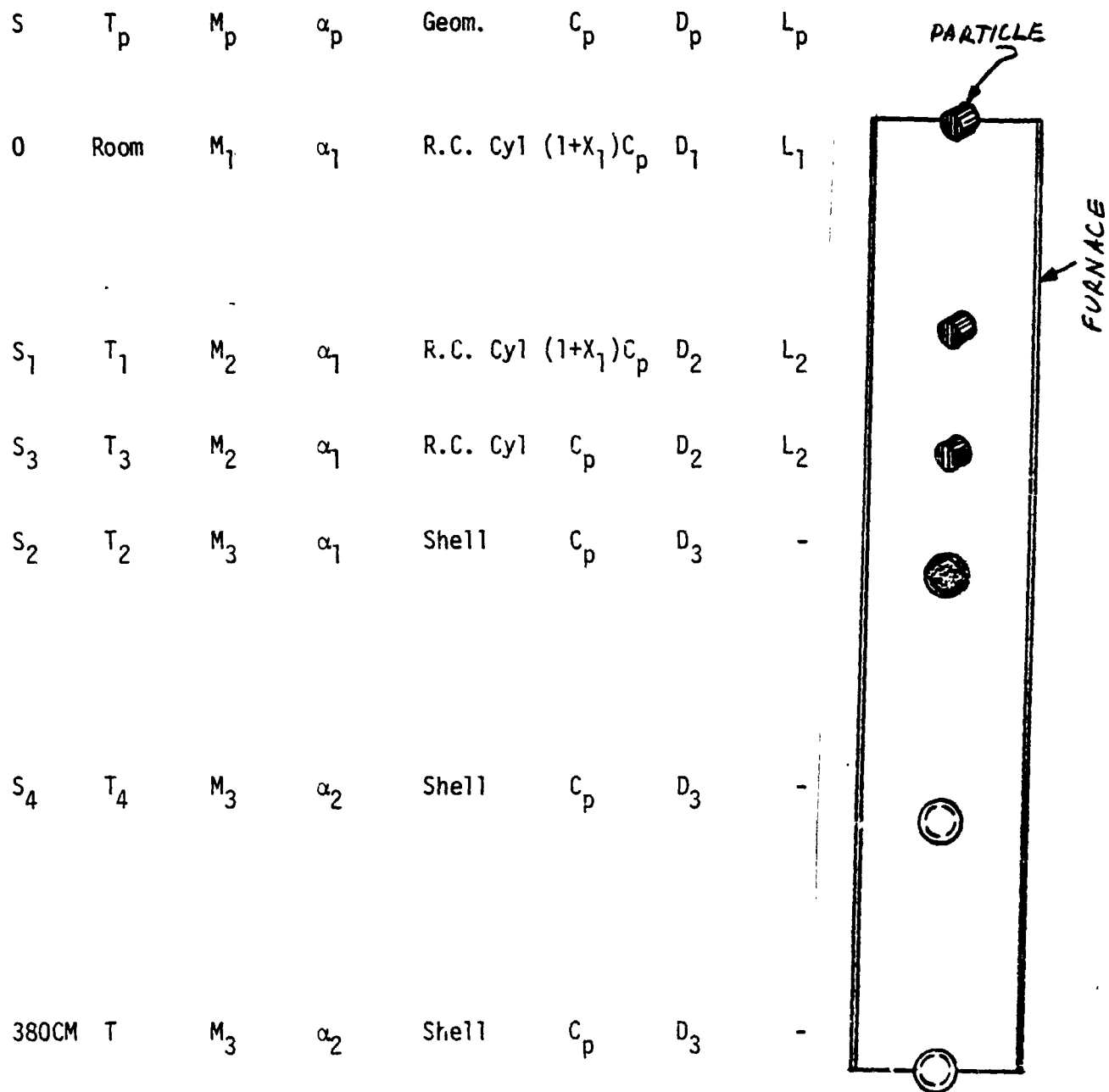


Figure 1. Temperature-Dependent Transformation of Gel-Particles Dropping Through Glass Furnace.

Radial Temperature Difference Model

A program, TGRAD, has been written to calculate the radial temperature profile history of a spherical gel particle. The gel particle was divided into eight equal-mass sub-volumes, or nodes. The inner node is a sphere and the remaining seven nodes are spherical shells. For nodes internal to the gel particle the program utilizes the forward finite difference approximation to the one-dimensional differential equation of heat conduction.

$$T_n' - T_n = \frac{\Delta t}{C_n} \left[ \frac{T_{n-1} - T_n}{R_{n-1, n}} + \frac{T_{n+1} - T_n}{R_{n, n+1}} \right]$$

where

$T_n'$  = Temperature of node n at the end of the time-step.

$T_n$  = Temperature of node n at the beginning of the time-step.

$\Delta t$  = Time-step.

$C_n$  = Thermal capacitance of node n.

$R_{n-1, n}$  = Thermal resistance between nodes n-1 and n.

The thermal capacitance of a node is given by

$$C = mC_p(T)$$

where

$m$  = Mass of the node.

$C_p(T)$  = Specific heat of the nodal material at the temperature T.

The thermal distance between adjacent nodes in the form of spherical shells is given by

$$R = \frac{D_o' - D_i'}{2\pi D_o' D_i'} \frac{1}{k(i)}$$

\*Appendix III was authored by R. J. Simms of KMS Fusion, Inc.

where

$D'$  = "Average" diameter of a shell, i.e., divides the shell into two shells of equal mass.

$D_0'$  = "Average" diameter of outer-shell

$D_i'$  = "Average" diameter of inner shell

$k(T)$  = Thermal conductivity of the nodal material at the temperature  $T$ , w/cm  $\cdot$   $^{\circ}$ C.

The boundary condition is that the heat input to the outermost shell is by convection and radiation; this is calculated from the same heat transfer relationship used in the GELSHEL code (described in Appendix II). Initially, the gel particle is at room temperature.

The specific heat and thermal conductivity of the gel particle are parameterized by linear approximations of the type  $A + B * T$  to published data. For specific heat, glass properties are used. For thermal conductivity, two extremes are used: glass properties for tightly compacted material and air for loosely compacted material.

The temperature of the furnace and furnace gas is a function of the distance from the top of the furnace. Hence, as the gel particle descends through the furnace, the ambient temperature changes. The rate of descent of the gel particle then determines the apparent rate of change of the furnace temperature. For short time periods of the order of 20 msec, a 20  $\mu$ g gel particle at the top of the furnace descends only about 2 millimeters which causes an ambient temperature change of only 12 $^{\circ}$ C. Hence, the furnace and gas (air) temperature was held constant for any given problem and the program was executed for just 20 to 50 msec problem time which was long enough to determine the maximum radial temperature profile of the gel particle.

For a furnace temperature of 1500 $^{\circ}$ C, the maximum radial temperature difference in a 20  $\mu$ gm, 296  $\mu$ m diameter gel particle is 80 $^{\circ}$ C for tightly compacted material and 1390 $^{\circ}$ C for loosely compacted material as shown in Figure 1. For a furnace temperature of 750 $^{\circ}$ C, the maximum temperature difference is 22 $^{\circ}$ C for tightly compacted material and 674 $^{\circ}$ C for loosely compacted material. For a 180  $\mu$ gm, 608  $\mu$ m gel particle, the maximum radial temperature difference is 105 $^{\circ}$ C, occurring 15 msec after injection into a 1500 $^{\circ}$ C environment (See Figure 2).

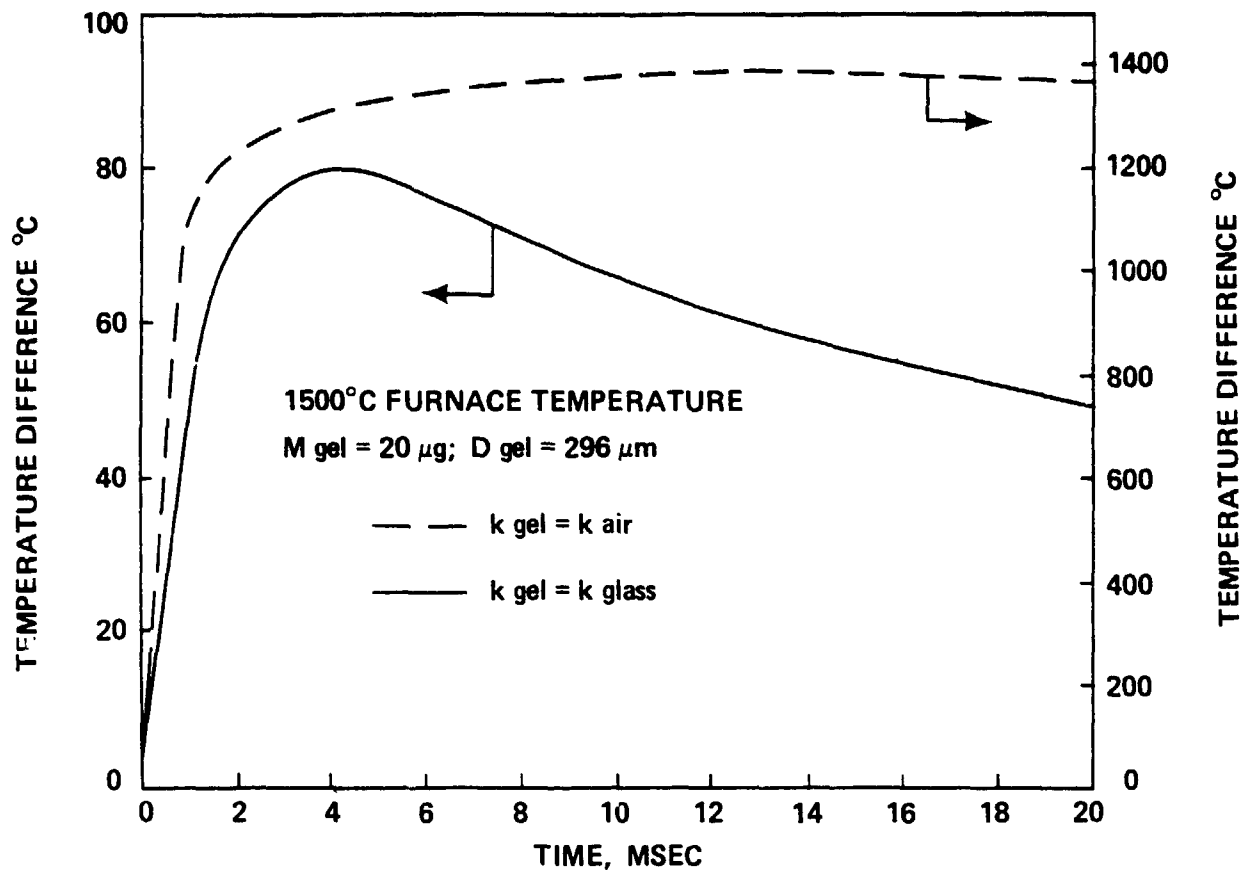


FIGURE 1. GEL PARTICLE CORE-TO-SURFACE TEMPERATURE DIFFERENCE

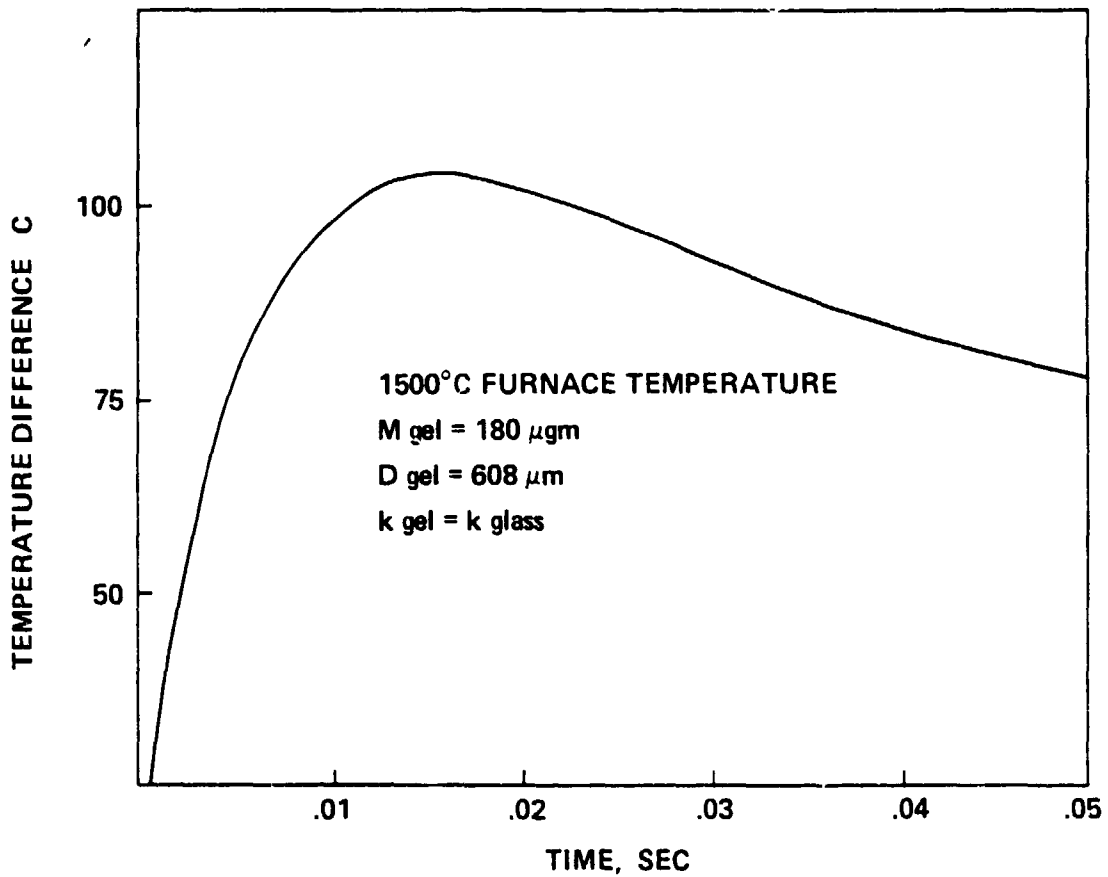


FIGURE 2. GEL PARTICLE CORE-TO-SURFACE TEMPERATURE DIFFERENCE

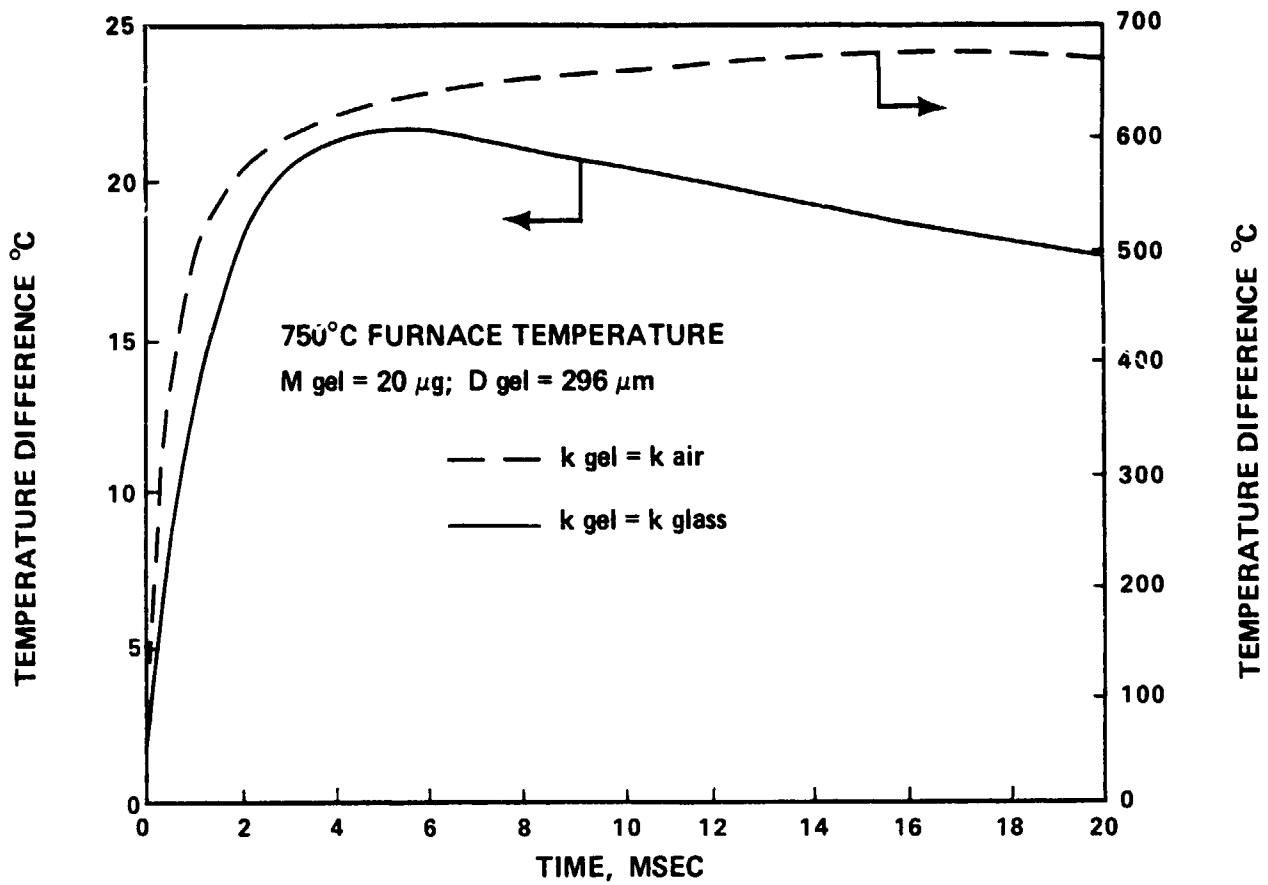


FIGURE 3. GEL PARTICLE CORE-TO-SURFACE TEMPERATURE DIFFERENCE

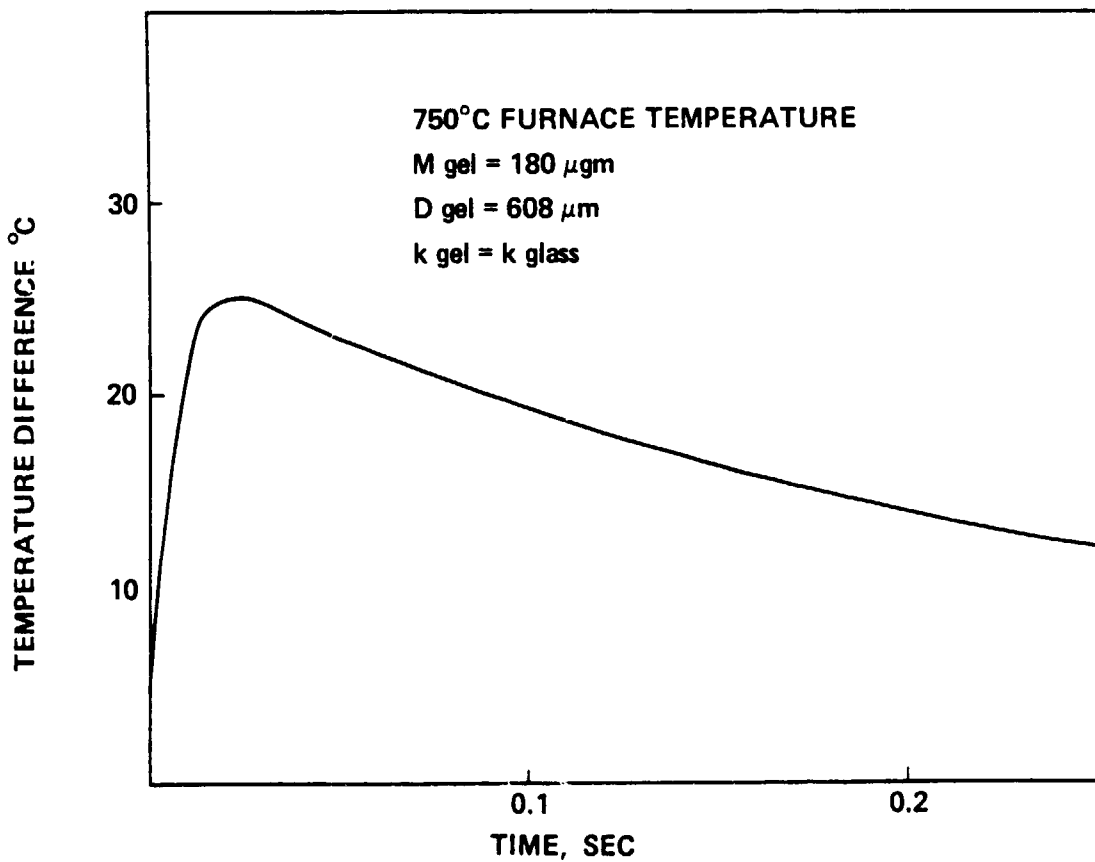


FIGURE 4. GEL PARTICLE CORE-TO-SURFACE TEMPERATURE DIFFERENCE

If the furnace environment is assumed to be 750°C, (shown in Figures 3 & 4) a more realistic condition, a maximum radial temperature difference of 25°C develops in the same particle 22.5 msec after injection. In all of these cases, the gradients maximize within approximately 20 msec and diminish rapidly with time. Consequently, one can safely make the simplifying assumption of a negligible temperature gradient for such gel particles in heat transfer calculations.

## APPENDIX IV

### A Model for the Prediction of Wall Non-Uniformity, in Thin, Liquid, Spherical Shells, Resulting from Acceleration (e.g., Gravity) Fields.\*

The purpose of this analysis is to develop a model that gives insight to the wall non-uniformity that is produced in a thin, liquid, spherical shell by gravity. A primary guideline for this development is that the analyses be extremely straight-forward; although it is feasible to develop very accurate models for this type of problem, such a project would be complex, long-range, and expensive.

The general notation is illustrated in Figure 1. Although it need not generally be the case, we assume that the liquid shell is bounded, both internally and externally, by spherical surfaces. This assumption is justified because we are primarily interested in shells of molten glass, for which the effects of surface tension are relatively large. The spherical region inside of the shell is occupied by a gas with a density that is negligible relative to the density of the liquid comprising the shell. Additionally, the region exterior to the shell is occupied by a gas: e.g., a furnace gas. Because of the very large viscosities of the molten glasses in which we are interested, we assume that two types of forces control the dynamic behavior of the shell:

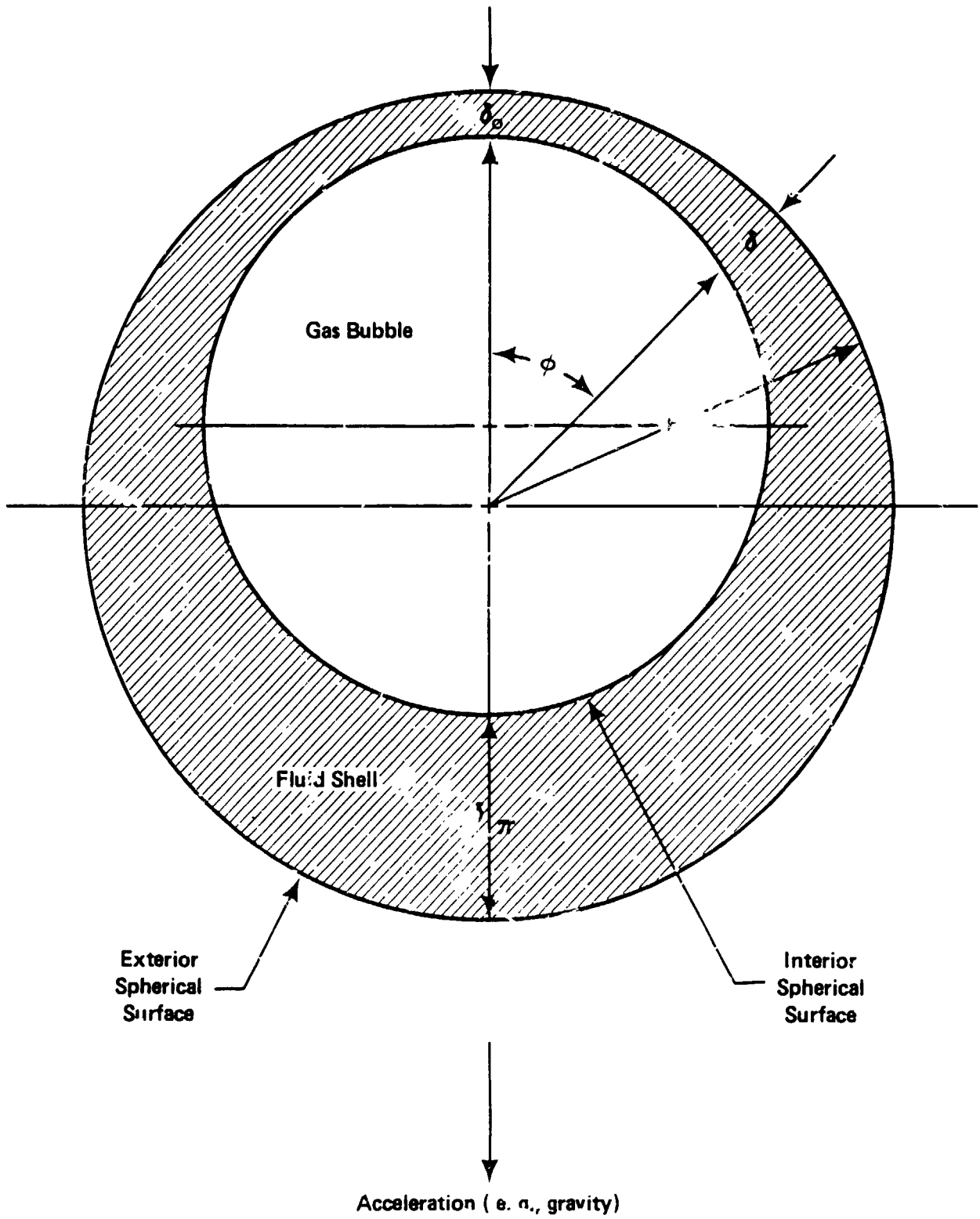
1. Body forces due to a constant acceleration field, e.g., gravity.
2. Forces caused by the viscosity of the liquids.

These assumptions place our model into a rather well-defined, very-important region of fluid mechanics, known as Low Reynolds Number Hydrodynamics or Creeping Flow. Although these types of problems have been studied intensely for over a hundred years, the problem in which we are interested has not been solved, and, as indicated above, cannot be solved within the guideline we have been working.

We therefore have adopted the following simplistic image. Consider that, as some time  $t$  (say,  $t = 0$ ), the interior and exterior surfaces of the shell are concentric. Immediately, the acceleration field causes the gas bubbles to "rise" within the liquid shell; or, conversely we may visualize that the liquid flows "down" the narrow space between the interior and exterior surfaces. This makes the shell thinner at the top and thicker at the bottom, leading to wall non-uniformity.

\*Appendix IV was authored by R. B. Jacobs of R. B. Jacobs Associates, consultant to current contract.

Figure 1.  
REPRESENTATION OF A GLASS SHELL  
WITH DECENTERED SURFACES



We assume that the shell does not rotate about any axis, and that, if it has any motion, the motion will be parallel to the uniform acceleration field. These assumptions are credible because tumbling of the shell tends to be damped. Then, because of the initial symmetry of the shell, the shell will always be axially symmetrical with respect to its diameter that is parallel to the acceleration field. It follows that the thickness ( $\delta$ ) of the shell is a function of only time ( $t$ ) and one spatial variable, the angle  $\phi$  shown in Figure 1.

A fundamental assumption in the following development is that the shell be thin. That is, if the radius of the exterior spherical surface be  $R$  and the thickness of the shell be  $\delta$ , we assume that

$$\frac{\delta}{R} \ll 1 \quad (1)$$

Note that the shell thickness,  $\delta(t, \phi)$ , is defined as a length, measured along a radius of the exterior spherical surface, between the interior and exterior spherical surfaces. It is apparent from the foregoing discussion that the minimum shell thickness will be at the top (at  $\phi = 0$ ) and the maximum shell thickness will be at the bottom (at  $\phi = \pi$ ). At  $\phi = 0$ ,  $\delta(t, \phi) \equiv \delta_0(t)$ ; at  $\phi = \pi$ ,  $\delta(t, \phi) \equiv \delta_\pi(t)$ . The wall non-uniformity (WNU) is defined as:

$$WNU = \frac{\delta_\pi - \delta_0}{\delta_0} = \left( \frac{\delta_\pi}{\delta_0} - 1 \right) \quad (2)$$

In order to proceed with our development we must make decisions regarding the conditions at the boundaries of our shell. Two most tenable conditions are that the shearing stresses are the same on each side of the interior surface, and are the same on each side of the exterior surface. Because the liquid shell is bounded by gas, both on the inside and on the outside, it would probably be satisfactory to assume that these stresses are zero at both surfaces. Even these conditions lead to the unacceptable complexities mentioned above. We therefore make assumptions that will yield the simplest model, and will also permit the development of wall non-uniformity controlled by viscous and acceleration effects:

1. There are only tangential velocity components.
2. The shearing stress at the interior surface of the shell are zero.
3. The velocity of the liquid at the exterior surface, relative to that

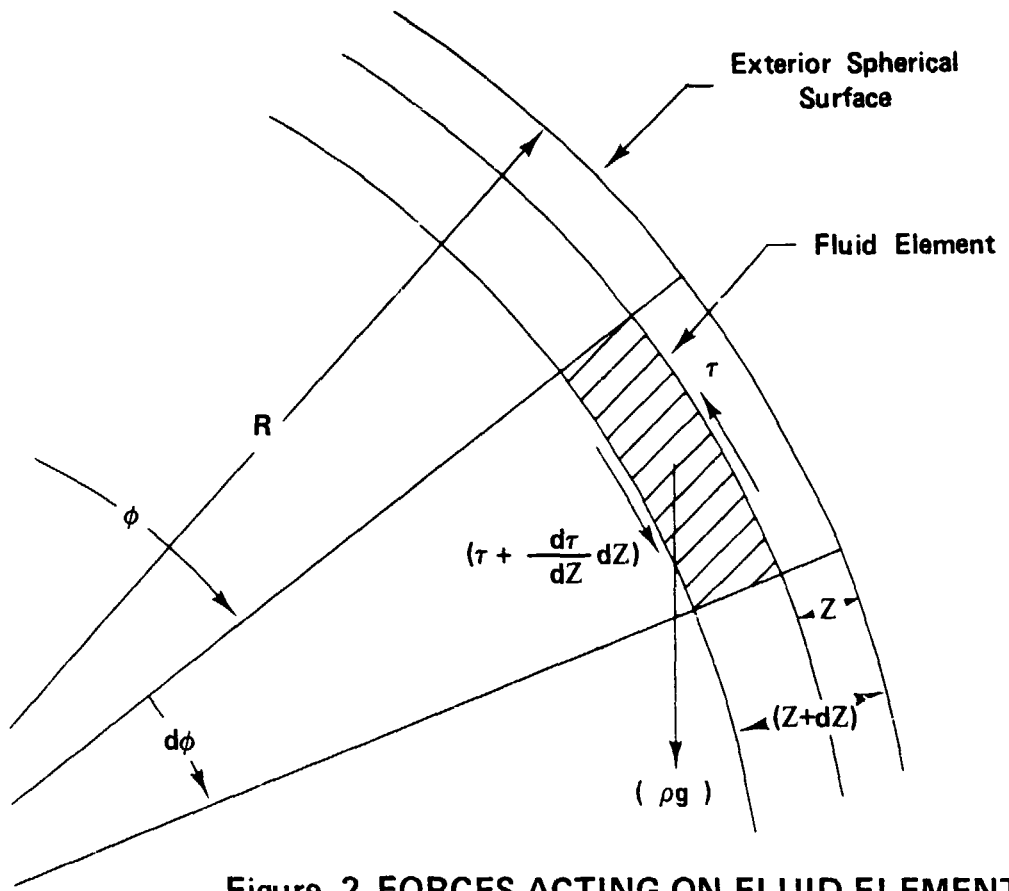


Figure 2 FORCES ACTING ON FLUID ELEMENT

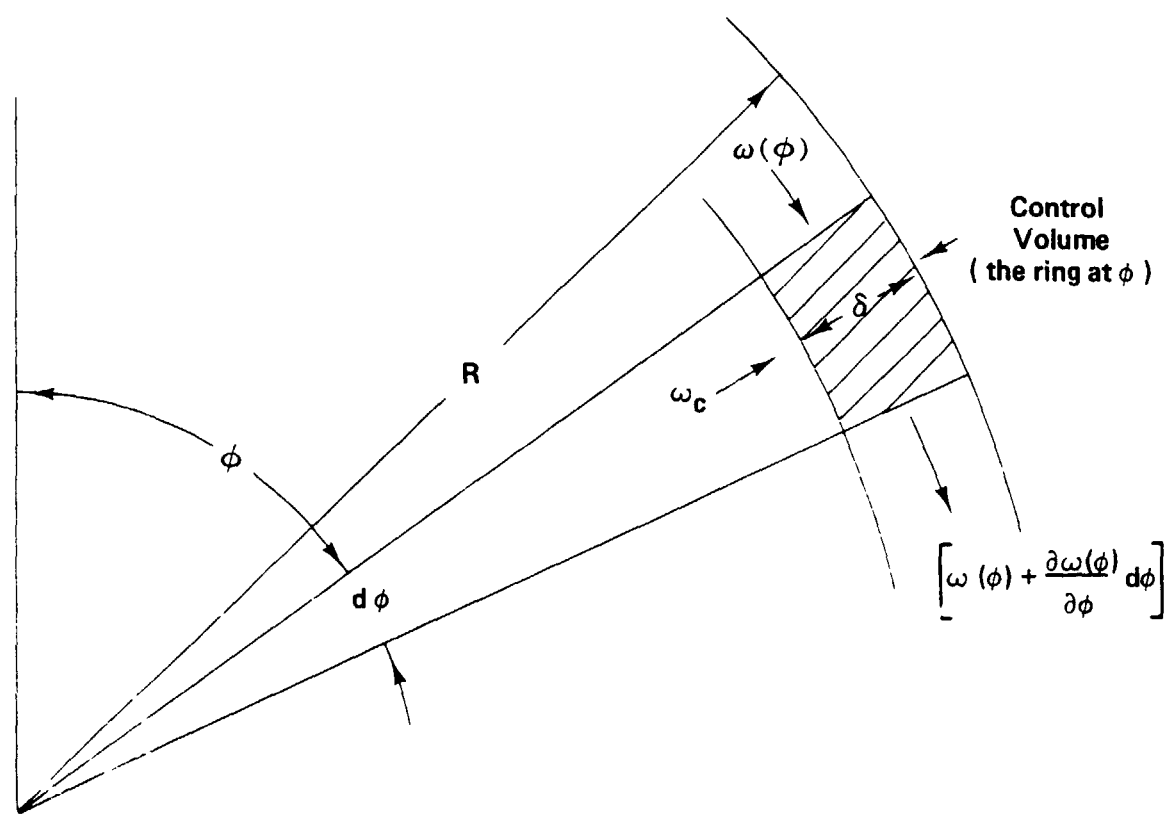


Figure 3 FLUID FLOWS TO CONTROL VOLUME

surface, is zero (no slip). Conceptually, we imagine that the shearing stresses, resulting from the fall of the shell through its surrounding medium, are sufficient to accomplish this.

4. At every instant, a steady-state velocity distribution exists across the shell wall; however, this distribution varies with time. This assumption is conservative relative to the purposes of this development. It leads to predicted values of WNU that are excessive; actual shells showed smaller non-uniformities than predicted.

Applying Newton's Second Law, in the tangential direction, to the fluid element in Figure 2 gives

$$\frac{d\tau}{dZ} = - \rho a \sin \phi \quad (3)$$

where

$\tau$  = shearing stress in the tangential direction,

$Z$  = a radial coordinate, measured inward from the exterior spherical surface,

$\rho$  = density of shell material, and

$a$  = acceleration.

Assuming that the shell material is Newtonian,

$$\tau = \mu \frac{dv}{dZ}, \quad (4)$$

where

$\mu$  = absolute viscosity, and

$v$  = velocity in tangential direction.

Substituting Equation 4 into Equation 3, and utilizing assumptions 2 and 3 in the preceding paragraph, we have

$$v = \frac{\rho a}{\mu} \sin \phi Z \left[ \delta - \frac{Z}{2} \right]. \quad (5)$$

Applying continuity considerations to the control volume in Figure 3 and noting that

$$w(\phi) = \int_{Z=0}^{\delta} \rho(2 \pi R \sin \phi dZ)v, \quad (6)$$

we obtain

$$\frac{d\delta}{dt} = - \frac{\rho a}{3\mu} \frac{1}{R \sin \phi} \frac{\partial}{\partial \phi} (\delta^3 \sin^2 \phi). \quad (7)$$

We define two dimensionless parameters:

1. Dimensionless wall thickness,  $\eta$

$$\eta = \left(\frac{\delta}{R}\right) \quad (8)$$

2. Dimensionless time,  $\tau$

$$\tau = \left(\frac{\rho a R}{3\mu}\right) t. \quad (9)$$

Introducing Equations 8 and 9 into Equation 7 yields

$$\frac{\partial \eta}{\partial \tau} = - \frac{1}{\sin \phi} \frac{\partial}{\partial \phi} (\eta^3 \sin^2 \phi) \quad (10)$$

Equation 10 is our final non-linear, partial differential equation which, when used with specific initial and boundary conditions, will permit us to obtain the shell-wall thickness as a function of time and position:

i.e.,  $\eta(\tau, \phi)$ .

By utilizing the assumptions made above, most particularly Equation 1 and the sphericity of the bounding surfaces, Equation 10 can be reduced to an ordinary differential equation. Let  $S(\tau)$  be the distance between the centers of the interior and exterior spherical surfaces. Then, because  $\eta \ll 1$  and  $\left(\frac{S}{R}\right) \equiv v \ll 1$ , we may derive that

$$\eta(\tau, \phi) = \left[ 1 - \frac{R_i}{R} - v(\tau) \cos \phi \right] \quad (11)$$

where

$R_i$  = radius of the interior spherical surface.

Substituting Equation 11 into Equation 10, we obtain

$$\cos \phi \frac{dv}{d\tau} = \left[ 3 \left( 1 - \frac{R_i}{R} - v \cos \phi \right)^2 v \sin^2 \phi + 2 \left( 1 - \frac{R_i}{R} - v \cos \phi \right)^3 \cos \phi \right]. \quad (12)$$

Equation 12 is an ordinary differential which may be integrated at  $\phi = 0$  and  $\phi = \pi$ . Performing the integrations, and substituting into Equation 11, we obtain

$$\eta_0 = \left\{ 4 \left[ \frac{1}{4\bar{\eta}^2} + \tau \right] \right\}^{-\frac{1}{2}} \quad (13)$$

and

$$\eta_\pi = \left\{ 4 \left[ \frac{1}{4\bar{\eta}^2} - \tau \right] \right\}^{-\frac{1}{2}} \quad (14)$$

where

$\eta_0$  = value of  $\eta$  at  $\phi = 0$ ,

$\eta_\pi$  = value of  $\eta$  at  $\phi = \pi$

$\bar{\eta}$  = value of  $\eta$  when shell wall is uniform.

Note that

$$\bar{\eta} = \frac{2}{AR}, \quad (15)$$

where

(AR) = aspect ratio of the shell.

$$(AR) = \frac{D}{\bar{\delta}}, \quad (16)$$

where

D = outside diameter of shell and

$\bar{\delta}$  = shell wall thickness when shell wall is uniform.

Substitute Equations 15, 16, and 9 into Equations 13 and 14. Combine Equations 8 and 2 to express WNU in terms of  $\eta_0$  and  $\eta_\pi$ . Combining the the resulting three equations and rearranging gives:

$$WNU = \left[ \sqrt{\frac{1 + T}{1 - T}} - 1 \right], \quad (17)$$

where

$$T = \left[ \frac{8\rho a D}{3\mu(AR)^2} \right] t. \quad (18)$$

Equations 17 and 18 express the wall non-uniformity (WNU), as a function of time (t), of all thin-walled shells which conform with the assumptions and limitations delineated in the development. We see that the wall non-uniformity is completely specified by the single, dimensionless parameters (T) defined by Equation 18.

Equation 17 is plotted in Figure 4, where T is considered as a dimensionless time. We see, for example, that WNU = 10% when T = .095.

We note that a characteristic time,  $t^*$ , can be defined for the system.

$$t^* = \left( \frac{3\mu(AR)^2}{8\rho aD} \right) \quad (19)$$

$t^*$  is, of course, determined by the shell geometry, shell material properties, and the acceleration. Examination of Equations 17, 18, and 19 shows that  $t^*$  is the real time required for the wall non-uniformity to become infinite.

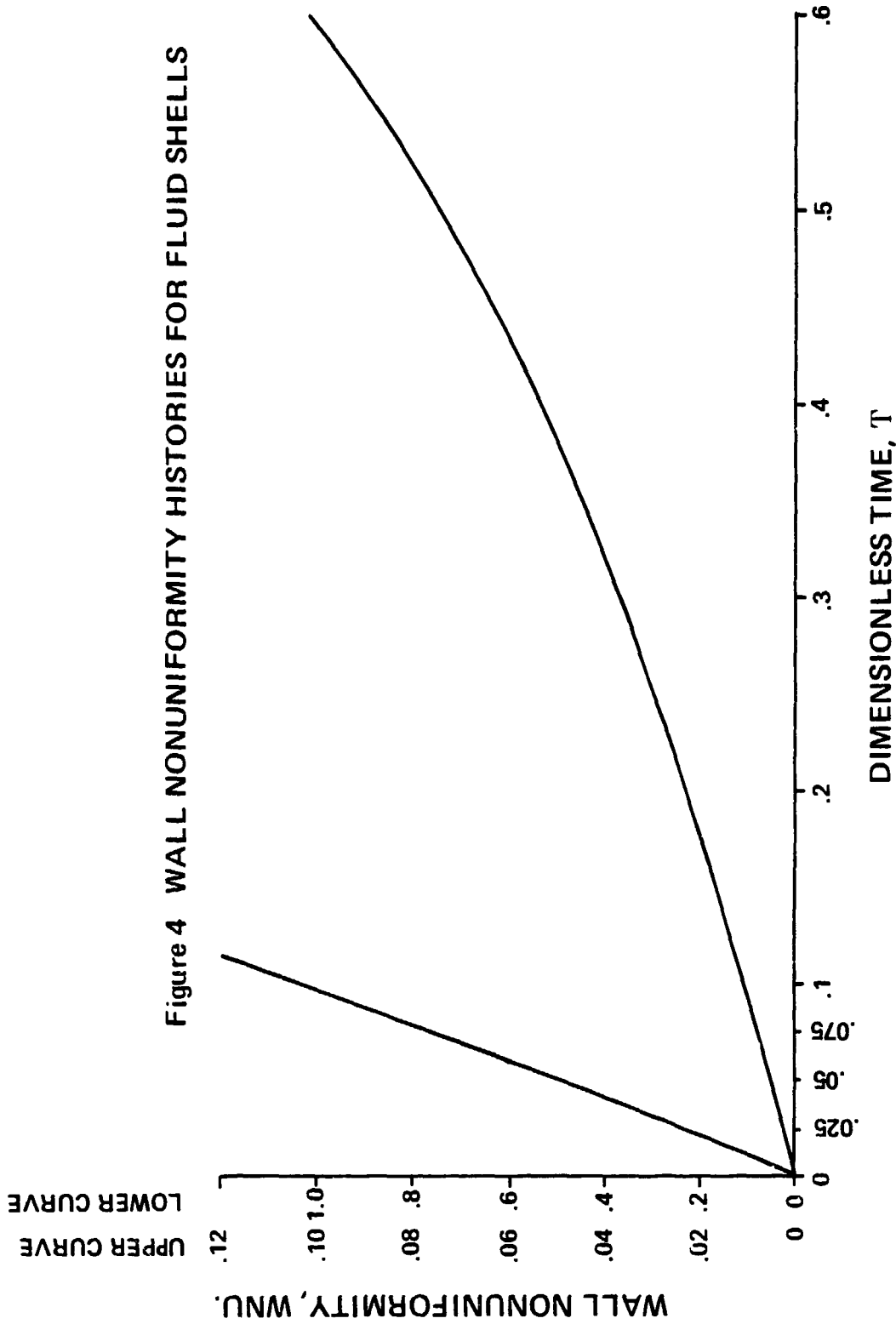


Figure 4 WALL NONUNIFORMITY HISTORIES FOR FLUID SHELLS